Faculdade de Engenharia da Universidade do Porto

Honeycomb Sandwich Structures made with Cork

Mafalda Manuela Vieira Pinto de Miranda Esteves

Integrated Masters in Mechanical Engineering

Supervisor: António Torres Marques
Co-Supervisor: Paulo Nóvoa

September, 2021

Resumo

A cortiça é um material leve e natural, extraído da casca das árvores *Quercus Suber L*, normalmente encontradas nas florestas em Portugal. É comum encontrar cortiça em rolhas, mas, hoje em dia, já se usa em aplicações de construções civis e aeronáutica, devido às suas propriedades de isolamento térmico e acústico.

Uma estrutura sanduíche é um tipo de compósito que utiliza duas peles com um núcleo entre as mesmas. As peles suportam as cargas de compressão e tração e o núcleo resiste às forças de corte. Na maioria dos casos, estes componentes são unidos com um adesivo.

Existem diversos tipos de núcleo, feitos por diferentes materiais. Os núcleos feitos de espumas, estruturas onduladas, treliças, à base de madeira e ninho de abelha (*honeycomb)* são apenas alguns exemplos. Este último tem como objetivo construir um núcleo furado, ou seja, mais leve, sem diminuir significativamente as propriedades finais. Estes furos podem ter diversas formas.

O objetivo deste estudo foi desenvolver uma estrutura sanduiche com peles em compósito de fibra de carbono e núcleo de cortiça, analisando em termos de esforços de flexão, compressão e impacto de baixa velocidade. Dois núcleos diferentes foram escolhidos: núcleo com furos hexagonais, representado o núcleo tradicional *ninho de abelha*; e núcleo com furos auxéticos, na forma "reentrante". Este último representa uma estrutura que depende do material e da geometria do mesmo, neste caso, dos furos. Além desta comparação de núcleos, o objetivo deste trabalho foi também comparar o núcleo de cortiça com outros núcleos tradicionais com matérias menos sustentáveis.

O tamanho do furo e o material da cortiça foi baseado nas propriedades especificas e numa simulação numérica, feita com o software ABAQUS ®, que representava ensaios mecânicos para analisar as propriedades. O tamanho escolhido foi um hexágono com dimensão de 10 [mm] e espessura de parede de 2 [mm]. Para o material selecionou-se a cortiça NL10, de massa específica 150 [kg/m^3], cujo fornecimento das placas da mesma assim como as fichas técnicas foi assegurado pela Amorim Cork Composites.

A parte experimental foi também corroborada pela simulação numérica dos ensaios, com boa concordância entre os dados experimentais e numéricos, feitos no software ABAQUS®.

Os ensaios mecânicos de compressão e flexão demonstraram propriedades superiores no núcleo auxético, em relação ao hexagonal. No ensaio de impacto por baixa velocidade, as capacidades de absorção de energia foram semelhantes em ambos os núcleos.

Observando os resultados do núcleo de cortiça nos diferentes ensaios, e comparando com os núcleos tradicionais, é possível ver que a cortiça demonstra propriedades mais baixas.

Assim, estes núcleos seriam mais competitivos para aplicações com menores esforços de corte e de compressão e/ou isolamento térmico, acústico e de vibração.

^

Página em branco

Abstract

Cork is a lightwieght, natural material made from the bark of the *Quercus Suber L.* tree, which can be found in Portugal's forests. The principal application is wine stoppers, but due to its unique thermal and vibration insulation and acoustic characteristics, it is now commonly found in construction and aeronautic applications.

A sandwich structure is a type of arrangement made up of two skins and a core sandwiched between them. The skins can withstand compression and tension, while the core is responsible for shear loads. These components are “glued” together, usually with an adhesive layer.

Cores come in a variety of shapes and materials. Cores made of foams, corrugated, wood based, truss, and honeycomb are only a few examples. The latter has a goal to build a lightweight core without sacrificing final attributes. The core is perforated, with holes of various shapes.

The design of a sandwich construction with skins made of carbon fibre prepreg, a common material, and a core made of cork was studied in flexural, compressive, and impact stresses in this study. The hexagonal core with hexagonal holes, which symbolises typical honeycomb cores, and the auxetic core with re-entrant form cells were chosen as cores. This one functions as a structure that is influenced not only by the material properties but also by the cell's shape. The purpose was also to compare cork cores to other less natural renewable traditional cores.

The size of the cell forms in the core holes was determined using a computer simulation of the mechanical studies, which included evaluating various cell sizes and wall thicknesses. The result was a hexagonal cell with a cell size of 10 [mm] and a wall thickness of 2 [mm]. The material was also chosen based on its specific properties and a computational simulation with a shear and compression test. NL10 (density = 150 [kg/m^3]), NL20 (density = 202.5 [kg/m^3]), and NL25 (density = 250 [kg/m^3]) were the options. The material utilised was NL10, and Amorim Cork Composites provided technical data sheets as well as cork boards. A numerical simulation performed with the software ABAQUS®, was done to support the experimental data.

Mechanical tests revealed that the auxetic core outperformed the other core in flexural and compressive loads. Both cores demonstrated equivalent absorption capabilities in low-velocity impacts.

When all the test findings are compared to the common cores, cork has lower properties, making it suitable for applications requiring reduced shear and compressive strength and /or specific thermal and vibration insulation and acoustic characteristics.

Página em branco

Acknowledgements

I'd like to thank my supervisor, Professor António Torres Marques, without whose knowledge, patience, recommendations, and consistent assistance throughout the process, I would not have been able to complete my project.

Professor Paulo Nóvoa, my co-supervisor, whose technical knowledge and guidance proved important to the development of this study. I'd also like to express my gratitude for providing the opportunity to expand my work at INEGI and for assisting me in doing so.

For all of Professor Marco Parente's comments and ideas during the creation of the numerical analysis.

To Engineer José Teixeira, from INEGI, for his work on the honeycomb core structures' development and production.

To Engineer Fábio Neto of INEGI for his assistance with the skins manufacturing.

To Engineers Miguel Figueiredo and Rui Silva, from LET (DEmec), for the support during the experimental testing.

To Engineer Marta Reinas and Dra Maria Martins from Amorim Cork Composite, who provided the cork and cork board technical data sheets.

To FEUP – Faculdade de Engenharia da Universidade do Porto - for the opportunity to do a master's degree in mechanical engineer.

To INEGI - Instituto de Ciência e Inovação em Engenharia Mecânica e Engenharia Industrial – for the space and materials provided in the developing of this project.

And finally, to my family, friends and boyfriend for the constant support and kind words, fundamental for finishing this thesis.

Página em branco

Contents

List of figures

List of tables

Abbreviations and Symbols

ASTM - American Society for Testing Materials

CFRP – Carbon Fibre Reinforced Polymer

CNC – Computer Numerical Control

EPS – Expanded Polystyrene

HDF – High Density Fibreboard

LVDT - Linear variable differential transformer

MDF - Medium Density Fibreboard

PC - Polycarbonate

PIR - Polyisocyanurate

PLA – Polylactial acid

PMI - Polymethacylmide

PP - Polypropylene

PS - Polystyrene

PU - Polyrethane

PUR – Polyrethane Rigid

PVC – Polyvinyl Chloride

UD - Unidirectional

TNT - Tessuto Non Tessuto , or in English nonwoven

XPS – Extruded Polystyrene

A – surface area; units SI: m^2 square meter

b – width; units SI: m meter

c – core's height; units SI: m meter

d – sandwich's height; units SI: m meter

D – Flexural Rigidity; units SI: $N.m^2$ Newton times square meter

E – Young's Modulus; units SI: Pa Pascal

E_f – Facing's Modulus; units SI: Pa Pascal

E_k – Kinetic Energy; units SI: J Joule

E_p – Potential Energy; units SI: J Joule

E_q – Equivalent Modulus; units SI: Pa Pascal

g – gravitic acceleration; units SI: m/s^2 meter per square second

G – Core Shear Modulus; units SI: Pa Pascal

h – height; units SI: m meter

I – moment of inertia; units SI: m^4 meter to the power of four

L - length; units SI: m meter

L_1 – length between the loading cylinders; units SI: m meter

l_h – wall's length of the hexagonal cell; units SI: m meter

m - mass; units SI: kg kilogram

P – force ; units SI: N Newton

S - slope

S_1 – length between the support cylinders; units SI: m meter

t - thickness; units SI: m meter

t_h – wall's thickness of the hexagonal cell; units SI: m meter

U – transverse shear rigidity; units SI: N Newton

v - velocity; units SI: m/s meter per second

Δ - deflection; units SI: m meter

σ – normal stress; units SI: Pa Pascal

δ - displacement; units SI: m meter

τ – shear stress; units SI: Pa Pascal

Chapter 1: Introduction

The search for new materials has always been a concern for humankind. Nowadays, the urge to have lightweight and environmentally friendly, with improved mechanical properties materials is increasing. As technology and ideas emerge, composite materials are evolving with different elements to test out different approaches. Here is where cork composites are a possibility.

A composite material is defined as an alliance of two or more materials, creating a new "material" with better specific characteristics than the ones observed in the constitutive materials solo.

The sandwich structures are a result of composite materials and present a beneficial bond between the components. The skins are rigid and provide high stiffness and strength to the structure, resisting to tensile and compressive stresses. The cores, usually with low modulus of elasticity, need to resist the shear stresses of the sandwich structure, as well as supporting the skins. Another inherent characteristic is the increased flexural stiffness of the sandwich structure. There are different types of core structure, such as honeycomb, foam, etc. (William D. Callister & Rethwisch, 2007). Some of the traditional cores use synthetic materials, contributing to the possible contamination of air and water during the manufacturing and waste disposal processes. The need for eco-friendly, biodegradable materials and the reduction of the carbon footprint during production is a growing issue (Sergi et al., 2021).

Cork is a natural, renewable material removed from the bark of the cork oak tree *Quercus suber L.* (Avillez et al., 2020). It is an interesting material due to its lightweight, thermal, and acoustic insulation performance, as well as permeability to fluids. The dimensional recovery is also an outstanding feature, among others (Sergi et al., 2021). The main applications are the wine stoppers, although many other industries, such as soil shoes, building and aeronautics, are interested in using cork (Avillez et al., 2020).

1.1 - Motivation and Research Objectives

As referred, cork is a promising material, and this work aims to test its hypothesis as an alternative to traditional cores.

Fortunately, there is some literature related to cork as a core material. However, there is still a lack of information on the possibility of transforming and testing agglomerated cork in honeycomb structures, reducing its weight.

The focus of this thesis is related to the honeycomb cell, and the typical cell structure is the hexagonal honeycomb. The shape of the cells proposed to compare will be hexagonal and auxetic (re-entrant shape). The re-entrant auxetic structure is a structure with a negative Poisson coefficient, and the idea is to study the advantages (or disadvantages) this specific structure can offer. The results will compare the structures behaviour to compression, bending and low-velocity impact response.

The experimental work will be supported with a finite element approach, using the software ABAQUS®, to obtain the best cell geometries and core dimensions.

1.2 - Structure of the Chapters

Chapter one clarifies the motivation and research objectives of the performed work and the subject of each chapter.

The second chapter provides the literature review about the sandwich structure, particularly focusing on cores and cork material. In the sandwich structures, the goal is to understand the concept, the primary components and, with particular attention to the core materials, approach the honeycomb cores. Also, analyse the progress of sandwich structures with a cork core. A review of the cork properties and applications in the modern world complements the chapter.

Chapter three is related to the numerical work. Firstly, will be discussed the procedure to choose the optimized size of the honeycomb hexagonal cell, as well as the type of cork. The second part of the chapter concerns the three detailed and more complex models representative of the experimental mechanical tests. The cell sizes and the models to verify the agreement with the experimental data were developed by using the finite elements software ABAQUS®.

The experimental work is described in the chapter four, including the preparation and assemble of the sandwich structures, as well as the description of the mechanical testing performed.

The results and their discussion from the previous part are presented in chapter five regarding the tests performed. The numerical results and experimental data will be compared in this section.

The sixth chapter contains the conclusions, withdrawn from the previous part, as well as some proposals for the future work on sandwich structures with cork, with or without honeycomb cores.

Chapter 2: Literature Review

2.1. Sandwich Structure

The base idea of the sandwich structure is to join two flat faces that will carry the bending, tensile and compressive loads, with a core between them. The purpose of the core is to support the shear loads. This concept is identical to an I-beam, composed of the web and flange (Campbell, 2010; Carlsson & Kardomateas, 2011).

Another interesting feature is the lightweight core. According to (Campbell, 2010), the thickness can increase by four times and, consequently, thirty-seven times the stiffness of the sandwich structure, with just a six per cent increase in the weight.

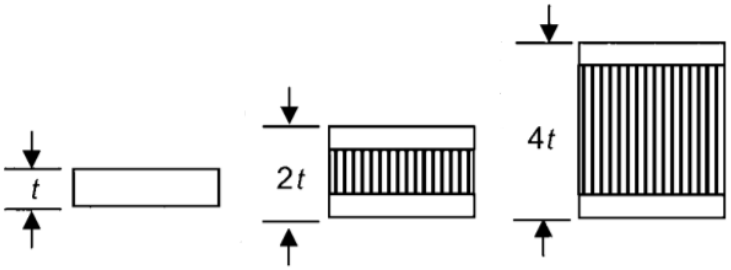

Figure 1 Comparison of different cores with different thicknesses (Campbell, 2010)

These optimized lightweight and high stiffness structures are very common to find in many industries, particularly in weight critical application, such as space structures, naval structures, aeroplanes components, etc (Carlsson & Kardomateas, 2011).

Figures 2 and 3 clarify the difference between flatwise and edgewise and in-plane and out-of-plane, which is important to understand how the loads are applied in the structure.

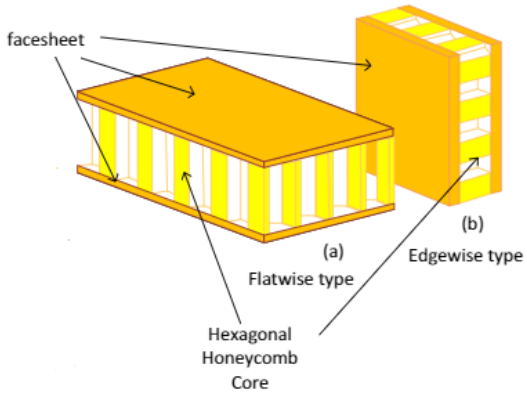

Figure 3 Difference between flatwise and edgewise(Arbintarso et al., 2019; J. Yan, 2013)

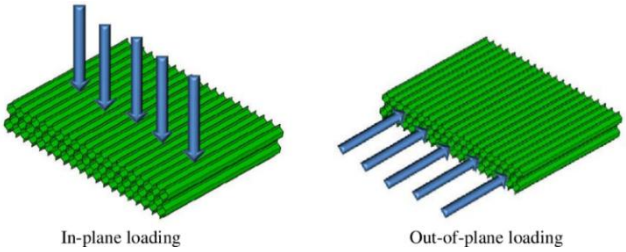

Figure 2 Difference between in-plane loading and out-of-plane loading (J. Yan, 2013)

2.1.1. Failure modes

Understanding how the loads affect the sandwich structures is crucial in order to predict the failures and optimize the properties of the structures.

The following sections are divided into four types of solicitations and in each one, the consequent failures modes will be described.

2.1.1.1. Bending

The bending solicitations can appear in a four-point bending test or in a three-point bending test. The three-point bending test has one loading bar between the two support bars, producing a compressive loading on top and a tensile loading in the bottom surface. The four-point bending, contrary to the first test, has two load cylinders, exposing a higher area to the stress. For this reason, the strengths are lower in the four-point bending test (Junior, Ferracane, & Bona, 2008).

In the four-point bending test, also known as pure bending, the predominant failures of the structures are compressive failure, when the stress in the face reaches the compressive strength of the material, and face wrinkling when the compressive strength of the material is higher than the stress in the face. The first mode occurs in high stiffness in the through-the-thickness direction cores. The face wrinkling is related to lower stiffness cores (Zimmermann & Wang, 2020).

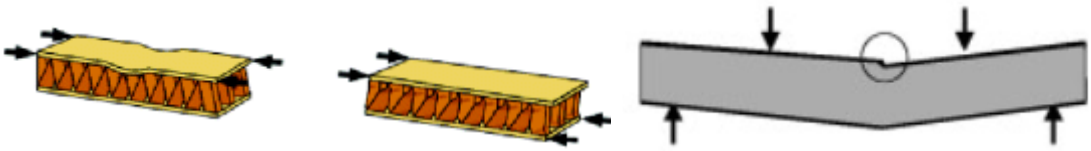

Figure 4 From left to right: face wrinkling; core shear failure (Heimbs, 2012) and compressive failure (Cabrera, Alcock, & Peijs, 2008)

For the three-point bending test, two events happen: the faces experience bending force and the core contacts with shear forces. Four failure modes are found: core shear failure and a combination of shear and compressive failure in the core; facing wrinkling and facing compressive failure. Depending on the intensity of the shear forces, the first failure mode to appear can be face wrinkling if the forces are low, or core shear failure if the forces are high (Zimmermann & Wang, 2020).

2.1.1.2. Compression

Similar to the previous section, an axially compressive force can cause facing compressive failure and face wrinkling. Furthermore, can origin global buckling and core shear instability. The first case is due to end conditions and material properties, whereas the shear instability in the core is related to the shear modulus and the thickness of the structure (Daniel, Gdoutos, Abot, & Wang, 2003; Zimmermann & Wang, 2020)

It is difficult to occur core compressive failure due to the lower stiffness and high ultimate strain of the core (Daniel et al., 2003).

Figure 5 Global buckling (Heimbs, 2012)

2.1.1.3. Impact

The low, medium, or high- velocity impact are a type of impact test, and it is first necessary to analyse the energies involved.

In this event, the sandwich structure and the impactor have kinetic energy. The sandwich absorbs the strain energy and, in particular, the face sheet absorbs the fracture energy. This last one contributes to tensile fibre damage, matrix fracture or a combination of both, in the case of composite skins. In addition, there is the energy used in buckling and crushing the core and, finally, energy to cause debonding of the face and core. Some energy is lost in friction, but usually is just a small fraction around 3 [%] of total energy (Chai & Zhu, 2011).

To summarize, the failure modes possible to identify in a velocity impact test are the following: core buckling, shear, and cracking; debonding; delamination in the top face sheet; and face sheet matrix cracking and fibre breakage, for composite skins. The bottom skin is often intact during most of the drop weight low-velocity impact tests (Chai & Zhu, 2011; Daniel, 2009).

Observing the final properties after impact, the shear, bending, compressive and tensile strengths are reduced. The compressive strength is the most modified. This is affected through several factors, namely the delamination of the impacted face sheet due to the resulting micro buckling of the fibres, and the indentation in the same face sheet, resulting in asymmetric structure (Schubel, Luo, & Daniel, 2007).

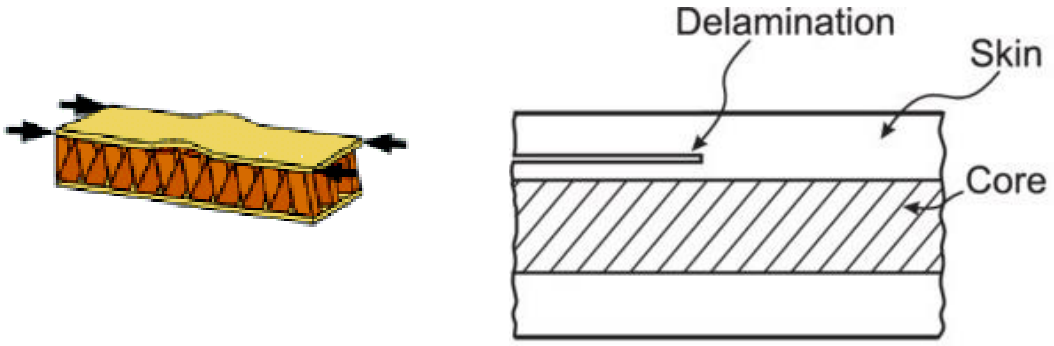

Figure 6 From left to right: debondig (Heimbs, 2012) and delamination (McGugan, Larsen, Bent F. Sørensen, Borum, & Engelhardt, 2008)

2.1.1.4. Fatigue

The fatigue solicitation starts when the structure is manufactured and begins the service life until it fails (McDaniels, 2017).

According to research found in (Schubel et al., 2007), for fatigue cycling of constant amplitude, the nucleation phase, which is the number of cycles until a crack is created, continues through most part of the fatigue life, with an almost unaltered stiffness. The defect propagation phase, on the other hand, happens very fast. So, it is important to study how the sandwich structure responds to the fatigue loading (McDaniels, 2017; Schubel et al., 2007).

In the study (Schubel et al., 2007), two test specimens, with honeycomb core were evaluated with fatigue load limit at 10^6 cycles, to understand the bending stiffness changes and the failure modes. The first specimen was undamaged, in contrast to the second specimen that had one partially debonded face.

The first specimen failed due to local buckling of the compressed face, whereas the damaged specimen collapsed in the debonding part, due to in-plane bending tensile stresses in the honeycomb cells (Schubel et al., 2007).

2 2. Skins

The skins or face sheets are a crucial part of the sandwich structure as they are responsible to handle tensile and compressive in-plane loads (Schiffer, Cantwell, & Kim, 2021). Therefore, it is expectable to look for some specific characteristics in a skin material. For example, high stiffness, high flexural rigidity, and high tensile and compressive strength are necessary. In addition, external attacks like humidity, fire, etc. are main criteria to select the skin materials to specific applications. (A. B. Pereira & Fernandes, 2019; Zenkert, 1995).

In face sheets materials are included two types: metallic and non-metallic (Zenkert, 1995).

2.2.1. Metallic Skins

In the first group, the most common metals are steel and aluminium, according to (Palomba, 2021). Applications with specific requirements of hygiene and corrosion resistance usually opt for aluminium skins (Davies, 2001).

One unique characteristic of these materials is the possibility to join the core and the skin through weld or braze. The use of adhesive is limited to particular case of the lack of heat resistance of the component (Njuguna, 2016). Another advantage is the isotropic features of these materials, allowing an easier understanding of the properties and mechanisms of damaging (B. Castanie, C. Bouvet, Y. Aminanda, J.-J. Barrau, & Thevenet, 2006).

2.2.2. Non – Metallic Skins

Plywood, cement, reinforced plastic, fibre composites, etc, are some examples of non-metallic skins (Zenkert, 1995). The most relevant type is the fibre composites, such as glass, and carbon fibre, and due to the importance for the purpose of the thesis, it will be a more detailed issue.

In general, fibre composites skins have two characteristics in comparison with metallic skins: easiness of manufacture and anisotropic behaviour. The latter refers to the different properties in distinct directions, according to the direction of the fibre. Despite the complexity, the anisotropy can be beneficial because it allows tailoring the properties of the skin to maximize the performance for a specific type of load (Zenkert, 1995).

The glass fibres are the most common, combining decent mechanical properties, low weight, and low cost. The carbon fibre, although with better mechanical performance, it is much more expensive (A. B. Pereira & Fernandes, 2019).

The fibres can be used in form of prepregs, with a resin mix, stacked ply by ply in order to obtain the desired properties. There are a lot of possible orientations for the fibres, but the three most common are 0 [º], called longitudinal, 90 [º], known as cross-ply and also angle or

off-axis plies with 45 [º] (World, 2016). The first one ensures resistance to axial loads, the cross-ply provide the strength and stiffness in the transverse direction and finally, the angle plies are responsible for resisting shear loads (DragonPlate, 2019; "Materials & Processes: Composites part design," 2016). Hence, depending upon the application, the stacking sequence and the fibre orientation are chosen.

2.3. Adhesive

The adhesive is the material that connects the core to the skin, allowing the creation of a very stiff structure. The main characteristics for the adhesive are the chemical compatibility with the skin and core materials, and the close or even better mechanical properties than the core. It is fundamental not having failure due to debonding, risking the integrity of the whole structure (A. B. Pereira & Fernandes, 2019).

Cured polyurethane (PU) glue is the most often used adhesive for sandwich structures. Furthermore, there are solid adhesive films that are thermally activated, resulting in reduced adhesive waste because they are manufactured to a specified size and do not require the mixing of materials like glues (A. B. Pereira & Fernandes, 2019).

As it was referred in the metallic skins, there is no need for an external adhesive when the core and the skins can be welded or brazed to each other. In this case, the weight of the structure will not increase due to the bond between the parts (Njuguna, 2016).

2.4. Core

Nowadays, there are various types of cores for specific applications. The geometry of the core will affect the shear stiffness, flexural stiffness, and energy absorption ability of the sandwich structure (Miranda et al., 2021). The material of the core is fundamental, as its density should be as low as possible. Typical materials include lightweight wood (balsa wood), polymers (polyurethane, etc) and lightweight metal (aluminium) (Xiong et al., 2018).

This chapter will review the type of cores, the geometry, the features and the characteristic properties of the traditional ones. Moreover, it is fundamental to know what type of industries the cores best fit in.

The start point is to divide the cores into two categories: the ones that provide homogenous support of the skins and the ones that do not provide homogenous support of the skins. Foams, with open and closed cells and balsa wood, belong to the first groups. The second group includes truss cores, textile cores, corrugated cores, and honeycomb cores. This latter will have emphasis owing to its importance for the thesis.

Homogenous support of the skin	Wood based	
	Foam	Closed cell
		Open cell
Non-homogenous support of the skin	Truss	Pyramidal, tetrahedral, Kagome, etc
	Textile	Diamond and Square
	Corrugated	Triangular, retangular, sinusoidal, etc
	Honeycomb	Hexagonal, square, triangular, etc.

Figure 7 Scheme of the cores

2.4.1. Homogenous support of the skins: Wood Cores

The main two wood-based cores used are balsa wood and plywood, due to their low density, low cost, etc.

Balsa wood is a very lightweight wood, and it can be exported mainly from South America, Ecuador, Papua New Guinea, etc.(Belleville & Ozarska, 2016). Its properties are higher in the direction of growth, comparing to the others. One way to address this issue is to use the end-grain shape, resulting in a core made of pieces bonded together with the fibre direction perpendicular to the plane of the core (Zenkert, 1995). Another solution, performed in a 2020 study, to overcome the difference between the properties in different directions was to create veneer layers oriented in the same end-grain direction, in this case, using 0º and 90º grain directions. The layers were bonded with an adhesive and resulted in lower density variations, and more balanced properties, so the design of such sandwich cores could be simpler (Keller, 2020).

The density of balsa wood can vary from 80 [kg/m3] to 220 [kg/m3], and so can the mechanical properties. Researchers found that density values around 150 [kg/m3] could have higher strength if compared to densities above and below that value, illustrating the heterogeneous nature of Papua Nova Guinea's balsa wood (Belleville & Ozarska, 2016). Balsa is also good at thermal insulation, but the smallest high density and the sensitivity to humidity make it less competitive, comparing to polymeric foams that offer more stability (Belleville & Ozarska, 2016; Cripps, 2019; Zenkert, 1995). The leading applications for balsa wood rely on marine, aerospace, wind energy industries, etc. (Belleville & Ozarska, 2016)

The other wood-based material is plywood, with a superior in-plane behaviour, comparing with conventional wood (Eyma, Luycker, Cantarel, Bouvet, & Castanie, 2019).

Moreover, plywood cores are quite suitable for fire resistance or thermal and/or acoustic insulation applications. Also, according to (Eyma et al., 2019), wood-based structures, such as plywood cores, can have an important role in crash and impact applications due to the capability to dissipate energy, as well as the high specific properties. Low cost and environmentally friendly are also advantages.

2.4.2. Homogenous support of the skins: Foam Cores

The typical foam cores are split into two categories, addressing the material: polymeric foams and metallic foams. First will be presented the polymeric foams followed by the metallic foams.

Within these two types of foams and concerning the structure, there are open and closed cells structures. Open cells provide more porosity to the structure and, besides lower stiffness and compressive strength, in comparison to the closed cells, they absorb more moisture, which could cause damage to the skins. Therefore, the closed cells are much more used in sandwich structures (Bharath, Bonthu, Gururaja, Prabhakar, & Doddamani, 2021; Njuguna, 2016). Nevertheless, open-cell foams are good for sound absorption applications (Campbell, 2010).

There are many polymeric foams, thermosets and thermoplastics, and the most common there will be succinctly mentioned. The best attributes are related to their lightweight and high strength per unit weight, as well as the capacity of energy-absorbing, thermal insulation, resulting in several applications in various industries, such as structural engineering applications, household applications, crash protections applications, and so on (Deb & Shivakumar, 2009; Linul, 2020). Nevertheless, this type of material generally needs sophisticated equipment and highly technical requirements (Zhao & Park, 2019).

Polyurethane

Polyurethane is, in general, a thermosetting material very common in a form of foam core for energy dissipation applications and mould constructions (Andami & Toopchi-Nezhad, 2020; Engelsmann, Spalding, & Peters, 2010). It is made of polyol and isocyanate, a blowing agent, and activators. The PUR foams can be flexible or rigid, according to the desired physical properties, being the latter the material with greater values of modulus of elasticity and yield stress.

Polystyrene (Styrofoam®)

Polystyrene, a common thermoplastic, is known for being a good thermal insulating material, quite common in insulating panels in a variety of industries (Davies, 2001; Engelsmann et al., 2010). It is common to see this material in form of expanded (EPS) or produced through a process of extrusions (XPS), both produced from polystyrene granulates. The latter is a more uniform foam, with closed cells and a compact surface.

In comparison to the PUR, the EPS has half the heat transmission capacity of PUR and for the approximate equivalent physical and mechanical properties, the weight of EPS is half of the weight of PUR. The density of polystyrene is around 15 to 20 [kg/m^3] (Davies, 2001).

According to (Caliskan & Apalak, 2017), who tested different EPS foam cores with different densities (10, 20, 30 [kg/m^3]) and thicknesses (10, 20 [mm]), in a low-velocity impact test, the higher density and thicker core specimen showed a lower permanent central deflection (Caliskan & Apalak, 2017).

Polyvinyl chloride (Klegecell® and Divinycell®)

The following material, one of the most used core materials, can be either thermoset or thermoplastic, according to the application, and this difference relies on the chemical bonds: the thermoset is crosslinked, and the thermoplastic is not. The thermoset polyvinyl chloride (PVC) has higher mechanical properties and better temperature resistance, but it is more brittle. On the other hand, the thermoplastic PVC has a tougher more damage resistant structure and it is easier to deform (Campbell, 2010).

In general, this foam is quite common in marine applications because of the high chemical resistance, good thermal insulation, and low water absorbency. According to the application, the density can vary from 60-250 [kg/m^3] (Zhou, 2016).

Polymethacrylimide (Rohacell®)

Polymethacrylimide foams, also abbreviated PMI are lightly cross-linked closed-cell foams and are known for the excellent mechanical properties and heat resistance, so the main application is in aerospace due to the high performance and high costs, in comparison with other polymeric foam cores (Campbell, 2010). The density has a larger interval: 30-300 [kg/m^3] (Biron, 2013).

Now, it will be discussed the metallic foam cores. This type of core has quasi-isotropic properties and one of the main advantages is the fact that they can be produced with integral skins, avoiding the use of adhesive bonding. Moreover, they have a relatively high Young's modulus (McCormack, Ronald, Kesler, & Gibson, 2001)

Aluminium

The most typical metal used in metallic foams is aluminium. The resulting foams have low density, good impact and erosion resistance, good energy absorption capability and high stiffness (Yu, Wang, Li, & Zheng, 2008)

There are two predominant processes to manufacture aluminium foams: injecting a gas into the liquid metal or use a substance (agent) to promote the foaming. The first process mentioned creates a larger volume of foam with low density, resulting in a more economical process. Both of them create foam with different densities, cell sizes, open or closed cells, etc (Sadek, 2016).

2.4.3. Non-Homogenous support of the skins: Truss Cores

The truss or lattice truss cores are not so common as honeycomb or foams, but are beginning to get more interest due to their unique properties (Abdullah, Azman, Hui, & Singh, 2021).

These structures connect the two face skins with a layer of a 3D lattice of straight beams, arranged in a periodic repetitive pattern. They can be multi-layered or single-layered (Chu, Gao, Xiao, & Li, 2019).

The unique properties mentioned before are related to the open-cell configuration that allows free movement of fluid and improves the thermal and transport properties, favouring multifunctional application opportunities (Li, Zhou, Ye, & Li, 2015). Besides, the macroscopic behaviour can be tailored to different applications. Their excellent specific strength and stiffness, good energy absorption and impact resistance capabilities also justify the interest in studying and developing this category of cores (Abdullah et al., 2021; (Yuan, Song, & Huang, 2016).

Nevertheless, the design is often complex and the bonding area between lattice and skins is small, resulting in the debonding of the core and face sheet, which significantly affects the structural strength (Abdullah et al., 2021; Li et al., 2015).

The common designs for lattice structures are octet, tetrahedral, block, pyramidal, 3D Kagome and X-type (Rejab, Siregar, & Guan, 2021; Yuan et al., 2016). The thickness of the strut influences the mechanical strength of the lattice, and the length affects the compressive strength (Abdullah et al., 2021).

Concerning the materials, it is common to find aluminium alloys and carbon fibre reinforced polymer (CFRP) (Ma, Wang, & Wu, 2012).

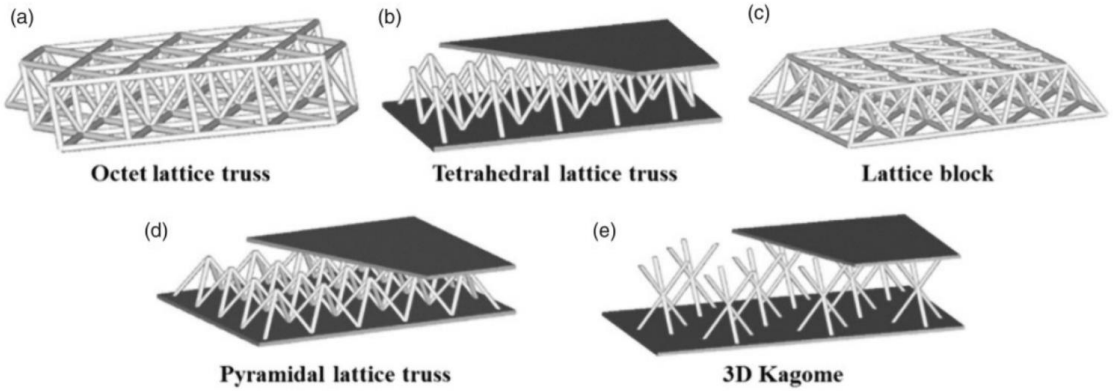

Figure 8 Some designs of truss cores (Rejab et al., 2021).

2.4.4. Non-Homogenous support of the skins: Textile Cores

The textile cores are also considered lattice structures, but instead of straight struts, they have plain wavy wires bonded to each other (Wadley, 2007; Wang, 2010).

In comparison to other cores and similar to the truss cores mentioned before, the textile cores have high specific strength at low relative density and can be used in multifunctional applications. Moreover, the manufacturing costs are low (Evans, 2003).

In the design of the cores, there are two main types: square, composed by horizontal and vertical wires, and diamond orientation, with diagonally align wires. A study, concerned about the strut waviness impact on the mechanical properties, compared the two orientations. They conclude that the stiffness of the square orientation is not influenced by the aspect ratio (ratio between the length and the height of the core), although the strength decreases with the increase of the height of the specimens. This happens because higher heights cause buckling of the wires parallel to the height direction. In contrast, the diamond orientation mechanical properties are affected by aspect ratios less than 4 but do not suffer from the buckling of the wires when the height of the core increases. For this reason, the diamond orientation is often preferred (Wadley, 2007).

In terms of materials, the textile cores use metals, such as stainless steel (Wadley, 2007).

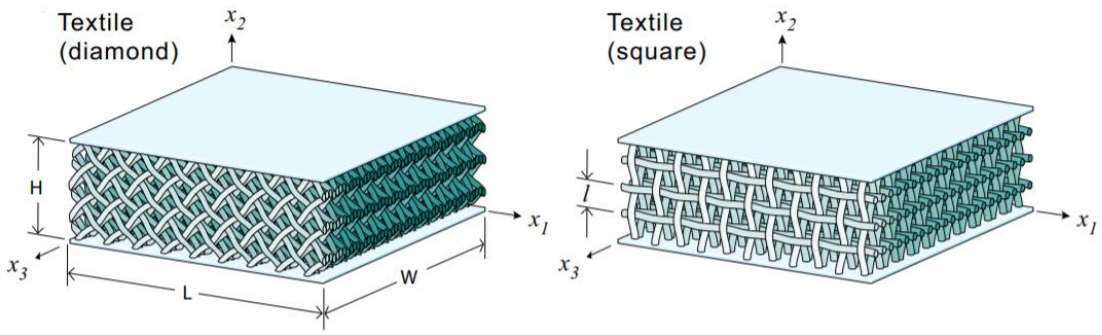

Figure 9 From left to right: textile core in the diamond orientation and square orientation (Wadley, 2007).

2.4.5. Non-Homogenous support of the skins: Corrugated Cores

The corrugated cores are part of the prismatic cores. They are distinguished for forming open channels in one direction, representing a two-dimensional periodic structure. Honeycomb cores can also be included in this category, but they will be presented in the following section (He, 2018; Xiong et al., 2018).

These structures have a high flexural stiffness-to-weight ratio and stabilize the face sheets by resisting vertical strains. Moreover, the ventilation characteristics outstand the corrugated cores from honeycombs and some foams since they avoid humidity problems. The major applications are in aerospace, aeronautics, civil engineering, etc. (Campbell, 2010; Zaid, Rejab, & Mohamed, 2016)

a. Core Geometry

It is fundamental to know what geometry of the corrugation pattern influences the mechanical properties of the final sandwich structure. The most known patterns are arc-shaped, sinusoidal, rectangular, triangular, and trapezoidal, being the latter two the most used. They are represented in figure 10 (He, 2018).

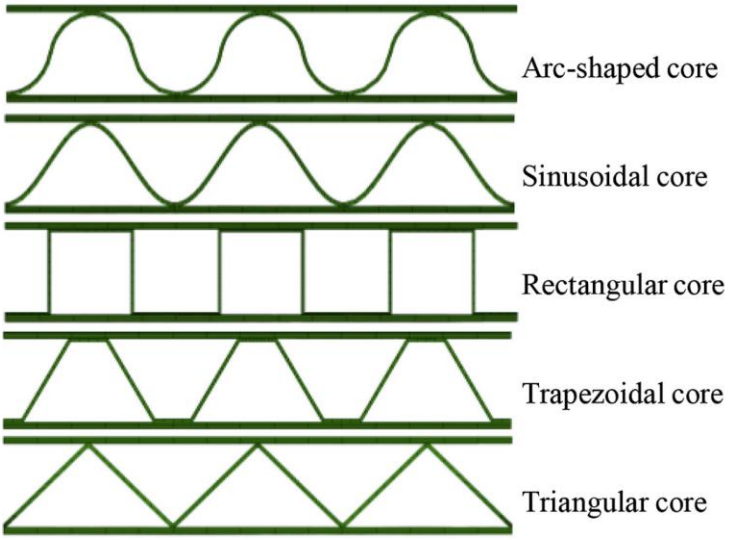

Figure 10 Types of corrugated cores, according to the geometry (He, 2018)

In the study (He, 2018), the five referred corrugated types were tested in low-velocity impact tests and planar compression tests. The core material was aluminium alloy, and it was the same for all geometries.

According to the study (He, 2018), under minor energy impact, the sinusoidal, the arc-shaped and the triangular had more damage and because of the lower bonding area, these specimens suffer debond more easily. On the other hand, the trapezoidal and rectangular shapes had higher energy absorber capacities.

In the compression test, the arc-shaped and sinusoidal had the lower out-of-plane stiffness's and lower ultimate compression stress, compared to the other three cores. The trapezoidal core had the highest ultimate strength (He, 2018).

Considering the conclusions of the study and acknowledging the fact that the forming process of the rectangular core is more difficult to perform, the trapezoidal core had the best balance performance for the engineering applications (He, 2018).

b. Materials

The typical materials can be metallic such as aluminium and stainless steel that provide excellent resistant properties. It is common to see sinusoidal corrugated aluminium core in the automotive industry (Zaid et al., 2016).

Fibre composite materials are not so common due to the insufficient transverse strength of the low-density corrugated cores. One way of overcoming this problem could be in using a hierarchical structure (S. K. D. Zenkert, 2009; S. K. D. T. D. Zenkert, 2009). According to the study (S. K. D. Zenkert, 2009; S. K. D. T. D. Zenkert, 2009),a novel hierarchical structure made of unidirectional carbon fibre SE-84LV prepreg had at least seven times higher specific strength, when compared to the monolithic corrugation, with the same material.

2.4.6. Non-Homogenous support of the skins: Honeycomb Cores

The idea of honeycomb structures is inspired in the natural architecture and the purpose of this structure is to reduce material, decreasing the weight of the overall structure and consequently diminish the costs. The cells are hollowed and adjacent to each other to form the core (Alphonse & Chandra, 2021).

There are many industries with sandwich structures and honeycomb cores and, in particular, they became more common in aviation and helicopter applications, as well as aerospace vehicles(Jędral, 2019).

Honeycomb cores combine low density with high strength and a good ability to absorb impact energy. Comparing to foams, they have higher work temperature. Because this structure is anisotropic, when loaded along the out-of-plane direction, the structure has high stiffness. In contrast, in the in-plane direction, the cell walls tend to bend, and the stiffness and strength are much lower (Jędral, 2019; Liang, 2017).

Two features that influence the mechanical properties and final performance of the core are the density and the cell size and shape. The density has a straightforward relation: the higher the density, the stronger will be the honeycomb. A smaller cell also elevates the strength of the honeycomb (Jędral, 2019).

a. Cell Shape

Concerning the shape of the cell, many shapes are possible. Traditionally, there is the hexagonal core, very structural efficient with isotropic properties in the plane of the hexagonal shaped cell, although the formability is limited (Campbell, 2010; Masters & Evans, 1996). Besides, there are the flexible core and the over expanded core, represented in figure 11. The first has the best formability, of all three, followed by the over expanded core, without causing the cells to buckle. The over expanded, as the name suggests, it is a regular hexagonal shaped cell expanded in one direction, increasing the shear modulus in that direction, and decreasing in the other one (Campbell, 2010).

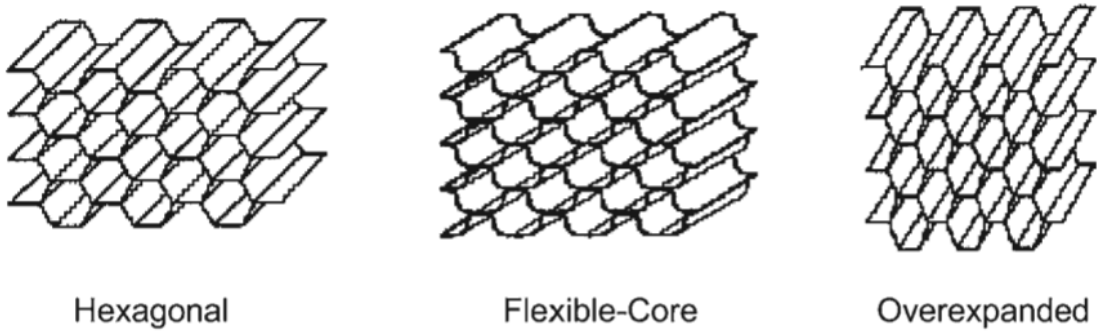

Figure 11 Types of honeycomb cells (Campbell 2010)

More efforts have been done to improve the honeycomb cores performance, especially when it comes to the cell shape. A study conducted by (Hamzah, Al-kawaz, & Hamzah, 2020) tried four different configurations of cells: hexagonal, circular, triangular and squared in flexural testing, and concluded the squared cell had superior performance, comparing to the others and the triangular had the lowest maximum load.

Furthermore, a lot of research has been done to create a honeycomb with auxetic cells. This option may be called “metamaterials” and it is characterized by geometric properties instead of just the material chemical composition. The negative Poisson’s ratio is the fundamental feature of the auxetic structures and can improve out-of-plane properties and adapt to curved structures (Liang, 2017). There is more than one configuration for auxetic cells, but for the thesis, the re-entrant auxetic structure is the main focus, represented in figure 12.

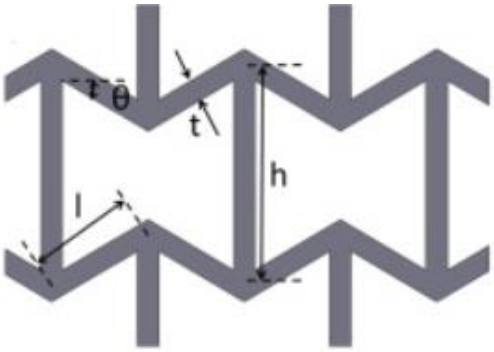

Figure 12 Auxetic Cell for honeycomb (Liang, 2017)

b. Materials

There are numerous typical materials for honeycomb cores, metallic and non-metallic. In the first group, there is aluminium, very common, and stainless steel, both used in thermal conductive applications, for example. In non-metallic materials, there are aramid fabric and paper, known by the trade name Nomex®; thermoplastics, such as polycarbonate (PC), polypropylene (PP), and so on (Jędral, 2019).

Aluminium

Aluminium honeycomb cores are quite used due to the lightweight and good mechanical properties and the recyclability. The latter characteristic is fundamental nowadays and because of that, aluminium honeycombs can be a good alternative to polymeric foams and fibre reinforced polymers to minimize waste (Palomba & Epasto, 2019). However, long term moisture exposure environments can degrade aluminium due to corrosion, which can lead to debonds between faces and cores (Kroplin, 2008).

The common alloys for honeycomb are 5052, for general purposes, 5056, for higher strength applications, 3003, for energy absorbance purposes and 2024, which can work up to 210ºC (Mirza, 2012; Zenkert, 1995). The density can go from 20 to 80 [kg/m^3] ("Datasheet - AluNID,").

Aramid (Nomex®)

Nomex® is the trade name for the aramid paper, very common to do honeycomb cores. This honeycomb material, in form of sheets bonded together and shaped with hexagonal holes, is dipped in a phenolic resin, and cured. The phenolic coat layers preserve the orthotropic ductile Nomex® core. The orthotropic properties are the consequence of the manufacturing process: the aramid fibres are oriented in the direction of the sheet coming off the machine and this direction is, therefore, stronger than the cross direction (Krause, 2014). Common applications are the aerospace industry include doors, floor, flaps, etc (Ke, 2020).

This material is particularly known for its fire-resistance properties. Besides, it is a lightweight, good thermal insulator, flame retardant and it has a high compressive out-of-plane resistance (Ke, 2020). Nevertheless, the material is sensitive to moisture that can alter the dimensions and properties. Moreover, the quality control and the limited temperature for bonding the components difficult the production (Kroplin, 2008). The typical density can go from 29 to 144 [kg/m^3]("Nomex® honeycomb - commercial," 2017).

Thermoplastics

Polycarbonate (PC) and polypropylene (PP) are two thermoplastics used in honeycomb cores.

PC is easily applied, also waterproof and washable material. Moreover, it is non-toxic and 100% recyclable. The densities can vary from 70 to 110 [kg/m^3], but for densities of 200 [kg/m^3], it is used in crash-absorber applications. Other than that, it is also common to find PC honeycomb in commercial refrigeration, wind tunnels, etc. ("Polycarbonate honeycomb core," 2020).

PP honeycomb, with densities from 80 to 120 [kg/m^3] is known for the chemical resistance properties and behaviour in aggressive environments. For that reason, it is used in support of filters, decreasing corrosive gas emissions. Polypropylene is also a good kinetic absorber, and if pair up with TNT, can be used as a flat surface for cutting tools ("Polypropylene honeycomb core ", 2017). TNT, *Tessuto Non Tessuto*, is an Italian acronym that translate to English means nonwoven (Aster, 2021).

2.4.7. Comparison of Cores

Now, it will be presented the density and a few specific mechanical properties of some typical cores, in table 1, followed by a graphic comparison of the cores. The relative density concerns the ratio of the core density and the density of the core material (Petras, 1999). All data was collected in the database CES Edupack.

Table 1 Examples of traditional cores and their properties (elaborated with data from: CES Edupack)

Core	Density [kg/m^3]	Relative density	Specific Shear Strength [N·m/kg]	Specific Shear Modulus [N·m/kg]	Specific Compressive Strength [N·m/kg]	Specific Compressive Modulus [N·m/kg]
Balsa Wood **Core**	138-169	0.507-0.647	19480.1	1.06 x 10^6	84040.8	2.64 x 10^7
PUR Foam **(Rigid)**	59.2-64	0.0477-0.0574	6520.3-7000.0	61824.3-78593.8	6490.71	98479-128594
PVC Foam **(Rigid)**	50-60	0.036-0.043	7500.0-7083.3	360000	15000.0-14166.7	615000-646000
PMI Foam **(Rigid)**	52.1	0.031-0.049	11516.3-15355.1	364683-406653	11516.3-17274.5	556622-614203
Aluminium Foam	480-520	0.17-0.2	-	3.64 x 10^6- 3.84 x 10^6	10416.7-19230.8	-
Aluminium honeycomb **(3003)**	22-22.8	0.00781-0.00863	16363.6-17456.1	4.17 x 10^6- 4.43 x 10^6	22318.2-23815.8	4.77 x 10^6 - 5.09 x 10^6
Nomex honeycomb	28.8-32	0.0235-0.0261	16770.8-11750.0	791667-968750	27430.6-31250.0	1.91 x 10^6 – 2.38 x 10^6
Polycarbonate (PC) honeycomb	62.7-65.3	0.0507-0.056	9409.9-9984.7	344498-366003	22009.6-23277.2	67567.6-215625
Polypropylene (PP) honeycomb	59.2-64.0	0.0648-0.0716	4780.4-8406.3	67567.6-215625	16891.9-18906.3	211149-781250

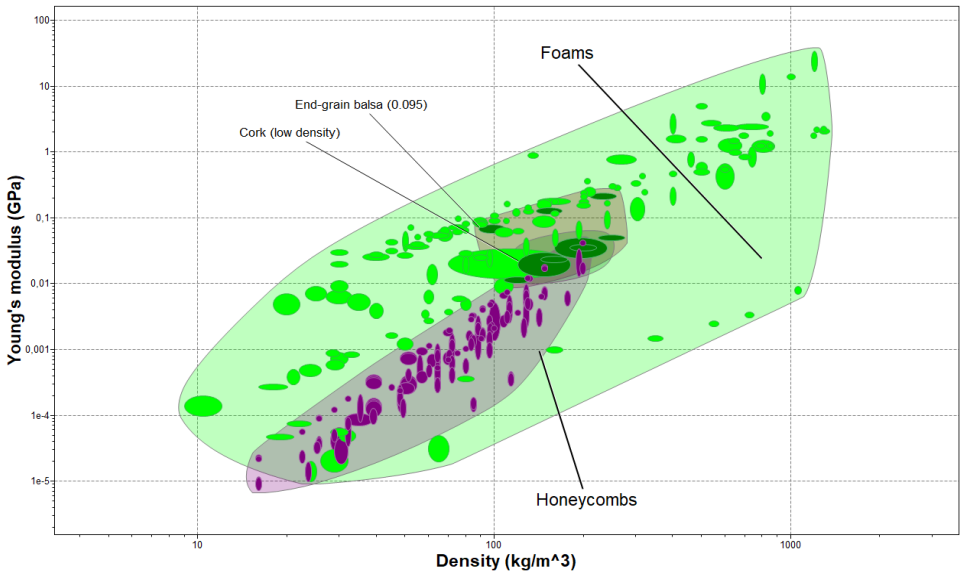

Figure 14 Density vs Young's Modulus of traditional cores (source: CES Edupack)

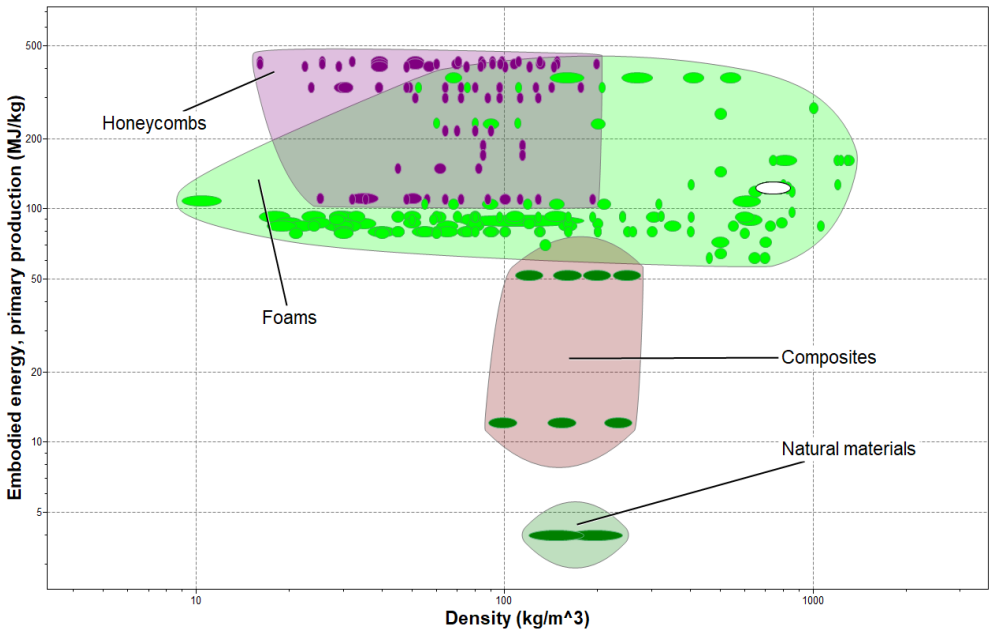

Figure 13 Density vs Embodied energy, primary production of the traditional cores (source: CES Edupack)

It is obvious to see the foams, in green, are the most versatile core, although most of the polymers are not recyclable and the production energy is quite high. The honeycombs also have a good ratio of Young's modulus and density, although the second graphic presents an elevated quantity of energy to produce, which is justified by the fact that there is lot of honeycomb polymers in the purple spot.

In the natural materials, where cork fits in, it is interesting to see that honeycomb cork could be a possible solution to substitute some traditional cores.

2.4.8. Latest developments and trends in cores

There are always new trends or developments to improve the sandwich structures and provide a bigger field of applications for these structures. The core is one of the main components that has suffered enormous updates. This section will be approaching some new studies related to core innovations.

A recent study (Zhang, Yan, Zhang, & Guo, 2021) presented a novel core combining a traditional aluminium honeycomb core with aluminium tubes. The idea is to improve the load-carrying capacity, the impact resistance and the structural stiffness of the core. The results of the impact response to a drop weight showed an increase in the peak load and stiffness of the honeycomb. Furthermore, the stress and deformation were distributed more homogeneously (Zhang et al., 2021).

Another study, with a similar idea but, in this case, the Nomex® honeycomb had just a central carbon-reinforced polymer tube in the structure, is shown in figure 15. The experience aimed to test the compressive and energy absorption properties and the results were promising. The elastic modulus increased by more than 50 [%], and the peak stress and energy absorption were raised by more than 600 [%] and 300 [%], respectively. Another characteristic of this hybrid core has the combination of excellent electromagnetic absorption and mechanical properties (L. Yan et al., 2021).

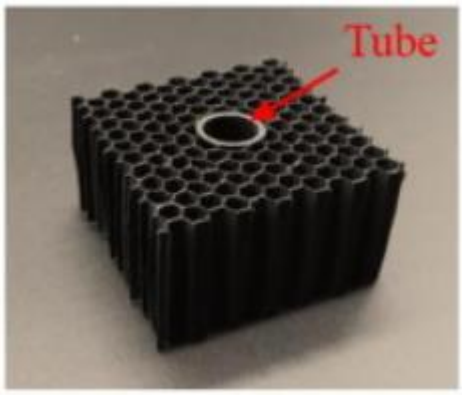

Figure 15 Example of the Nomex honeycomb core with a central carbon-reinforced polymer tube (L. Yan, Zhu, Chen, Zheng, & Quaresimin, 2021)

Besides the typical hexagonal honeycomb cell, it is common to see new studies about auxetic cells. In a study comparing the thermo-mechanical properties of auxetic and non-auxetic honeycomb, it was found that, with an identical temperature distribution, the auxetic honeycomb had superior performance. The auxetic cells core had reduced thermal stresses levels and the thermal shock resistance was quite high (Hu & Wang, 2021).

Despite de importance and growth in the use of honeycomb cores, the foams have also some improvements. In (Najafi & Eslami-Farsani, 2021) it is presented a hybrid core with PU foam and agglomerate cork, with the purpose to improve the mechanical properties and

resistance to marine environmental conditions. Five tests were conducted, namely, three-point bending, edgewise and flatwise compression, high-velocity impact, and quasi-static indentation. The results showed an enhanced structure.

Another way to improve foam cores properties is to introduce new elements, such as stiffeners. In this study (Liu, Tao, Li, & Zhao, 2021), the flexural properties of a PVC foam core with stiffeners are analysed and the results show an increase of 25 [%] in shear stiffness and a reduction of the deflection around 19 [%]. Plus, the ultimate load increased by more than 20 [%]8 and the failure mode went from indentation failure to core failure.

Finally, a concerning problem is the use of non-renewable materials. The search for environmentally friendly materials and manufacturing processes continue to increase. One idea could be using polylactide acid (PLA) polymers, in cores and skins, and according to the study (Lascano et al., 2021) that tested PLA honeycomb with PLA-flax skins for flexural and compressive loads, the results showed a possible candidate to medium-to-high technological applications. Nevertheless, there was a poor adhesion between the skin and the cores and new developments are needed to clarify the standard properties (Lascano et al., 2021).

2.5. Cork

Cork is a much known natural material commonly used for many centuries due to its unique properties. The most common application is the stoppers for wines or other beverages, representing around 67.4 [%] of the manufactured cork (Avillez et al., 2020). However, many industries are exploring the potential for building and aeronautic applications, soil shoes, and so on. (Avillez et al., 2020)

The following chapter will present the chemical composition of cork, the micro and macrostructure, and the mechanical and physical properties, comparing with other materials. The end of the section concerns some related applications.

2.5.1. Composition

Cork is the bark of the tree, providing a protective layer against animals and erosion agents and every nine to twelve years, production harvest the cork from the cork oak tree (Quercus suber L.). Portugal is the major producer worldwide, containing a third of the total cork oak forest, around 34 [%], followed by Spain with 27 [%] and Morocco with 18 [%] (Avillez et al., 2020).

The chemical composition has five main components:

- Suberin, 45 [%], responsible for the elasticity and compressible properties;
- lignin 27 [%], which is present in the cell walls;
- polysaccharides 12 [%], related to the structure;

- non-structural compounds extractives 12 [%], such as polyphenols, triperpenes and chain fatty acids, important for impermeability and protection of the material and can be easily extracted,
- and ashes 4 [%](Gil, 2007; Manrique, 2016).

The cork's composition is affected by the season of harvest, the genetic origin, the age, the region, among other factors (Gil, 2009). Table 2 summarizes the composites mentioned before. The percentages are from the study of Pereira (1988), performed in four different regions with cork oaks forests, in Portugal.

Table 2 : Chemical composition of four diferente virgin cork locations, namely: Herdade da Palma, in Alcácer do Sal; Herdade da Cardazana, em Grândola; Monte dos Olheiros in Mora and Herdade de Gouveia in Montemor-o-Novo (H. Pereira, 1988)

Component	% -dry weight
Suberin	35.2-41.2
Insoluble Lignin	19.5-21.0
Soluble Lignin	1.2-1.6
Polysaccharides	15.7-21.3
Extractives (total)	14.1-16.9
Dichloromethane	6.3-7.9
Ethanol	4.5-4.8
Water	1.9-3.2
Ash	0.53-0.91

2.5.2. Macroscopic and Microscopic Structure

The first harvest is called virgin cork and, in contrast with the successive harvests, it is irregular in structure, density and thickness. It is used in cork board, insulation, shoe soles, etc. The first reproduction cork is more uniform than the virgin, although only the second reproduction cork and next reproductions are commonly used for wine stoppers (Silva, Sabino, Fernandes, Correlo, & Reis, 2005). It is very important to search for structural defects in order to achieve the best quality, which is deeply linked to the morphology and quantity of pores present in the cork. These pores result from the lenticulars channels present in the radial direction. For the wine stoppers, these defects affect the selection, whereas in building applications is not so critical. In figure 16, it is possible to see these pores, represented with Po, along with some other elements of the composition, such as the waxes and suberin (W), the primary wall (P), the secondary wall (S) and the tertiary wall (T).

Cork has an anisotropic behaviour. However, in applications with agglomerated cork, the randomly oriented granules despise the anisotropy effect.

There are three directions defined: radial direction mentioned before, parallel to the radius of the tree; axial direction, parallel to the vertical line of the tree; and tangential direction, as the name suggests, tangent to the circumference of the tree (Gil, 2007). Figure 17 represents all three directions mentioned before, as well as the cellular disposition.

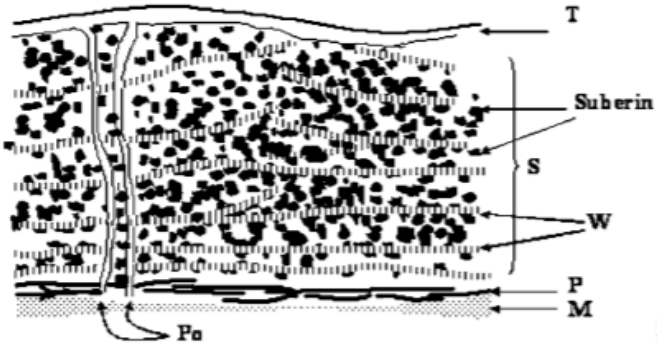

Figure 16 Representation of the cork oak cell wall: tertiary wall (T), secondary wall (S), waxes and suberin (W), primary wall (P), medium lamella (M) and pore (Po) (Silva et al, 2005))

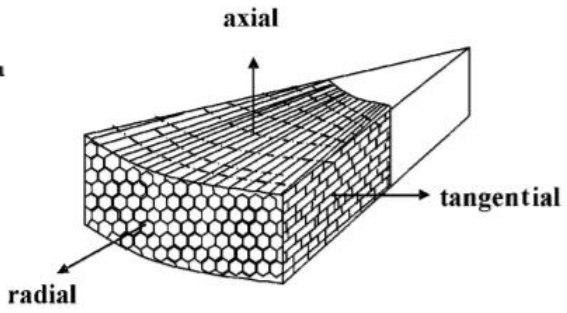

Figure 17 The three directions of the material: axial, tangential, and radial, with de cellular disposition in cork growing section (Silva et al, 2005)

In 1664, Hooke first examined the microstructure of cork, under the microscope. With the advance of technology, cork is now understood as a tissue of thin-walled cells, forming an alveolar structure, similar to a honeycomb, with close-cells. The cells assemble in columns parallel to the radial direction, as rectangular prisms.

In the radial section, the cork cells appear as a heptagonal, hexagonal, and/or pentagonal polygon. Furthermore, they can go from 4 to 9 sided polygons. As one can see in figue 17, the structure resembles a brick wall from a tangential and axial perspective.

A decisive characteristic of the cell walls is their undulation, or corrugation, present in the lateral faces. The pattern often varies, and the corrugations can be so strong that near cell collapse, in particular cases. These corrugations are associated with the compression developed during the growth of the bark.

Since the cork cells are closed and hollow, the cell walls represent most of the mass, and the interior gas influences the properties (H. Pereira, 2015; Silva et al., 2005).

2.5.3. Properties

This subchapter will address the properties of the cork and the relation of the cell structure with them. The first one will be the density, followed by the physical properties, such as thermal insulation, permeability, damping and sound response. In the end, the mechanical properties are presented.

2.5.3.1. Density

Cork is considered a very light material and, as it was mentioned, the mass is essentially concentrated in the cell walls. The density depends on the corrugation of the cell wall: the

density is higher when the corrugation is higher. Usually, boiling the cork, a traditional procedure, straightens the walls, leading to lower desired density. The season when the cells grow is also a factor: in the spring, the cells are taller and thinner; in the autumn, the cells are denser. Due to the low density and closed-cell morphology, cork also floats. (Pereira, 2015; Silva et al., 2005).

2.5.3.2. Physical Properties

Concerning thermal insulation, the two fundamental characteristics are the presence of "air" inside the cells and their small size. Of all the three mechanics of heat transfer, conduction, convection and radiation, only conduction can be remotely effective. Convection is only meaningful if the volume of gas is high, and if the cell size is small, radiation is insignificant. Nevertheless, the cell walls are as much conductive as the gas inside, which has low thermal conductivity. For this reason, it is acceptable to use cork as an insulation layer in applications susceptible to fire, for example.

Table 3 captures the thermal conductivity and the water absorption at 24 hours of the previous discuss traditional cores. Thermal conductivity measures the rate at which heat is conducted by the material (Bird, Stewart, & Lightfoot, 2002). The water absorption at 24 hours is a test that consists in emerging the material in water and see how much weight the sample has gain, after 24 hours ("Edupack ", 2020).

Table 3 Physical properties concerning the cork board and the traditional cores (elaborated with data from: CES Edupack)

Core	**Density [kg/m^3]**	**Thermal Conductivity [W/m°C]**	**Water absorption at 24 hours [%]**
Balsa Wood **Core**	138-169	0.0752-0.0919	180-220
PUR Foam **(Rigid)**	59.2-64	0.0267-0.0305	0.15-0.19
PVC Foam **(Rigid)**	50-60	0.029-0.031	3.53-4.2
PMI Foam **(Rigid)**	52.1	0.028-0.032	1.66-2.6
Aluminium Foam	480-520	7-14	0.001-0.002
Aluminium honeycomb **(3003)**	22-22.8	1.27-1.41	0.001-0.002

Nomex honeycomb	28.8-32	0.0252-0.0279	4.28-4.74
Polycarbonate (PC) honeycomb	62.7-65.3	0.0329-0.0364	0.135-0.165
Polypropylene (PP) honeycomb	59.2-64.0	0.0357-0.0394	0.019-0.021
Cork board	144-176	0.0356-0.0436	3.6-4.4

The low density and the high porosity of the cork also affect sound transmission, especially in expanded corkboard applications. The sound transmission is small because the waves are absorbed, diminishing the magnitude of the reflected sound. The same happens to the reverberation. The damping characteristics are also excellent, which is fundamental in applications such as shoe soles ((Gil, 2007); Pereira, 2015; Silva et al., 2005).

2.5.3.3. Mechanical Properties

Figure 18 represents the typical compression curve of cork. It is possible to observe three different zones. The first region consists of a first elastic bending of the cell walls and is about 7 [%] strain. The second is almost horizontal and represents the plateau stress. The progressive buckling of the cells walls results in 70 [%] of the strain. In the end, the cells collapse, causing the sudden rise of the curve. It is the third mechanism.

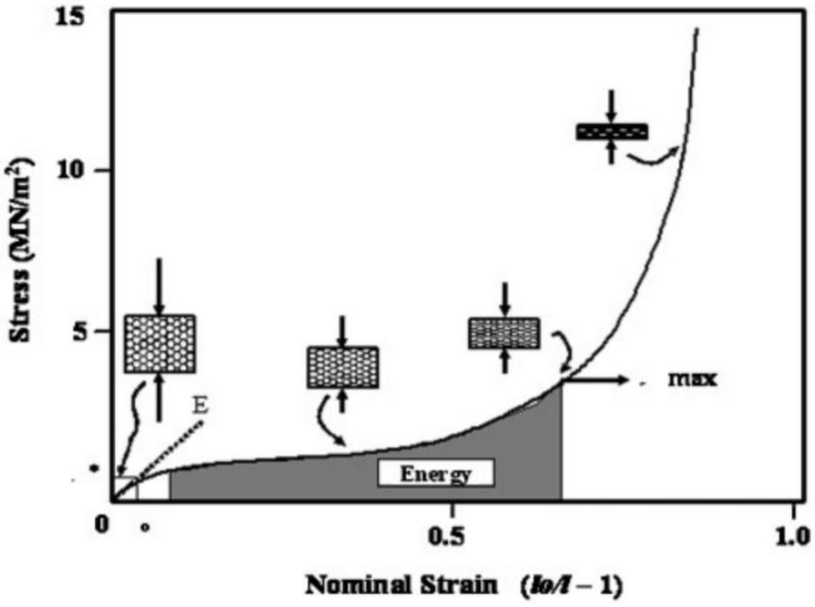

Figure 18 Compressive stress-strain curve for cork (Silva et al, 2005)

The boiling treatment, considered before, softens the cell walls and the differential of pressures causes tensile stresses to align them, due to water absorption. The strength and anisotropy of the material decrease consequently. In addition, when compressed in the radial direction, a sharper yield point appears, due to the reduction of the amplitude of the corrugations. When the amplitude is higher, the yield transition is smoother.

Figure 19 shows tensile behaviour, and it is very different from the previous compression stress-strain graphic. For every direction is expected a different response, although both tangential and axial directions have similar curves. The middle region, in the radial direction, is quite irregular. Microcracks propagated through a few cells, before the material expands, can explain the irregularity. ((Gil, 2007); Pereira, 2015; Silva et al., 2005).

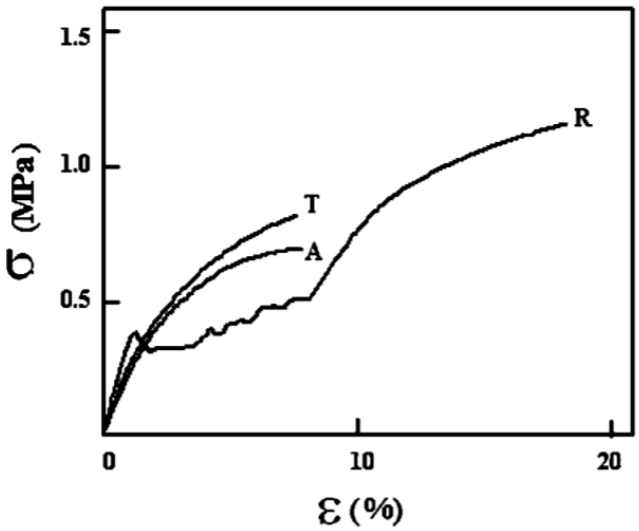

Figure 19 Tensile stress-strain curve for cork in three directions: tangential (T), axial (A) and radial (R) (Silva et al, 2005)

Next, Young's modulus is analysed. It is expected different modulus for tensile and compressive behaviour and for this material, tensile strength is much higher than compressive strength. It is simple to see that the tensile stress decreases the corrugation of the wall, whereas the compression increases, diminishing the stiffness.

Lastly, the Poisson coefficient is a function of the cells disposition and the corrugation of the walls, hence different directions of compression result in different Poisson coefficient. If the cork is compressed in the radial direction, the cells wall will fold and pack, increasing the corrugation and causing a slight expansion in the tangential or axial direction. In this case, the Poisson coefficient has a small positive value. If the compression is in the tangential or in the axial direction, the lateral cell walls will bend and straighten, and if the strains are high enough, it will decrease the size in the radial direction (Silva et al., 2005).

The specific properties of the cork board are found in table 4, withdrawn from the database Edupack.

Table 4 Specific mechanical properties of the cork board (elaborated with data from: CES Edupack)

Core	Density [kg/m^3]	Specific Shear Strength [N·m/kg]	Specific Shear Modulus [N·m/kg]	Specific Compressive Strength [N·m/kg]	Specific Compressive Modulus [N·m/kg]
Cork Board	144-176	5603.2	36875.0	1250.0	31875.0

2.5.4. Applications

The use of cork in many industries is related to its unique properties and renewable and sustainable features. Some specific applications will be presented, as well as some of the manufacturing processes.

2.5.4.1. Cork Stoppers

Because of impermeability to liquids and gases, compressibility, chemical inertness and resilience, cork is an excellent material for stoppers. The impermeability property is the effect of the suberin present in the cell walls (Gil, 2009).

After harvest, the cork planks need at least six months to oxidise the polyphenols and stabilise the texture. The next step is to boil the plank in water for one hour, so the cells can expand, creating a more uniform, smoother, and cleaner structure. After dried and stored for some weeks, the stoppers are punched and based on their quality, sorted to the agglomerate stopper, discs or other products. Each raw cork stopper is cut to size, polished, and graded (Silva et al., 2005).

2.5.4.2. Building applications

In construction works, thermal insulation, acoustic performance and vibration insulation are leading properties of this material (Gil, 2009). Agglomeration of granules of corks, also called black agglomerates or insulation corkboards, are manufactured in a closed autoclave at high temperature and pressure, without adhesives. The expansion and thermomechanical degradation of the cork cell walls creates natural adhesives between the granules. The expanded black cork is made of the lowest quality or residual corks, from winter virgin cork or other types reject in other applications (Silva et al., 2005). Hence, this type of cork is used in interior or exterior walls, providing the thermal and acoustic insulation desired (Silva et al., 2005).

Another application is the “floating floor” as a product of the composition cork with MDF (medium-density fibreboard) or HDF (high-density fibreboard). Different layers of both materials are glued and assembled by a plate pressing (Gil, 2009).

2.5.4.3. Aeronautic applications

For aeronautic applications, the low weight combined with high bending stiffness is fundamental, and cork needs to compete with synthetic foam and honeycomb cores in sandwich structures. Yet these composites transmit noise, which is reduced with glass fabric, increasing the weight, and decreasing the space. So, for this reason, cork agglomerate is already presented as a good alternative (Soares, 2017). A study performed on different types of cork cores agglomerates that mixed cork granules with epoxy resin, demonstrates the core shear stress limit was better than similar materials, reducing the crack propagation area, in a three-point bending test (Devezas, Silva, & Gil, 2009).

2.5.4.4. Aerospace applications

Similar to previous applications, aerospace industries also look for materials with low weight. Another fundamental property is the capacity to withstand the very high temperatures and vibration attenuation that the space vehicles are subjected too (Soares, 2017).

Norcoat®- Liège is cork based material used in the thermal protection system as an ablative material. It is made by hot pressing the cork particles agglomerated with phenolic resin (Soares, 2017).

2.5.4.5. Other applications

The shoe soles are typical products with cork agglomerates, due to the high coefficient of friction and damping capacity. The shock absorption, the cushioning, the ground insulation, and the impermeability provide comfortable walking (Gil, 2009; Silva et al., 2005).

The cork-rubber, a common cork based material, is made of mixed rubber and cork granules, introduced into a heated mould for polymerization. It is present in gaskets for automobiles and oil containers(Gil, 2009; Silva et al., 2005).

Chapter 3: Numerical Simulation

It is key to have a lightweight structure to compete with different materials, without the need to significantly sacrifice the mechanical properties. To find the optimized structure, a few simulations, with simple designed models, were carried out using the software ABAQUS.

The simulations were based on four different mechanical tests, according to the standards mentioned in the respective section.

To choose the dimensions of the honeycomb cell size, the three tests simulated were a three-point bending test, a compression test, and a low velocity impact test. The cell studied was the hexagonal cell. The auxetic cell was adjusted once the dimensions were determined in order to preserve the same thickness wall and area reduced as the hexagonal cell.

On the cork material, the second purpose of this chapter, there were three options, NL10, NL20 and NL25, with different densities and different elastic properties. The choice was founded on two tests: a compression test and a shear test.

Finally, at the end of this section, the models concerning the experimental data will be presented. These models are more complex than the previous ones and the tests performed were: three-point bending test, a compression test, and a low velocity impact test.

3.1. Structures

An arbitrary hexagonal dimension was chosen: 10 [mm] size and 2 [mm] thick, which means, 4 [mm] between cells in the honeycomb core. This first structure represents, approximately, a 50 [%] loss of mass, comparing with the same dimensions without the hexagonal holes. Moreover, it is a reasonable dimension to machine on cork. The second and the third structure had a thinner distance between cells, 1.5 and 1 [mm], respectively. Lower than 1 [mm] could be difficult to machine the cork board.

The table 5 summarizes the cell dimensions in each structure as well as weight loss in continuum test specimen referred before.

Table 5 Cell dimensions and weight loss for the three selected structures

Structure	Size of the cell [mm]	Thickness [mm]	Weight loss [%]
1: D10	10	2	~ 50
2: D11	11	1.5	~ 62
3: D12	12	1	~ 74

Figure 20 displays the three structures.

Figure 20 Structure Display: from the left to the right: structure 1 , D10 [mm], thickness 2 [mm]; Structure 2: D11 [mm], thickness 1.5 [mm]; Structure 3, D12 [mm], thickness 1 [mm]

3.2. Selection of the structure

3.2.1. Three-point bending test

Simulation Model

The next method tests the behaviour of the structure to a bending loading and the standard was ASTM C393/C393M-11. The test specimens' dimensions are 200 [mm] length, 75 [mm] width and 15 [mm] thickness. The tool, a discrete rigid part, is a 25 [mm] diameter cylinder, with 75 [mm] long, to reach all of the structure. A boundary condition, that will prevent the structure to move forward on the loading direction, will represent the loading bar. Therefore, there will not be the need to create it as a rigid part. To reduce the CPU time and complexity of the model, a quarter of the specimens and tools are represented.

The material specifications, concerning the core, vary depending on the structure. The Poisson ratio and density, common to all structures were 0.24 and 1.5e-10 [ton/mm^3], respectively. According to CES Edupack data base, the Young's Modulus is 37.5 [MPa].

The step selected was Static, general, with NLgeom to account for geometric nonlinearity. The start increment time is 0.1 and the maximum number of increments is 100.

In interaction module, we choosed a contact property with a tangential behaviour with a friction coefficient of 0.7 and applied between the top surface of the core and the exterior surface of the tool. The friction coefficient is an average value, taken from the article about Cork properties (Silva, Sabino, Fernandes, Correlo, & Reis, 2005).

Two boundary conditions were necessary in order to assure the symmetry in two axes: in this case, the two interior sides of the structure could not move in the perpendicular direction to the respective plane. The supporting bar was selected with the displacement

boundary condition, placed 25 [mm] from the start of the structured, preventing this “line” to move in the loading direction. The fourth condition was applied in the tool, and it causes it to displace in the Z-axis in six different values to observe the evolution of the core to different loads.

The mesh, finally, has a type of element shape hex for the core, with C3D8 element, with 11340 elements. The tool has a quad element shape, with a R3D4 element.

Results

The six displacements are represented in Table 6, along with the equivalent applied force, for the three structures: D10, for the 10 [mm] cell, D11 for the 11 [mm] cell and D12 for the 12 [mm] cell. This force was measured by the relation between the force (P), the maximum displacement (δ), the mechanical (E) and geometric properties (I) and length (L), displayed in equation (2).

Equation 1

$$\delta = \frac{PL^3}{48EI}$$

Table 6 displacements and respective force applied for each structure, in bending test.

Displacement [mm]	Force Applied [N]		
	1. D10	2. D11	3. D12
2.5	0.92	0.30	0.07
5	1.84	0.60	0.14
10	3.70	1.21	0.28
12	4.44	1.45	0.33
15	5.55	1.81	0.41
20	7.39	2.42	0.55

The “stronger” structure, in this case, the first, has a higher equivalent modulus, leading to a higher force for the same displacement. The following graphic represents the force applied [N] versus the displacement [mm] caused to the structured.

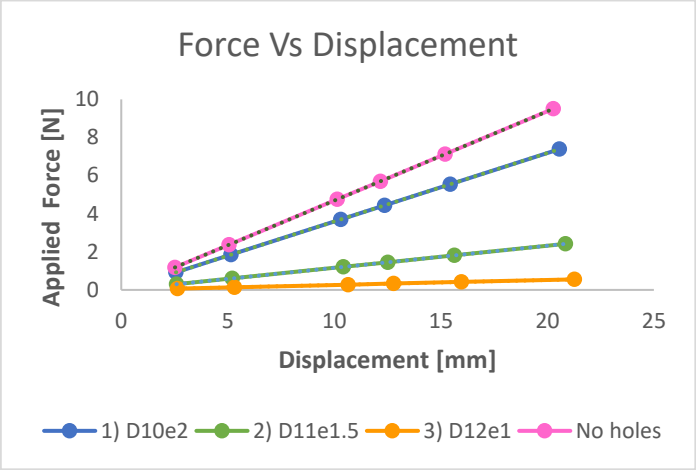

Figure 21 Force vs Displacement for the bending results.

As expected, the stronger structure, closest to the continuum core, is the first, with higher thickness. The slope of each curve determines the "strongest" core and, table 7 summarizes the slopes of each curve, as well as the difference between the continuum structures.

Table 7 Slope results from the force vs displacement graphics, for the three structures, and a structure with no holes.

Structure	Slope	Difference [%]
No holes	0.469	-
1	0.359	-23
2	0.116	-75
3	0.026	-94

Conclusions

Observing the table, the inferior performance of the third structure is noted, with over 90 [%] less slope than the continuum core.

The first structure has just a 23 [%] decrease, whereas the second structure has over 70 [%] less slope.

3.2.2. Compression test

Simulation Model

In the compression test, a quarter of the structure was represented to simplify the problem and the standard used was ASTM C365/C365M − 11a. The total dimensions of the specimens were square 90 [mm] and 15 [mm] thickness.

The step selected was static, general, as it was done in the model before, although in this case the minimum increment was lower.

There were four boundary conditions: two for the symmetry in two axes; one to clamped the bottom of the structure, preventing it from moving in any undesired directions; and finally, a boundary condition to cause a displacement at the top surface.

The mesh had C3D8 elements type, Hex shaped, with 3490 elements.

Results

Three displacements were applied, except in the third structure, since the software reported excessive deformation, and the model would not convert. The surface area (A) for the boundary condition was considered when calculate the applied force (P). Equation (3) was used, being σ the normal stress applied in area A.

Equation 2

$$\sigma = \frac{P}{A}$$

The displacements and forces are demonstrated in table 8.

Table 8 Results of the force applied to each structured, due to the displacement impose, in the compression tests.

Displacement [mm]	Force Applied [N]		
	1) D10	2) D11	3) D12
1	3604.91	841.30	142.24
3	15543.48	3663.62	674.74
4	27741.57	6957.63	-

The following figure represent graphically the table 8.

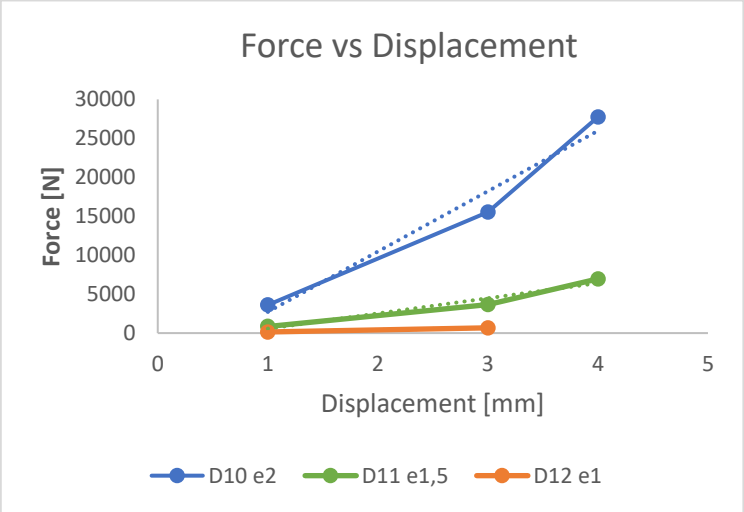

Figure 22 Force vs Displacement for the compression results

The value for a displacement of 4 [mm] in the third structure was not reached, as the model did not converge due to excessive deformation.

The slopes of the curves, in each structure, represent the resistance to compressive loadings. The slopes of each one, as well as the decrease of them, compared to the reference structure is represented in table 9.

Table 9 Slope results from the force vs displacement graphics, for the three structures

Structure	Slope	Difference [%]
1	7748.90	-
2	1949.10	-75
3	266.25	-97

Conclusions

The second and third structures are quite similar in this test since they have a lower value for the surface area, resulting in a lower force for the same displacement. This means the first structure is able to absorb a greater part of the compressive energy, compared to the other two.

3.2.3. Low Velocity Impact

Simulation Model

This test was adapted to the simulation model and, unlike the previous two tests where only the core is included in the simulation, the low-velocity test includes, also the skins, as the presence of this element affected the core. The standard used was ASM D7136/D 7136M – 05.

The dimensions of the structure were 100 [mm] length, 150 [mm] width and 5 [mm] thickness. The skins were around the same size, except for the thickness, which was around 1 [mm]. For the reasons mentioned before, a quarter of the structured was represented.

In the skin properties, carbon fibre reinforced polymer was selected, and its properties were taken from the database CES Edupack. The density was 1.55e-9 [ton/mm^3], the Young's modulus was 109500 [MPa] and finally, the Poisson ratio was 0.306. This composite is extremely strong and light, and the binder resin is usually thermoset epoxy (Nguyen, Khawaeizmi, & Kim, 2020).

The impactor, a discrete rigid part had a "bullet" shape, with a 16 [mm] diameter sphere and 15 [mm] long. A property of inertia was created in order to assign a mass of 5.5 [kg], in this case, 1.375 [kg].

The step was dynamic explicit, NLGeom on and time step = 0.003.

In order to simulate the sandwich structure, a tie constraint was applied between the core and the skins. The impactor had a rigid body constraint, and a contact property was set up to replicate the interaction between the structure top skin and the impactor. The contact type had a tangential behaviour with a 0.25 penalty, allowing a relative stiff motion of the surfaces, according to the ABAQUS Manual. This is an average value and it was taken from an article concerned with the friction properties of carbon fibre (Sarkar, 2016).

Two boundary conditions assume the symmetry of the structure in two axes, identically to the previous two tests, and a velocity condition was placed in the impactor. The values and corresponding energy, explained in the results table are displayed in table 10. In addition, displacement/rotation boundary condition was placed in the impactor, concerning all rotations and displacements, except in the loading direction avoided the impactor to move forward on any of these directions.

Table 10 Velocities applied in the low velocity impact test and the kinetic energy

Velocity [m/s]	Energy E_k [J]
1	0.69
2	2.75
5	17.19
7	33.69
10	68.75

The mesh for the structure and skin was hex shape, and the element type was C3D8, with 738 elements. The impactor had R3D4 elements and a quad shape.

Results

The applied velocities (v) were transformed in terms of kinetic energy applied (E_k) to the structure, as can be seen in equation (4). The term m is the mass of the impactor. For each

energy, equal to all cases, the deformation in the loading direction was observed, represented in the following graphics.

Equation 3

$$E_k = \frac{mv^2}{2}$$

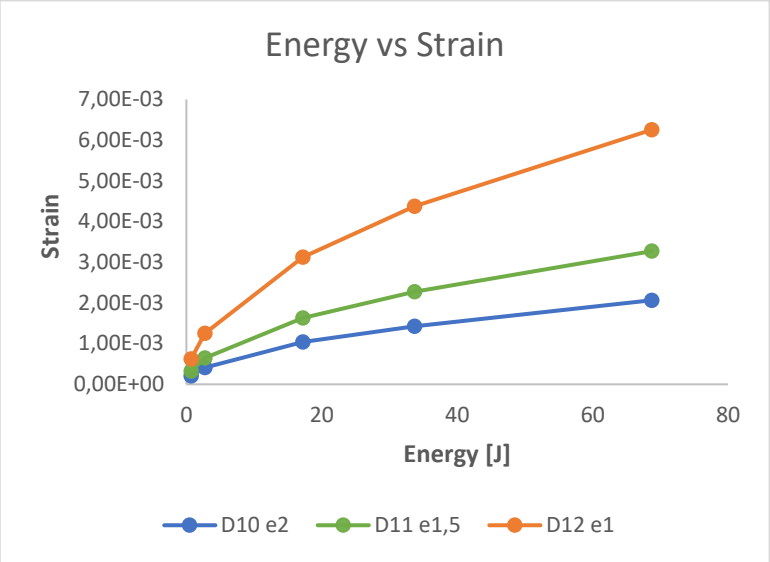

Figure 23 Energy vs Strain for the low velocity impact results

Conclusions

Considering the last result for the higher energy, the difference between the green structure is about 58 [%] higher strain than the first structure. The strain in the third structure is around 202 [%] higher in comparison to the first structured.

3.3. Selection of the material

As referred, three materials, with different densities, were available. In order to select the better fit, three structures were designed, based on the same value for the mass and maintaining the middle structure (D11) for the NL10. The characteristics of the three structures are exhibit in table 11.

Table 11 Cell dimensions and densities of the three selected structures

Structure	Size of the cell [mm]	Thickness [mm]	Density [ton/mm^3]
NL10	11	1.5	1.50e-10
NL20	11.8	1.07	2.02e-10
NL25	12.22	0.9	2.40e-10

In the next table, it is possible to see the specific properties of the three materials. The specific properties are based on the properties divided by the respective density.

Table 12 Specific properties of NL10, NL20 and NL25. Elaborated with the technical data from Amorim Cork Composites

Material	Specific Compression Modulus [N·m/kg]	Specific Compression Strength [N·m/kg]	Specific Shear Modulus [N·m/kg]	Specific Shear Strength [N·m/kg]
NL10	34000	2000	39333.3	6000
NL20	29629.6	2469.1	29135.8	4444.4
Nl25	28750.0	2500	25000	4166.7

It is clear to see that NL10 has superior specific properties in almost every field of the table. Nl20 and NL25 have closer specific properties.

3.3.1 Compression Test

Simulation Model

For this test, the same process to the previous compression test was performed, using the standard ASTM C365/C365M − 11a. The material properties inserted in ABAQUS material model are presented in table 13.

Table 13 Modulus of the three structures for the compression test

Structure	Density [ton/mm³]	Compressive Modulus [MPa]
NL10	1.50e-10	5.1
NL20	2.025e-10	6.0
NL25	2.40e-10	6.9

Results

Once again, the displacements were translated in terms of forces, correlating the applied pressure and the surface area, as seen in equation (3).

The following graphic presents the force [N] versus the displacement [mm] for the three structures.

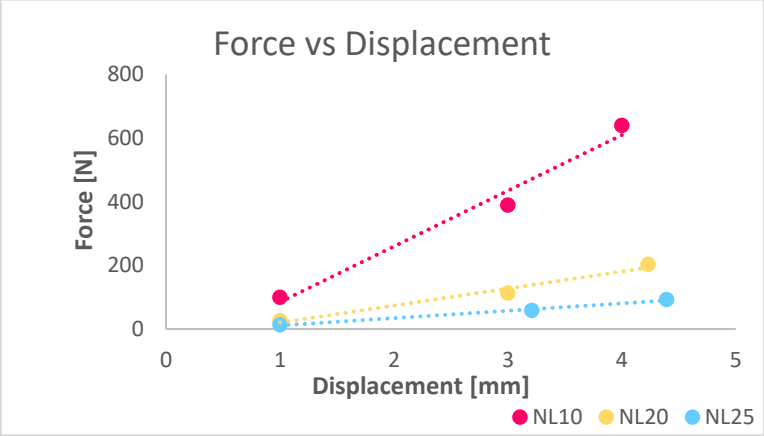

Figure 24 Force vs Displacement for the compression results.

It is clear to see the NL10 has a much thick structure. The difference between the NL10 slope and the other two is quite higher: around less 69 [%] and 87[%], respectively to NL20 and NL25.

Conclusions

In this simulation, NL10 has a better compressive behaviour, because the other two materials have a very thin structure, between cells.

3.3.2. Shear Core Test

Simulation Model

A different structure was selected to meet the standard ASTM C 273 – 00, about, 60[mm] x 30 [mm] x 10 [mm]. For this test, it is necessary to have two plates, where the core will be placed between, in this case, with 70 [mm] x 30 [mm] x 5 [mm], as rigid bodies.

The material properties are summarized in table14.

Table 14 Shear Modulus of the three structures for the shear core test

Structure	Density [ton/mm^3]	Shear Modulus without holes [MPa]
NL10	1.50e-10	5.9
NL20	2.025e-10	5.9
NL25	2.40e-10	6.0

The step is similar to the previous tests, as the mentioned static general step.

For the interaction module, two tie constraints were created to attach the plates to the surface of the core. Moreover, a contact property, with normal and tangential behaviour, with coefficient friction of 0.7. This value is the average result of the interaction between steel (plate) and cork found on (Silva et al., 2005).

The boundary conditions caused a displacement in both plates, in opposite direction. Two different sets of displacements were created to simulate tension and compression loading. In addition, since there is only one-quarter of the plate represented, two symmetry conditions are necessary.

The mesh for the plates includes R3D4 elements, with quad shape, and for the honeycomb, the best fit for the mesh has hex-dominated, C3D8 element type, with 1160 elements.

Results

For each tension/compression test, there are two graphics force versus displacement: in each test. It is necessary to apply two forces, in opposite directions, one for each plate, and these forces will cause shear stresses in both surfaces of cork specimen in contact with them. Therefore, for that matter, in the following subchapter, there will be two graphics, one for each plate. Furthermore, in each case, the shear modulus G is calculated based on the shear stress τ caused on the core surface, based on the equations (4) and (5).

Equation 4

$$\tau = \frac{P}{Lb}$$

P represents the applied force and, *L* and *b* are, respectively, the total length and width of the test specimens.

Equation 5

$$G = \frac{S\,t}{L\,b}$$

Where S is the slope of the graphic of force versus displacement, mentioned before, and t represents the thickness.

Tensile

The force versus displacement graphs for the top and lower plates are shown next. The NL20 and NL25 are clearly close, however the NL10 stands out with a larger shear modulus due to the higher slope in both the upper and lower plate.

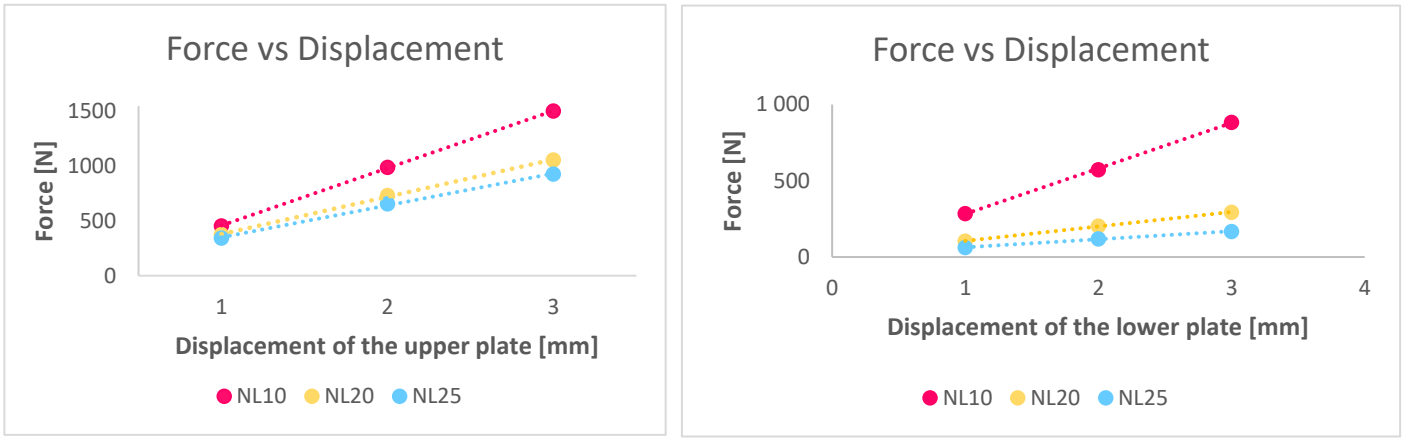

Figure 25 Force vs Displacement of the plates graphics for the shear core test - Tensile

Table 15 Shear Modulus for the three structures/materials - Tension

Structure	Upper Plate		Lower Plate	
	G [MPa]	Difference [%]	G [MPa]	Difference [%]
NL10	0.509		0.415	
NL20	0.133	-74%	0.132	-68%
NL25	0.0733	-86%	0.0733	-82%

Compression

The force versus displacement graphs for the top and lower plates are shown next. The NL10 has a greater slope, resulting in a higher shear modulus, as similar seen in the graphics from figure 26.

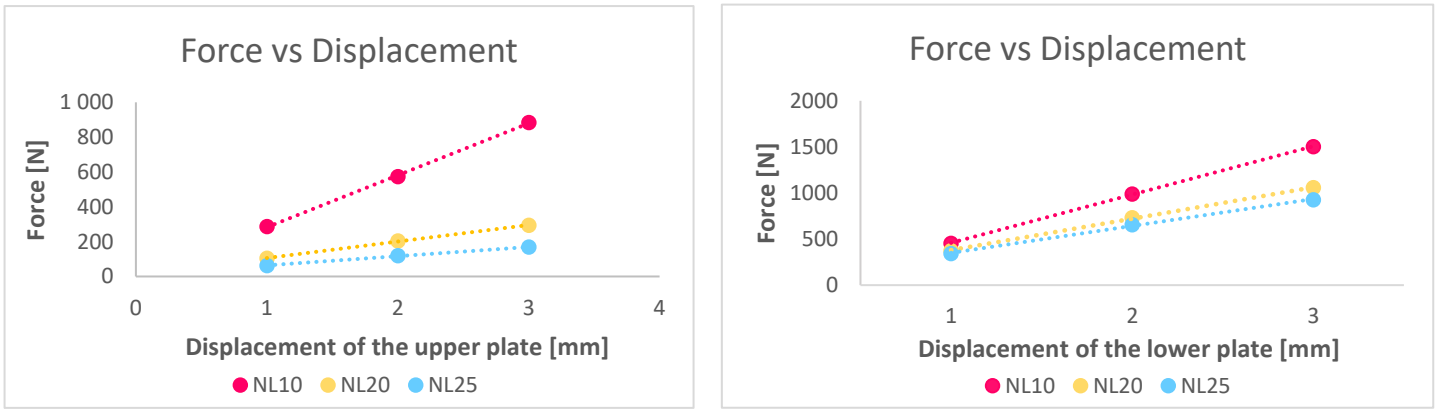

Figure 26 Force vs Displacement of the plates graphics for the shear core test - Compression

Table 16 Shear Modulus for the three structures/materials - Compression

Structure	Upper Plate		Lower Plate	
	G [MPa]	Difference [%]	G [MPa]	Difference [%]
NL10	0.509	-	0.415	-
NL20	0.133	-74%	0.132	-68%
NL25	0.073	-86%	0.073	-82%

Conclusions

In both modes, NL10 has a higher shear modulus, where the difference is over 65 [%], in every value. Again, the structure of the specimen is quite important for the shear properties.

3.4.Hexagonal Cell Size and Material: Final Remarks

Based on all done, two decisions need to be taken: choose the optimized dimensions of the cell and what material to use.

The first decision is a compromise between weight and mechanical properties. Structure number 3 has the worst properties, quite low compared to the other two, so this option is ruled out. Between the structure 1 and 2, the difference of weight is a reduction of 12 [%] but does not replicate in the properties because the second structure, in some tests, shows an over 40 [%] worst performance than the structure 1. For that reason, structure 1 seems to be a better fit.

For the material, NL10 had a better response in both tests, in comparison with NL20 and NL25, which have "thinner" structures, resulting in lower equivalent properties. This is true for the middle structure (D11, NL10), which was the starting point. If there were to be simulations using the first structure (D10, NL10), as a starting point, it would probably have similar results as the difference between equivalent properties is even higher, according to the analytical approach from (Sun, 2018) to calculate the equivalent modulus of hexagonal honeycomb. Table 12's specific properties also suggest to NL10 as a superior option.

Equation 6

$$Eq = E \cdot 2.3 \cdot \left(\frac{t_h}{l_h}\right)^3$$

According to this equation, the equivalent properties of NL10, Nl20 and NL25 with the two types of starting point structures are presented in table 17.

Table 17 Equivalent Modulus for different corks and different structures, according to Equation 6 (Sun, 2018)

Cork Type	Size of the Cell [mm]	Equivalent Modulus [MPa]	Size of the Cell [mm]	Equivalent Modulus [MPa]
NL10	10	4.521	11	1.431
NL20	11.2	1.161	11.8	0.427
NL25	11.6	0.666	12.2	0.259

3.5. Simulation Model

The three different models used to represent the three mechanical testing described in chapter four will be presented in this section.

The models were created to be as close as possible to the experiments. The material properties of the core and the skin were the same in all three tests: three-point bending, compression, and low velocity impact. As a result, the materials in this subchapter will be displayed first. Following that, for each test, the parts, the step used, the interaction and boundary conditions, and finally the mesh size/elements will be described.

3.5.1. Material properties

NL10 cork was used for the core, and UD Carbon prepreg was used for the skin.

Some authors (B. Soares et al., 2011; F.A.O. Fernandes, R.T. Jardin, A.B. Pereira, & Sousa, 2015) argue that cork should be treated as a hyperplastic solid in terms of the core material. These materials are isotropic and non-linear, according to ABAQUS manual users. Furthermore, for materials with an instantaneous elastic response to large strains, it is a valid model. Mullins effect is a damage model in ABAQUS that is suitable for this type of material.

ABAQUS was used to enter the properties, which are summarised in table 18. Some were derived from Amorim Cork Composites' technical data, while others came from two cork-related research (B. Soares et al., 2011; F.A.O. Fernandes, R.T. Jardin, A.B. Pereira, & Sousa, 2015).

Table 18 NL10 cork properties inserted used in the models representing the mechanical testing, inserted in Abaqus

Type of Property	Property	Value	Source
General	Density [ton/mm^3]	1.50e-10	Technical data from Amorim Cork Composites
Hyper elastic model	Uniaxial Test data: ASTM C-365 Stress vs Strain curve	Figure 27	(B. Soares et al., 2011)
	Poisson's Ratio	0	(F.A.O. Fernandes, R.T. Jardin, A.B. Pereira, & Sousa, 2015)
Damage Model: Mullins Effect	r	1.8	(F.A.O. Fernandes et al., 2015)
	m'	0.01	
	ß	0.1	

The letters r, m' and ß are parameters to define the damage.

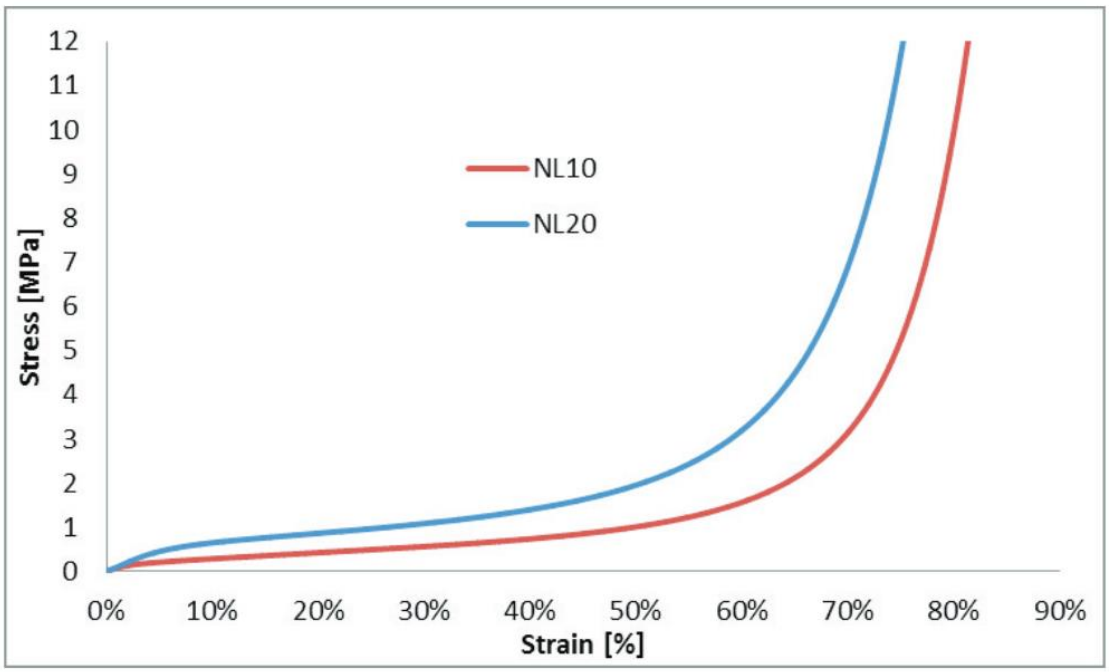

Figure 27 Uniaxial compression test ASTM C-365 Stress vs Strain curve of NL10 and NL20. (B. Soares, L. Reis, & Sousa, 2011)

The section with the NL10 cork applied to the core had 2 [mm] thickness, resulting in a 4 [mm] thick wall and the core was represented with shell elements.

UD Carbon prepreg, which was represented as an elastic material type Lamina, was used to make the skins. The damage model of fibre reinforced composites was described using the Hashin Damage. The damage evolution was also included in this model. The properties of the skin materials were gathered from various sources, just like the core material. Table 19 summarises the characteristics.

There were eight plies in the section applied to the skins, with a stacking sequence of $[0/+45/90/-45]_s$.

Table 19 UD Carbon Prepreg properties inserted used in the models representing the mechanical testing, inserted in Abaqus

Type of Property	Property	Value	Source
General	Density [ton/mm^3]	1.55e-9	CES Edupack 2020
Elastic: Lamina	E1 [GPa]	129	Technical data sheet from Composite Materials (Italy) s.r.l.
	E2 [MPa]	8219.88	
	Nu12	0.34	CES Edupack 2020
	G12=G13 [MPa]	3740	
Hashin Damage	Longitudinal Tensile Strength [MPa]	2294	

	Longitudinal Compressive Strength [MPa]	1152	Technical data sheet from Composite Materials (Italy) s.r.l.
	Transverse Tensile Strength [MPa]	79	(Xue, Wang, Zhang, & Wu, 2015)
	Transverse Compressive Strength [MPa]	190	
	Longitudinal Shear Strength [MPa]	140	
	Transverse Shear Strength [MPa]	88	
Damage Evolution	Longitudinal Tensile Fracture Energy [N/mm]	81.5	(Benzaama, Mokhtari, Benzaama, Gouasmi, & Tamine, 2018)
	Longitudinal Compressive Fracture Energy [N/mm]	81.5	
	Transverse Tensile Fracture Energy [N/mm]	0.277	
	Transverse Compressive Fracture Energy [N/mm]	0.277	

3.5.2. Three-Point Bending Test

The ASTM C393/C393M-11 standard was followed for the three-point bending simulation. Honeycomb core, skin, loading bar, and support bar were designed in the module part. A quarter of the model was represented, and shell elements were used to reduce CPU time.

The loading and support bar were created as discrete rigid components. The loading bar had a diameter of 16 [mm] and a length of 40 [mm]. The support bar was also 40 [mm] long and 13.5 [mm] in diameter.

The dimensions of the skin and honeycomb were 37.5 x 100 [mm^2]. The core was 10 [mm] tall, and the skins were 1 [mm] thick. The hexagonal core had hexagonal holes, and the auxetic core had auxetic holes.

The Step selected was dynamic explicit, with NLgeom on and the total time period was 1 [s].

There were four constraints and one interaction property in the module interaction. To simulate the adhesive between the skins and the core, two tie constraints were used. The loading and support cylinders were defined as rigid bodies by the other two constraints. A friction coefficient of 0.25 was defined by the interaction property. This value has been taken from the study (Silva et al., 2005). A general contact interaction was selected, using the previous mentioned interaction property.

There were two boundary conditions in the sandwich and three on the cylinders in the load module.

Two sides of the sandwich were symmetrical to represent one quarter of the original structure. The support cylinder was clamped, which means it was constrained in all degrees of freedom. The loading cylinder was restricted to only moving in the Z direction due to a displacement constraint. The same cylinder was also subjected to a displacement condition, causing it to move downwards and bend the sandwich.

Finally, S4R elements were used to mesh the honeycomb and skin in the mesh module. The honeycomb contained 950 elements, while the skin contained 348. Shell elements were used in the three models because they were simpler than solid elements and reduced CPU time.

The next image displays the model with the hexagonal core.

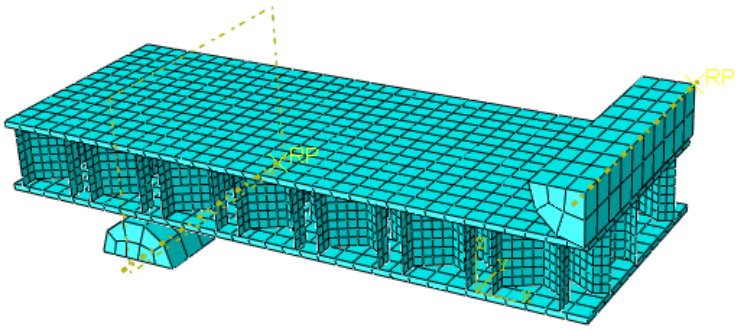

Figure 28 Hexagonal Core Model for three-point bending test

Moreover, the following picture shows the auxetic model for the three-point bending test.

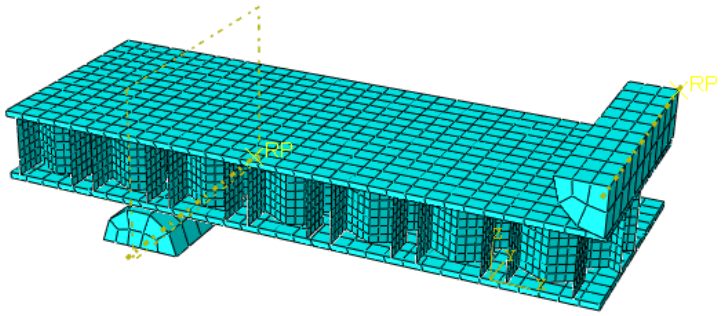

Figure 29 Auxetic Core Model for the three-point bending test

3.5.3. Compression Test

The compression test followed the ASTM C365/C365M-11a standard. Only the honeycomb was developed in this test. The one quarter of honeycomb has the same holes as the previous test, but the outside dimensions are different: 45 x 45 x 10 [mm^3]. In addition, a rigid body plate with dimensions of 60 x 60 x 1 [mm^3] was created. Shell elements are used in both.

The step selected in the step module is the same as the one mentioned previously.

Two constraints were created in the interaction module to connect the core to the plates. Furthermore, the plates were designated as a rigid body. In general contact, a contact property with a friction of 0.7 was defined. (Silva et al., 2005).

In the honeycomb, the load module has two symmetry criteria. Except in the vertical direction, the upper plate was clamped, and the upper bottom plate had restrictions in all degrees of freedom. A displacement movement was also imparted to the top plate, causing the core to move and compress.

The meshed honeycomb core used S4R elements, with a total of 2864 elements.

The next two pictures display the mesh for each model: on the left there is the hexagonal core and, on the right, there is the auxetic core.

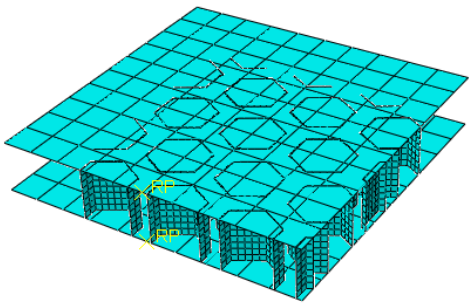

Figure 30 Hexagonal core model for the compression test

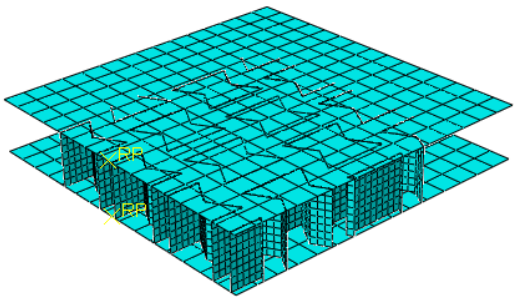

Figure 31 Auxetic core model for the compression test

3.5.4. Low Velocity Impact

Finally, the ASTM D7136/D7136M-05 standard is used for the third session.

The honeycomb, skin, and impactor were designed in 3 parts. The honeycomb, as well as the skin, had the following dimensions: 30 x 30 x 10 [mm^3]. The impactor had a hemispherical tip with a diameter of 16 [mm] and a length of 40 [mm]. This part was made as a discrete rigid, and shell elements were employed, just like the rest of the parts. Aside from the attributes applied to the sandwich components, the impactor had an inertia property, which gave it a mass of 0.943 [kg], a fourth of the original model's mass.

The step was dynamic explicit, with a time period of 0.020 [s] and NLgeom was on.

Similar to the three-point bending test, the same interactions properties are applied.

Two conditions defined symmetry in two axes of the sandwich in the load module, and the other sides of the sandwich without these conditions were pinned to limit the sandwich's linear degrees of freedom. Other two conditions were added to the impactor: one boundary condition that allowed only vertical movement and a predetermined field that included an initial velocity.

The element types in the mesh of the honeycomb and the skins were S4R. There were 298 elements in the skin and 1040 elements in the honeycomb core.

The following two pictures display the meshed model for both cores.

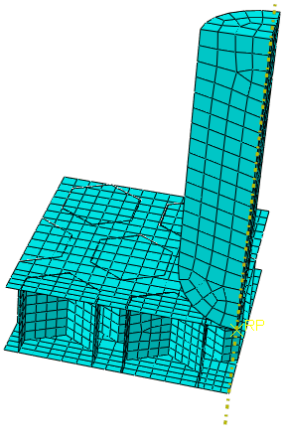

Figure 32 Hexagonal Core model for the low-velocity impact test

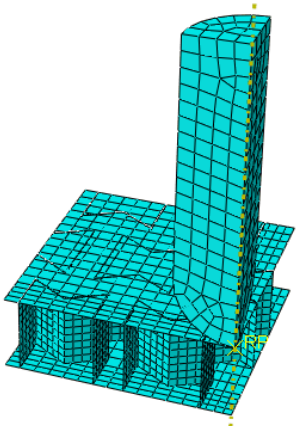

Figure 33 Auxetic Core model for the low-velocity impact test

Chapter 4: Experimental Procedure

This section will concern the preparation of the materials for the experimental testing, namely the skins, the honeycomb cores, and the assembly of them in a sandwich structure through a bond of an adhesive.

The skins were prepared at INEGI.

4.1. Preparation of the Skins

The skins are made of a prepreg fibre carbon, UD REM TAPE ± T700 Carbon Prepreg. The resin present in the prepreg is Toray Semi-Toughened 350°F Epoxy Resin and this thermoset resin provides excellent mechanical properties to the final prepreg. The percentage of resin volume in the prepreg is around 36 [%].

The first step to prepare the skins was to cut the proper size to fit in the hot press from the prepreg tissue conserved in freezer. From the UD prepreg, plies with 45 [º] fibre orientation were cut resulting in some waste material. For the 0 [º] and 90 [º] the cut allowed almost no waste.

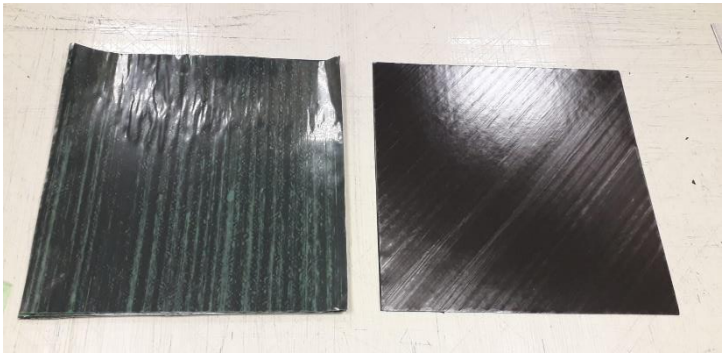

Figure 34 From left to right: a prepreg fibre carbon 90 [º] oriented with the plastic wrap; a stack of some prepregs and the first, on top, is 45 [º] oriented

The prepreg comes with a plastic wrap attached to one side and a harder plastic in the other side. After the skins are cut in all the desired directions, the plastics are removed and the skins in a specific orientation are glued together through the natural glue from the resin. The stacking sequence is the following: $[0/+45/90/-45]_s$. Therefore, eight plies are necessary for each skin.

After the stacking sequence is complete, the prepregs are ready to be placed on the hot press. A bleeder fabric is applied to one side in order to absorb the excess resin and to give a good surface where the adhesive will be placed on. Both sides have the plastic release agent. The skin with just this plastic will have a shining finish.

Figure 35 Skins are ready to go to the hot press. On the left the top side has the bleeder fabric and plastic release agent; on the right, the top side just has the plastic

The time, the temperature and the pressure were chosen based on the guidelines of the manufacturer. In order to fit two skins at the same time in the hot press, a steel sheet was placed between them, and the temperature and time of cure were slightly higher. The cure lasted 60 [min], at 135 [ºC] and 0.5 $N.mm^{-2}$ [5 bar].

Figure 36 Left: before starting the cure, the skins are place inside the hot press; Right: during the cure process

Finally, the skins are taken from the hot press and when the fabric and plastics are removed, they will be ready to use.

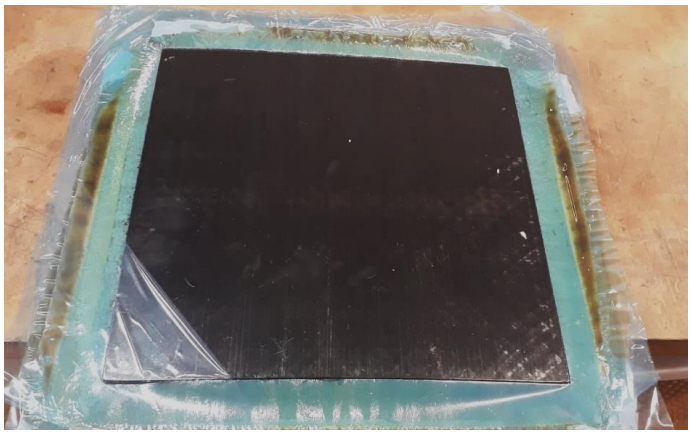

Figure 37 The skins after they exit the hot press. Some resin excess is seen on the sides

4.2. Preparation of the Cores

The first thing to prepare the cores was the development of the draw of the hexagonal and auxetic cores in the software *SolidWorks*. After that, the draws were transferred to the CNC machine, in this case, from the Portuguese company *Ouplan*®.

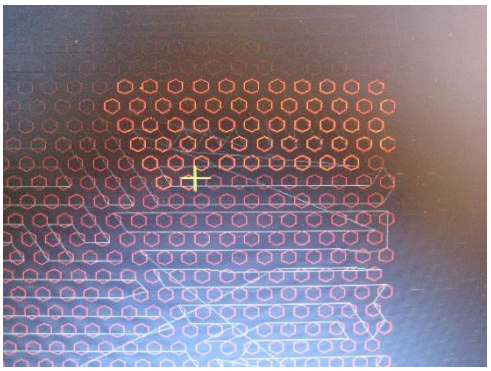

Figure 39 Draw of the hexagonal core

Figure 38 CNC machine

The CNC machine used a 2 [mm] tool at 15000 [rpm]. Figures 35 and 34 demonstrate the CNC machine building the hexagonal and auxetic core.

Figure 41 Making of the hexagonal core

Figure 40 Making of the auxetic core

Table 20 demonstrates the characterization of the core before and after the hexagonal/auxetic perforation, including dimensions, mass, and density data.

Table 20 Characterization of the cork cores, before and after the machining

Core	Dimensions [mm]	Before machining		After machining		
		Mass [g]	Density [kg/m^3]	Mass [g]	Density [kg/m^3]	Density variation [%]
Hexagonal	300.5 x 300.0 x 9.59	132.04	153.0	66.61	77.0	-49.6
Auxetic	300.5 x 300.0 x 9.52	137.28	160	78.05	91	-43.1

The auxetic core has a little greater density than the hexagonal core, as can be seen. The hexagonal and auxetic cores have relative densities of 0.50 and 0.57, respectively.

4.3. Preparation of the Sandwich Structures

Once the core and the skins were ready, it was time to add the adhesive layer and building the test specimens.

The polyurethane adhesive, from *Sika*®, was a mix of two components: SikaForce® - 7710 L100 and SikaForce® - 7010.

To minimize the weight, the adhesive layer was placed in a metal sheet and put on top of the machined core. The idea was to occupy only the core and avoid any adhesive between the holes and the skin. This technique, applied in both of the cores, is illustrated in the following pictures.

Figure 44 Adhesive applied into the metal sheet

Figure 42 Adhesive application the auxetic core

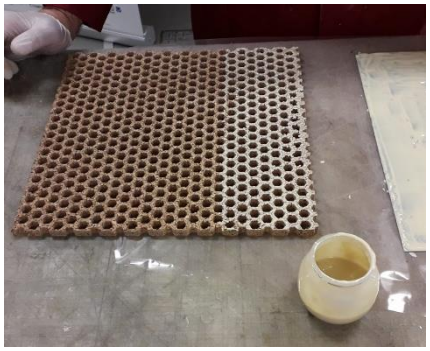

Figure 43 Adhesive application the hexagonal core

After the two skins were glued to the cores, the sandwich structures were allocated in a stove for six hours, at 65 [°C] to cure the adhesive. The final step was to cut the boards into test specimens dimensions, using a water cut saw, as seen in picture 45. They were dried out with intense airflow.

Figure 45 Saw used to cut the test specimens

4.4. Mechanical Testing

Three mechanical tests were performed to the test specimens: compression, three-point bending and low velocity impact. The experimental conditions will be present in this section.

Both **compression** and **three-point bending** test were conducted in the same machine. This device had a servo-hydraulic actuator, controlled by an electric unit, also responsible for the data acquisition.

The load data was measured with a 10 [kN] strain-gage load cell, whereas the deflection, in the three-point bending test, or the displacement, in the compression tests were collected LVDT transducer.

In figure 46, it is possible to see the configuration for the compression test. The imposed displacement was 10 [mm] at a 0.5 [mm/min], in agreement with the standard ASTM C365/C365M.

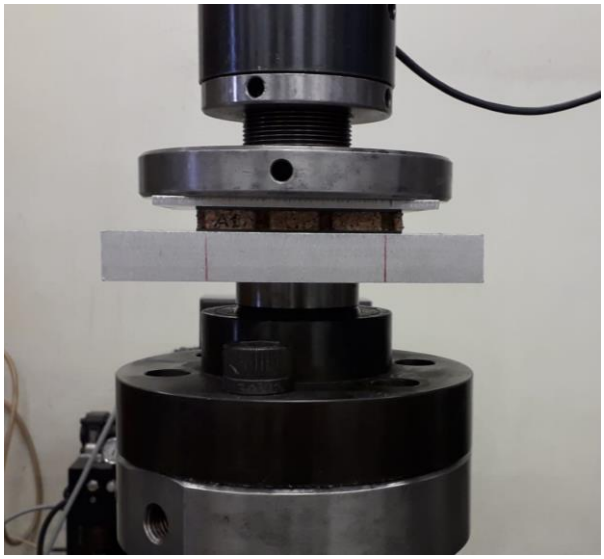

Figure 46 Compression test configuration

The three-point bending test configuration are seen in figures 47 and 48. In the first one, the test had just begun, and the test specimen is slightly deformed, whereas in the second, the test specimen is quite bent. The diameter of the loading cylinder is 16 [mm], placed in the middle of the test specimen, and the support cylinders have 13.5 [mm] diameters. Following the standard ASTM C 393 – 00, the selected rate was 2.5 [mm/min], and the distance between the support cylinder was 150 [mm].

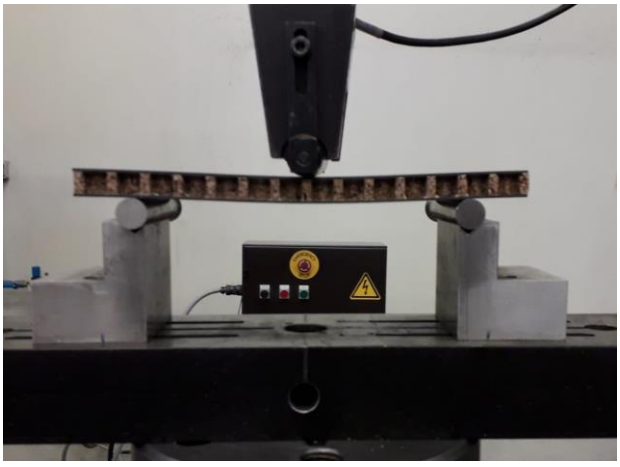

Figure 48 Three-point bending test specimen configuration, at begin of the test

Figure 47 Three-point bending test specimen configuration, during the test

The **low-velocity impact** tests followed the standard ASTM D 5628 – 96 and were carried out by using a drop weight impact testing device. This testing device was connected to a computer that recorded the data. The impactor had 40 [mm] length and a semi spherical 16

[mm] diameter tip. The total weight of the impactor was 3.772 [kg]. The selected impact energies were 8 [J] and 16 [J], which corresponds to a drop height of 0.217 [mm] and 0.434 [mm] respectively. The impactor reaches the test specimen with a velocity of 2.059 [m/s] and 2.913 [m/s] with an initial energy of 8 [J] and 16 [J], respectively, assuming the conservation of energy principle and applying the equations 7 and 8.

Equation 7

$$E_p = m \cdot g \cdot h$$

Equation 8

$$E_k = \frac{1}{2} \cdot m \cdot v^2$$

Where E_p denotes potential energy, m denotes the impactor's mass, g denotes gravity acceleration, and h is the impactor's height. E_k is the kinetic energy converted from the potential energy in the second equation, and v is the impactor's velocity.

After the drop weight event, the depth of the result was measured by a comparator measuring instrument.

Figure 43 displays the drop weight machine during a test, with low velocity impact tests configuration.

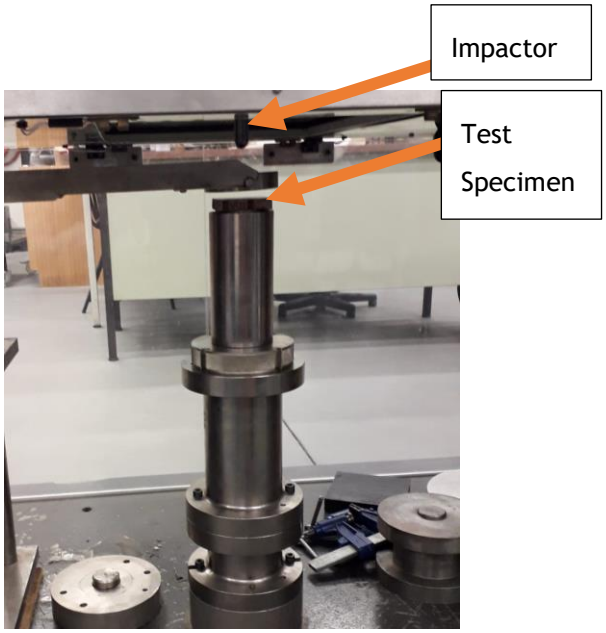

Figure 49 Low velocity impact tests configuration

Chapter 5: Results and Discussion

In the following section, the results from the mechanical testing will be presented and compared to the numerical simulation.

5.1. Three-point Bending Test

5.1.1. Test Specimens

Table 21 shows the parameters of the test specimens prior to mechanical testing, including their size and weight.

Table 21 Test specimens' dimensions, weight and density of the three-point bending test

Test Specimen	Dimensions [mm]	Average [mm]	Weight [g]	Average [g]
Hexagonal #1 (H1)	198.0 x 75.01 x 11.8	198.3 x 74.79 x 12.03	71.44	72.65
Hexagonal #2 (H2)	198.0 x 74.35 x 12.04		72.2	
Hexagonal #3 (H3)	199.0 x 75.02 x 12.16		74.3	
Auxetic #1 (A1)	200.0 x 75.05 x 11.87	198.67 x 74.68 x 11.98	72.78	73.66
Auxetic #2 (A2)	199.0 x 74.1 x 12.05		73.26	
Auxetic #3 (A3)	197.0 x 74.59 x 12.02		74.93	

The standard size of the test specimen was 200 x 75 x 12 [mm^3]. In comparison to the sandwich with hexagonal core, the auxetic specimens have a little more weight.

The test specimens were subjected to a 40 [mm] deflection at a rate of 2.5 [mm/min], with no evident failure in the top and bottom skin.

5.1.2. Load-Deflection Curve

Three test specimens for the hexagonal and auxetic cores were produced for the three-point bending test. The load-deflection curve of the six structures, three for each core, is shown in figures 50 and 51.

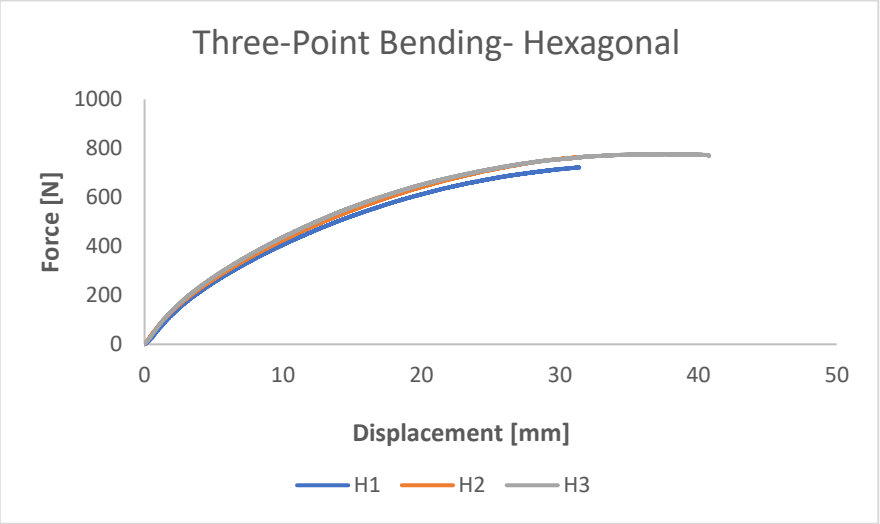

Figure 50 Force versus displacement of the hexagonal cored sandwiches in three-point bending test

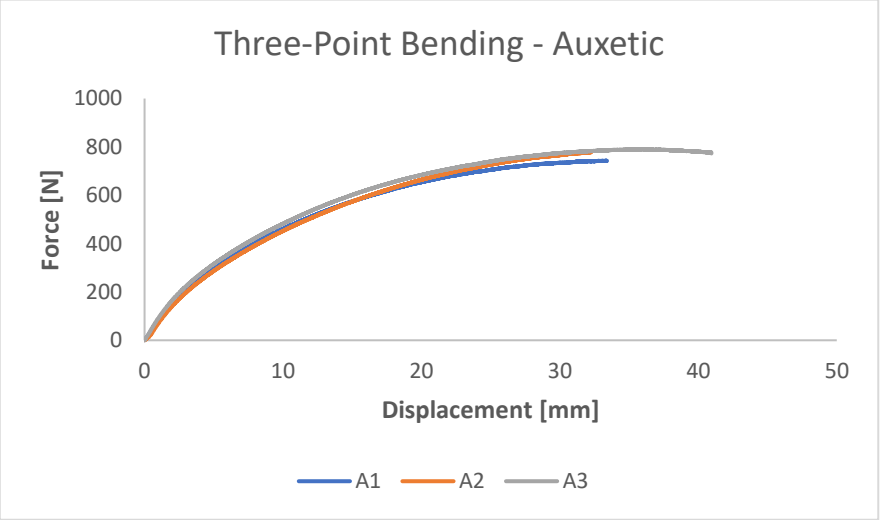

Figure 51 Force versus displacement of the auxetic cored sandwiches in three-point bending test

The next graphics were developed by calculating the average of the three test specimens of each core. Both of the cores have fairly similar curves, as can be seen. The elastic zone is represented by the first linear section of the curve.

The auxetic cores curves are somewhat higher than the hexagonal core when compared side by side, as seen in figure 52.

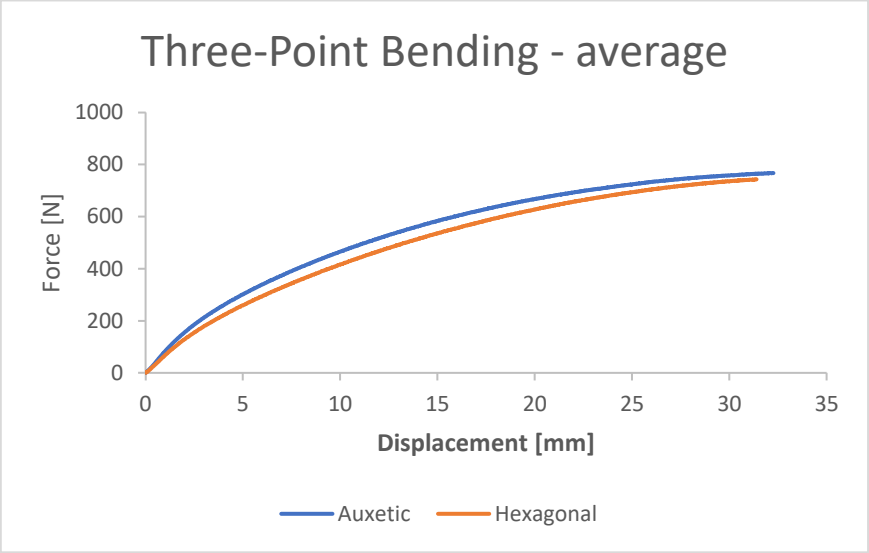

Figure 52 Force versus displacement of the average of the hexagonal and auxetic cored sandwiches in three-point bending test

Throughout the curve, the auxetic core has a slightly higher load for the same deflection.

5.1.3. Flexural Rigidity, Transverse Shear Rigidity and Core Shear Modulus

The flexural rigidity (D) can be determined using the equation 7, according to ASTM D7250/D7250M-06. This equation can only be used if the facing modulus (E_f) is known.

Equation 9

$$D = \frac{E_f \cdot (d^3 - c^3) \cdot b}{12}$$

Where d and b are the sandwich's height and width, respectively, and c is the core's height.

The flexural stiffness of each test specimen is shown in the table below, with the hexagonal average value being somewhat higher. The hexagonal cored sandwiches have thicker and wider test specimens, which could explain their superior resistance to bending loads.

Table 22 Flexural Rigidity of the test specimens in the three-point bending test

Test Specimen	Flexural Rigidity [N.mm^2]	Average [N.mm^2]	Standard Deviation	Coefficient of Variation [%]
H1	2.05×10^8	2.12×10^8	6.95×10^6	3
H2	2.13×10^8			
H3	2.19×10^8			
A1	2.08×10^8	2.11×10^8	2.50×10^6	1
A2	2.12×10^8			
A3	2.13×10^8			

The equation 10 from the preceding mentioned standard is used to compute the transverse shear rigidity (U).

Equation 10

$$U = \frac{P \cdot (S_1 - L_1)}{4 \cdot \left[\Delta - \frac{P \cdot (2 \cdot {S_1}^3 - 3 \cdot S_1 \cdot {L_1}^2 + {L_1}^3)}{96 \cdot D}\right]}$$

The applied load and deflection, respectively, are P and Δ. The load span is L_1, which in this case is zero, and the distance between the support cylinders is S_1.

If the graph of transverse shear stiffness vs applied force was linear, 10 values of transverse shear rigidity would be chosen, and the average of this parameter for the sandwich would be calculated. For each test specimen, a linear curve was discovered.

The transverse shear rigidity described in equation 8 is found in Table 23. Transverse shear stiffness is increased in auxetic cored sandwiches.

Table 23 Transverse Shear Rigidity of the test specimens in the three-point bending test

Test Specimen	U - Transverse Shear Rigidity [N]	Average [N]	Standard Deviation	Coefficient of Variation [%]
H1	1348.45	1460.11	99.92	7
H2	1541.09			
H3	1490.80			
A1	1579.55	1635.76	180.39	11
A2	1490.17			
A3	1837.56			

Finally, the core shear modulus (G) has determined with following expression:

Equation 11

$$G = \frac{U \cdot (d - 2 \cdot t)}{(d - t)^2 \cdot b}$$

Where t is the thickness of the facing.

As with transverse shear rigidity, a linear curve of core shear modulus versus applied force was plotted, and 10 points were chosen to average each specimen, as given in table 24.

Table 24 Core Shear Modulus of the test specimens in the three-point bending test

Test specimen	G - Core Shear Modulus [MPa]	Average [MPa]	Standard Deviation	Coefficient of Variation [%]
H1	1.51	1.66	0.13	8
H2	1.71			
H3	1.75			
A1	1.76	1.82	0.19	10
A2	1.67			
A3	2.03			

5.1.4. Numerical Results

The comparison of experimental and numerical data will be shown in this part. The force vs displacement image will be displayed first, followed by the experiment parameters. Finally, in the numerical simulation, there is a direct comparison between the auxetic and hexagonal cores.

Only the elastic half of the experiment was included in the simulations for both hexagonal and auxetic cores, as shown in figures 53 and 54.

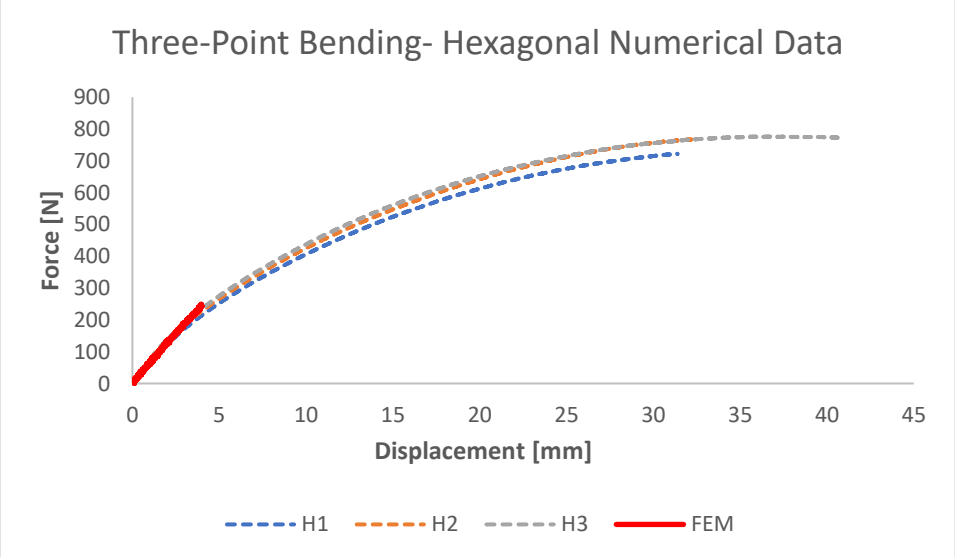

Figure 53 Force vs Displacement for the hexagonal core - experimental and numerical data

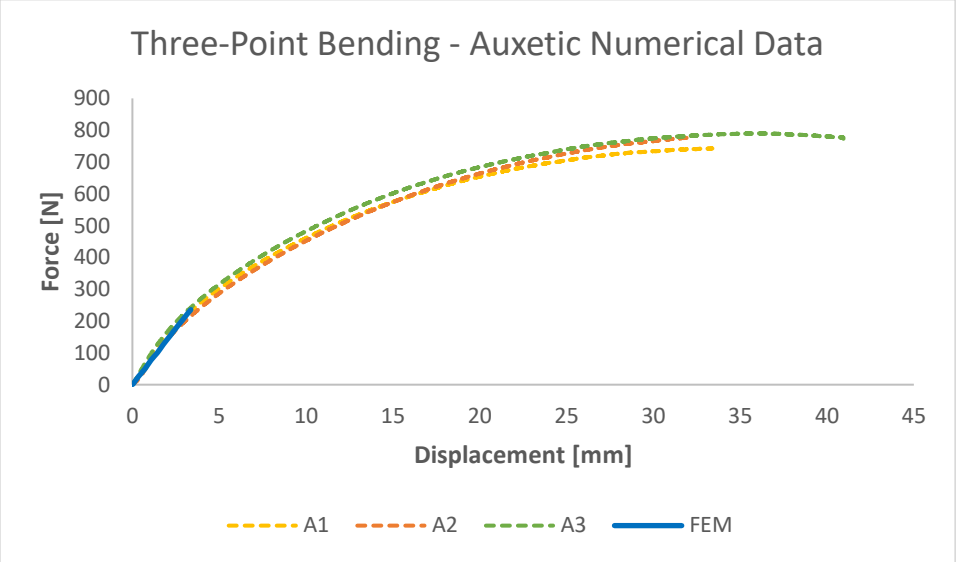

Figure 54 Force vs Displacement for the auxetic core - experimental and numerical data

The numerical data appears to be in good agreement with the experimental data in both graphics.

The flexural rigidity, transverse shear rigidity, and core shear modulus from experimental and numerical data are represented in Table 25. The average of the test specimens was used to calculate the experimental data.

Table 25 Flexural Rigidity, Transverse Shear Rigidity and Core Shear Modulus of hexagonal and auxetic core in numerical and experimental analyses

Core	Type of Data	Flexural Rigidity [N.mm^2]	Transverse Shear Rigidity [N]	Core Shear Modulus [MPa]
Hexagonal	Experimental	2.12×10^8	1460.11	1.66
	Numerical	2.13×10^8	1397.86	1.70
Auxetic	Experimental	2.11×10^8	1635.76	1.82
	Numerical	2.13×10^8	1593.43	1.76

For both cores, the difference between the two analyses is minor, around 3 to 4 [%] difference. The numerical and experimental findings are in good agreement. The auxetic core has a higher transverse shear rigidity and core shear modulus than the hexagonal core, as shown in the experiment.

The force versus displacement curve for the cores in the numerical simulation is shown in the next figure.

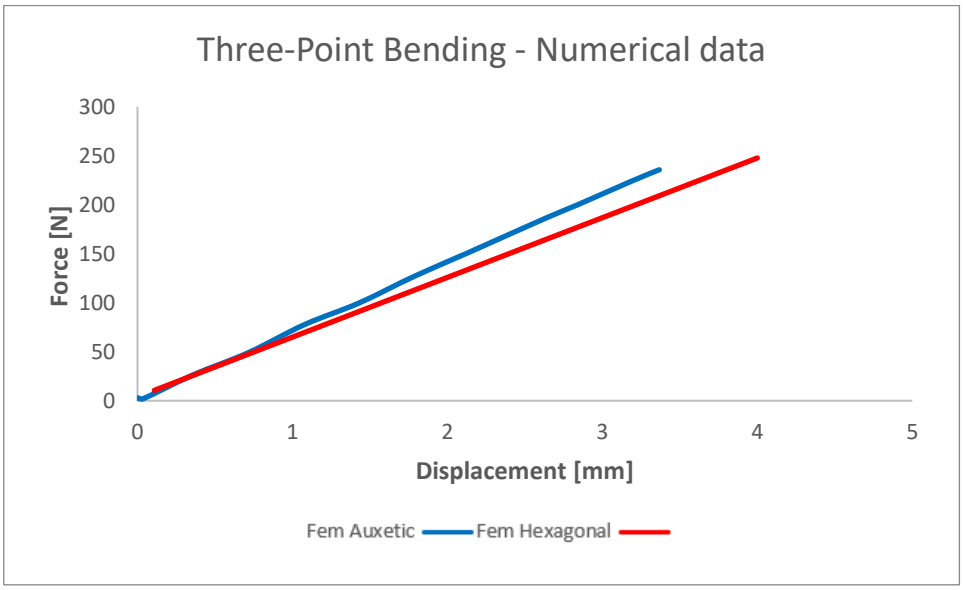

Figure 55 force versus displacement curve for the cores in the numerical simulation

5.2. Compression Test

5.2.1 Test Specimens

Two test specimens were created for each core. Each one's dimensions, weight, and density, as well as the average value for each type of core, are listed in Table 26. The analysis of this test was based on the ASTM C365/C365M – 11a.

Table 26 Test specimens' dimensions, weight, and density of the compression test

Test Specimen	Dimensions [mm]	Average [mm]	Weight [g]	Average [g]
Hexagonal (H1)	90.23 x 90.23 x12.09	90.26 x 90.26 x 12.10	39.63	39.73
Hexagonal (H2)	90.3 x 90.3 x 12.10		39.83	
Auxetic (A1)	89.76 x 89.76 x 12.03	90.07 x 90.07 x 11.97	39.96	40.08
Auxetic (A2)	90.38 x 90.38 x 11.90		40.19	

5.2.2. Load-displacement and stress-strain curves

The images for the load-displacement curve and the corresponding stress-strain curve are then provided, taken directly from the data acquisition system where the test was conducted.

The superficial area perpendicular to the loading and the height of the core were taken into consideration in order to compute the stress and strain, and they are recorded in table 27 for each test specimen.

Table 27 Test specimens' superficial area and core's height of the compression test

Test Specimen	Superficial area [mm^2]	Core's height [mm]
H1	8141.45	9.59
H2	8154.09	9.59
A1	8056.86	9.52
A2	8168.54	9.52

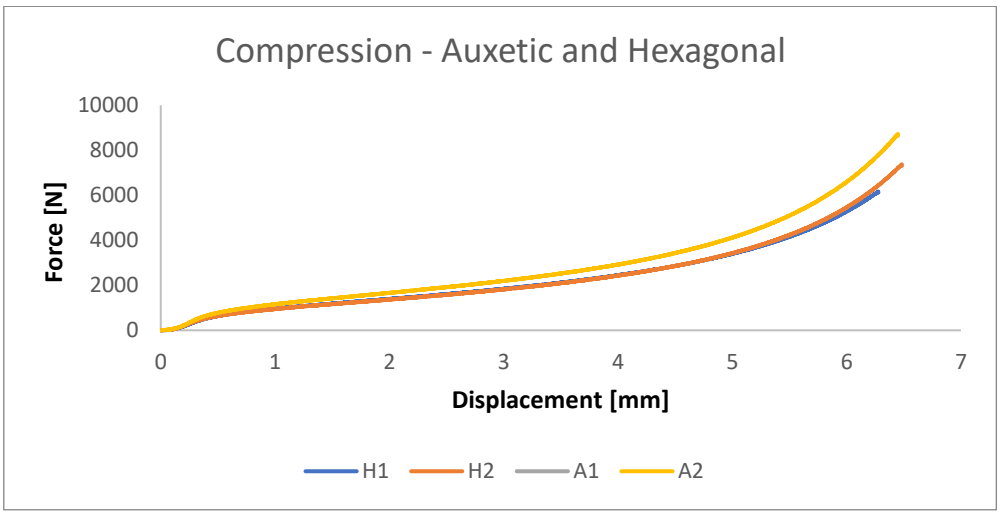

Figure 56 Force versus displacement of the test specimens in compression test

The load-displacement and stress-strain curves are depicted in the diagrams below. To make it easier to compare the test specimens, they are all represented in the same figure.

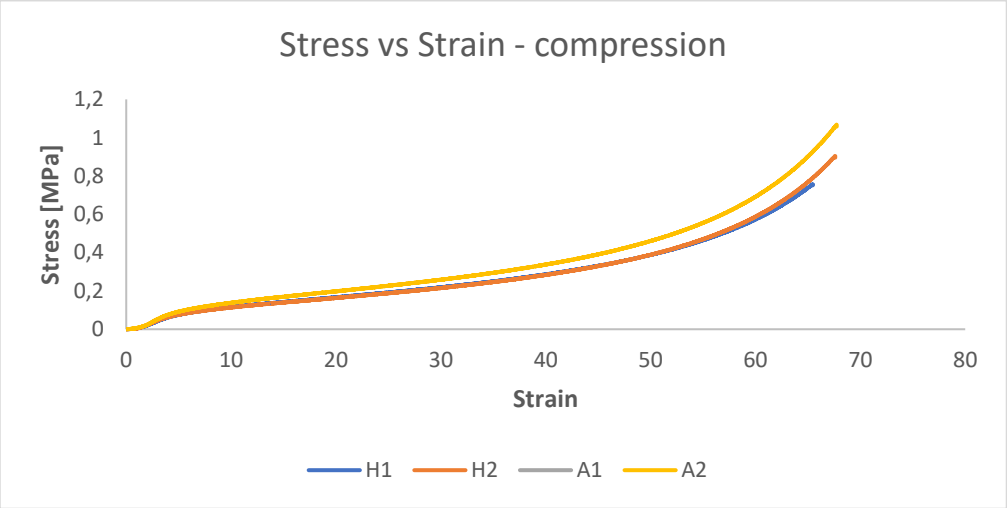

Figure 57 Stress versus Strain of the test specimens in compression test

The curves of both test specimens for each core are remarkably similar. The auxetic core has a superior curvature, which is expected given the structure's higher surface area.

5.2.3 Compressive Modulus and Compressive Strength

The compressive modulus was calculated by isolating the elastic zone of the stress-strain curve and finding the slope of the linear curve. The stress value that defines the elastic zone's limits was used to determine the compressive strength. The compressive modulus as well as the compressive strength of each specimen are shown in the table below.

Table 28 Test specimens' Compression Modulus and Compression Strength of the compression test

Test Speci-men	Compression Modulus [MPa]	Compression Strength [MPa]
H1	2.295	0.053
H2	2.366	0.055
A1	2.731	0.071
A2	2.934	0.063

In comparison to the hexagonal core, the auxetic core has a higher modulus and compression strength.

Another important statistic is the compressive strength at 2 [%] and 10 [%] strain. The values of the mentioned parameters are listed in the table below.

Table 29 Test specimens' Compression Strength at 2% and 10% strain of the compression test

Test Specimen	Compression Stress [MPa]	
	2% Strain	10% Strain
H1	0.042	0.128
H2	0.080	0.145
A1	0.0915	0.173
A2	0.0949	0.175

The auxetic cored sandwiches require additional stress in both strains to produce the same plastic strain.

5.2.4. Post-test: elastic recovery of specimens

The thickness of the specimens was carefully measured immediately after the test and for the next four weeks afterward. The following graph depicts the recovery of the specimens over the specified time, focusing on the residual deformation.

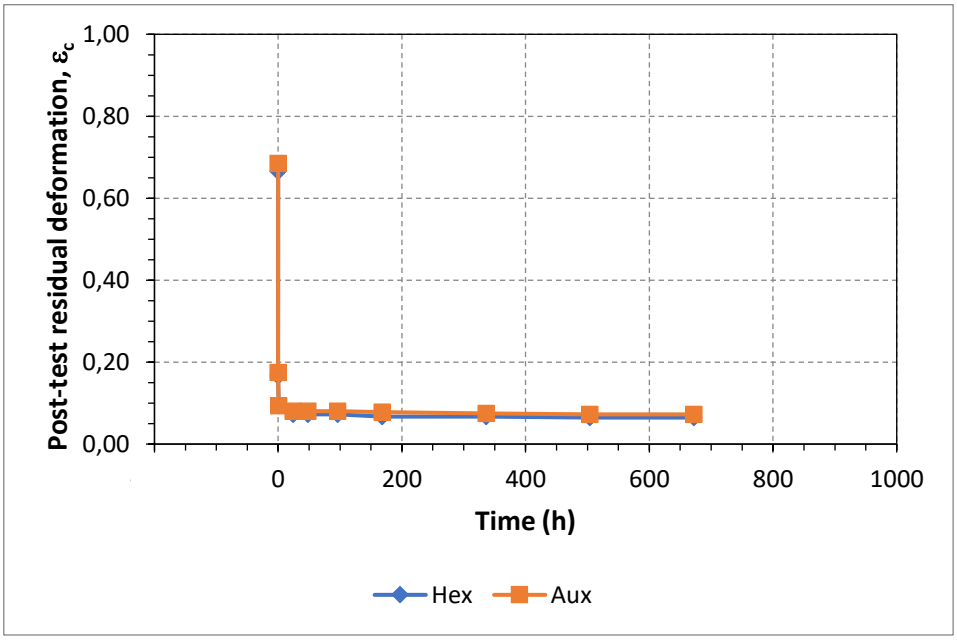

Figure 58 Test Specimens elastic recovery

Both cores showed an equal recovery trajectory, and according to the graph, the specimens recover nearly 75 [%] in the first minute following the test. The rest of the recovery is almost meaningless over time.

5.2.5. Numerical Results

The numerical results will now be displayed, and they will be compared to the experimental data. Only the elastic zone is depicted in the simulations. As a result, the graphics' compression modulus and elastic phase were the only variables that could be compared.

For each core, the compression modulus will be displayed first, followed by graphics of force versus displacement and stress versus strain.

The two simulated cores, hexagonal and auxetic, will be examined at the end.

Hexagonal Core

In the force versus displacement and stress versus strain graphics, the simulation is shown to be close to the experimental data.

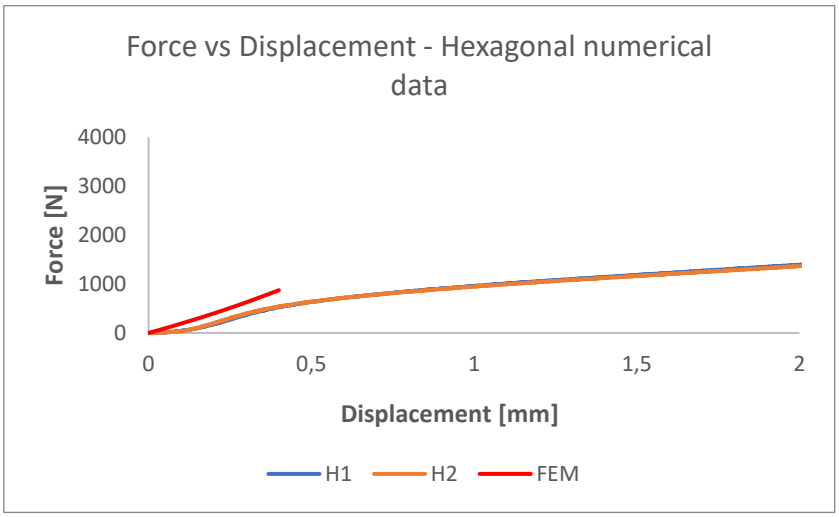

Figure 59 Force vs Displacement in compression test - hexagonal numerical data

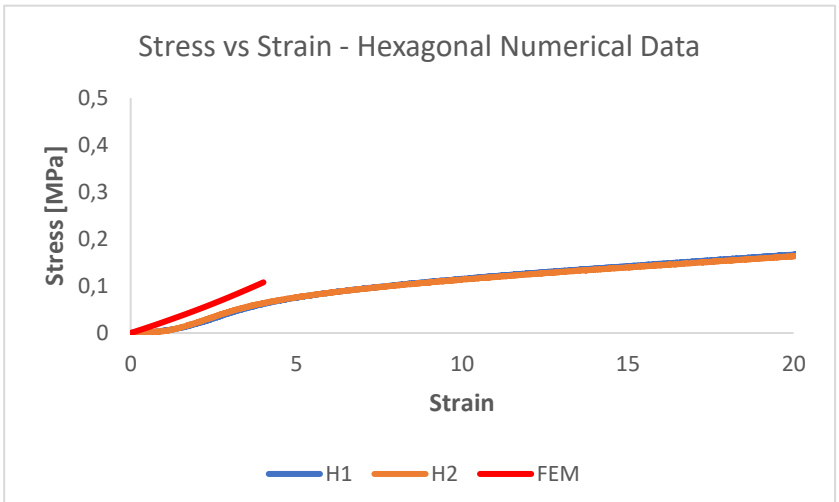

Figure 60 Stress vs Strain in compression test - hexagonal numerical data

The force and stress values in the simulation are slightly higher. The compression modulus obtained in the experiment is 18 [%] lower than that obtained in the simulation. The values are shown in Table 30. The experimental value is a composed of the two test specimens' results.

Table 30 Compression Modulus for the hexagonal core - experimental and numerical data

Analyse	Compression Modulus [MPa]
Experimental	2.33
Numerical	2.75

Auxetic Core

The auxetic core is now investigated. In comparison to the previous core, the numerical data in images 61 and 62 appears to be closer to the experimental values.

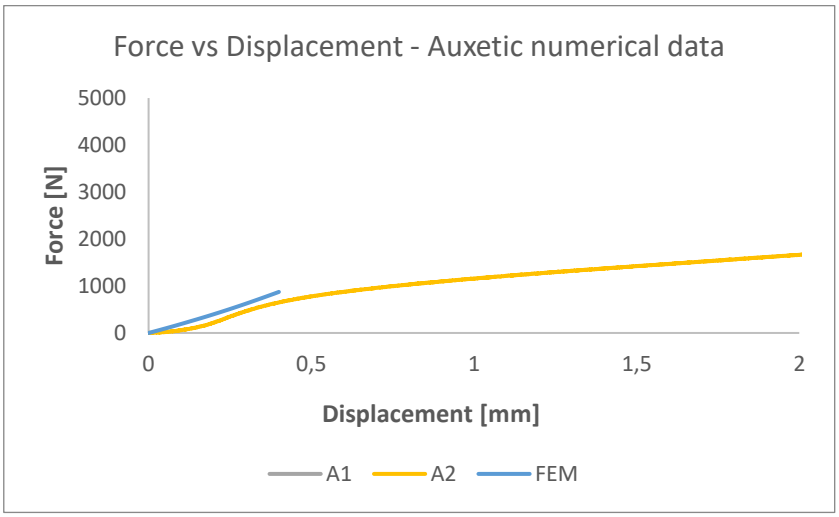

Figure 61 Force vs Displacement in compression test - auxetic numerical data

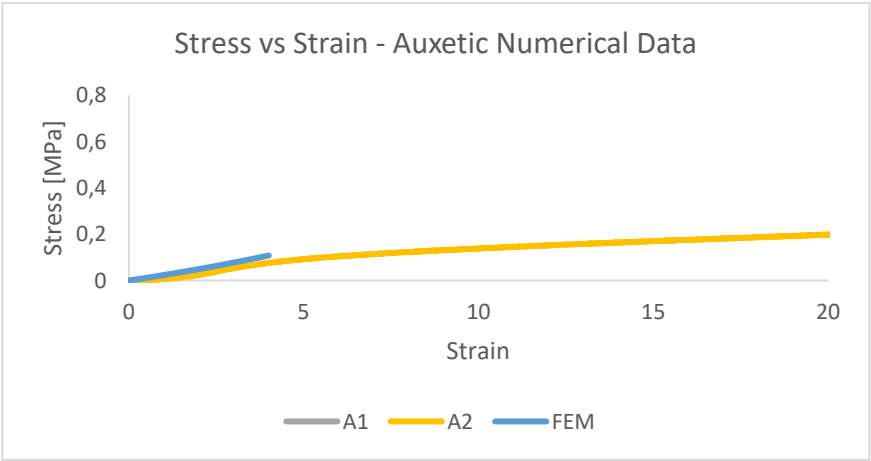

Figure 62 Stress vs Strain in compression test - auxetic numerical data

Information on the auxetic compression modulus can be found in Table 31. The values are very close, with only an 8 percent difference between them.

Table 31 Compression Modulus for the auxetic core - experimental and numerical data

Analyse	Compression Modulus [MPa]
Experimental	2.83
Numerical	3.06

The simulations, particularly the auxetic core, have a good agreement with the experimental data, with a difference of less than 10%.

The auxetic and hexagonal cores will now be compared using numerical data. The graphs show the relationship between force and displacement, as well as stress and strain.

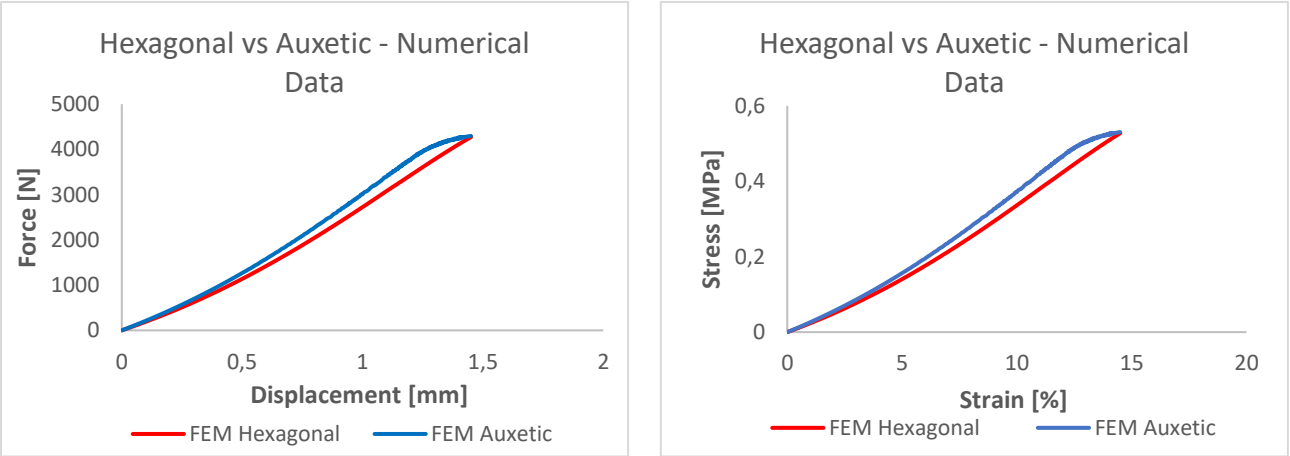

Figure 63: Left to Right Force vs Displacement and Stress vs Strain in compression test - auxetic and hexagonal numerical data

The curves are nearly identical until the auxetic core exceeds the hexagonal core around 0.5 [mm] displacement and 5 [%] strain.

The auxetic core has a higher compression modulus, which was also observed in the experimental data.

5.3. Low-velocity Impact

5.3.1. Test Specimens

The low velocity impact involved two velocities, i.e., two impact energies, and two test specimens for each hexagonal and auxetic cored sandwiches. Table 32 contains information on the specimens.

Table 32 Test specimens' dimensions, weight, and density of the low velocity impact test

Test Specimen	Impact Energy [J]	Dimensions [mm]	Average [mm]	Weight [g]	Average [g]
H1	8	60.10 x 60.10 x 11.99	60.23 x 60.23 x 11.94	17.45	17.56
H2		60.36 x 60.36 x 11.89		17.66	
H3	16	60.13 x 60.13 x 11.91	60.28 x 60.28 x 11.92	17.26	17.30
H4		60.43 x 60.43 x 11.93		17.33	
A1	8	60.31 x 60.31 x 11.92	60.27 x 60.27 x 11.92	19.15	18.93
A2		60.22 x 60.22 x 11.92		18.71	
A3	16	60.41 x 60.41 x 11.79	60.38 x 60.38 x 11.81	18.45	18.73
A4		60.34 x 60.34 x 11.82		19.0	

5.3.2. Force vs time, Energy vs time and Velocity vs time curves

This section will show the force vs. time, energy vs. time and velocity vs time graphics. Both energy levels, 8 [J] and 16 [J], will be examined in the first and second phases, respectively. They will be followed by the values of the parameters that are relevant to the analysis.

The dashed lines in figure 64 represent the 8 [J] energy, whereas the continuous lines reflect the 16 [J] energy in the force-time curve of the low velocity impact testing. The force, which is the test specimen's reaction to the impactor, represents the sandwich structure's ability to withstand the impact.

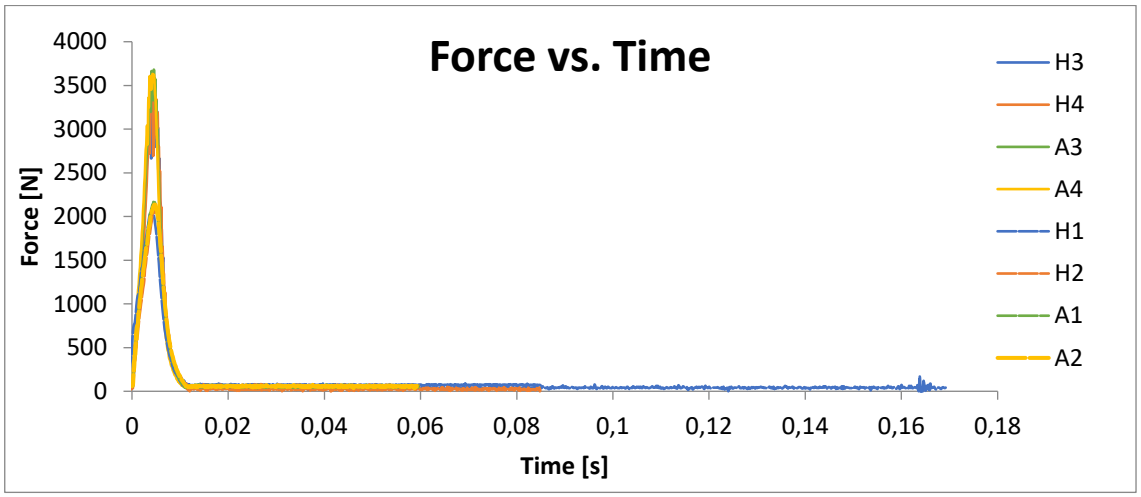

Figure 64 Force versus Time of the test specimens in the low velocity impact tests

Impact Energy: 8J

The force-time curve can be used to determine the maximum force for each specimen. Although their peak values are comparable, the auxetic core has a little higher peak force, as seen in table 33. The energy level at the point of peak force, as well as the contact duration, are shown in the same table. Both hexagonal cores have the maximum and minimum values for the energy level at peak force. In comparison to the auxetic core, the hexagonal core has a longer contact duration.

Table 33 Peak Force, Energy at peak force and contact duration the test specimen at 8 [J] impact energy

Test Specimen	Peak Force [N]	Energy at peak force [J]	Contact duration [s]
H1	2052.07	6.92	0.0130
H2	2088.53	7.64	0.0127
A1	2174.12	7.24	0.0109
A2	2136.38	7.29	0.0118

Impact Energy: 16J

The auxetic core, like the previous 8 [J] impact energy, has larger peak force values than the hexagonal core. The values, however, are wider apart in this case. In the graphics of Figure 64, there are recurring "peak" forces that indicate enduring skin injuries. This issue was not so highlighted for 8 [J]. In table 34, it is possible to see the peak force values. The energy at peak force is found in the same table, and the energy for the auxetic core is higher in this case. The contact duration for the hexagonal core is slightly longer, as evidenced by the preceding impact energy. However, the distinction is barely visible.

Table 34 Peak Force, Energy at peak force and contact duration the test specimen at 16 [J] impact energy

Test Specimen	Peak Force [N]	Energy at peak force [J]	Contact duration [s]
H3	3382.79	14.18	0.0110
H4	3471.25	13.06	0.0110
A3	3680.86	14.61	0.0109
A4	3632.14	14.33	0.0100

The absorbed energy, as well as the ratio between the absorbed energy and the impact energy, will be considered now as part of the energy balance. The energy vs time curve for all eight test specimens is shown in figure 65. 8 [J] and 16 [J] impact energies are shown by the dashed and continuous lines, respectively. The larger the impact energy, the higher the absorbed energy, as expected. The energy that is not absorbed is primarily "spent" in rebounding the impactor backwards.

The total absorbed energy can be determined by the constant value of energy at the end of the curve.

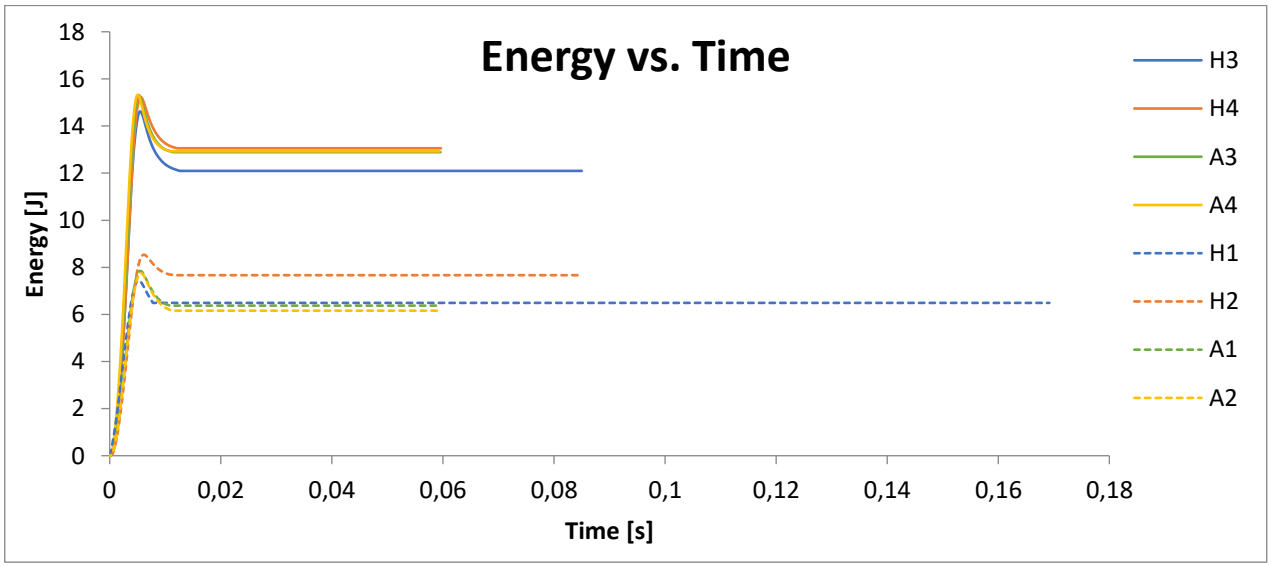

Figure 65 Energy versus Time of the test specimens in the low velocity impact tests

Impact Energy: 8J

In comparison to the auxetic cored sandwich, the hexagonal core absorbed more energy. The hexagonal cored specimens have a higher ratio of absorbed energy to impacted energy, which offers a more comparable parameter.

Table 35 Impacted Energy, Absorbed Energy, and ratio AE/IE the test specimen at 8 [J] impact energy

Test Specimen	Impacted Energy [J]	Average [J]	Absorbed Energy [J]	Average [J]	Ratio AE/IE
H1	7.44	7.93	6.45	7.08	87%
H2	8.43		7.65		91%
A1	7.84	7.79	6.37	6.27	81%
A2	7.75		6.16		79%

Impact Energy: 16J

Unlike the previous impact level, the auxetic core absorbs more energy, despite the fact that the AE/IE ratio is near for all specimens.

Table 36 Impacted Energy, Absorbed Energy, and ratio AE/IE the test specimen at 16 [J] impact energy

Test Specimen	Impacted Energy [J]	Average [J]	Absorbed Energy [J]	Average [J]	Ratio AE/IE
H3	14.62	14.92	12.09	12.57	83%
H4	15.22		13.05		86%
A3	15.31	15.31	12.89	12.91	84%
A4	15.31		12.92		84%

When the impactor strikes the test specimen, the velocity vs time curve can be analysed. The velocity then lowers to zero when the impactor reverses direction, i.e., becomes negative, and then gradually increases, right after the contact ends.

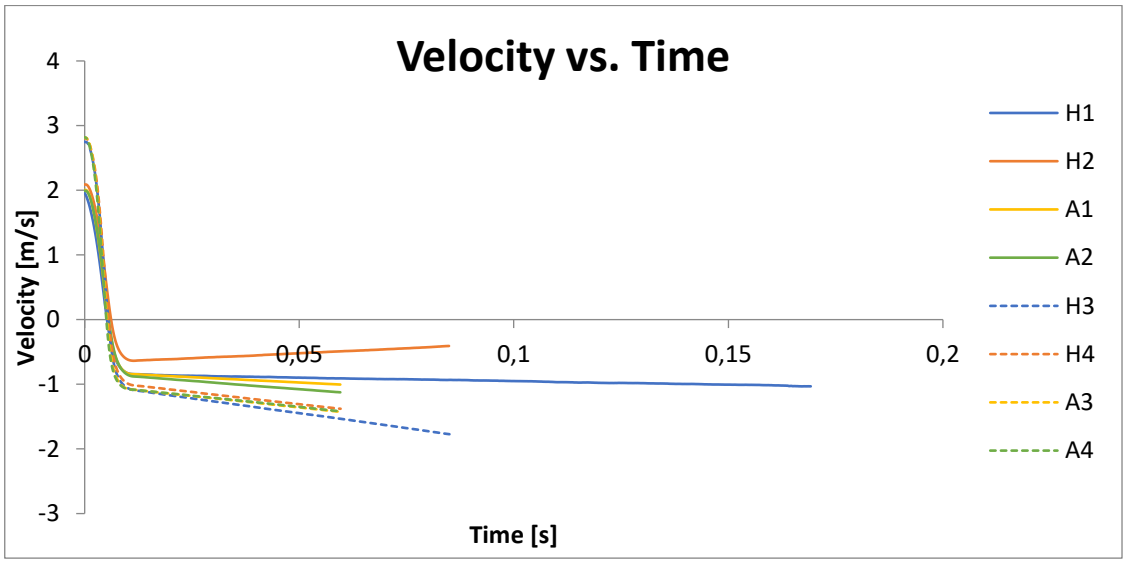

Figure 66 Velocity versus Time of the test specimens in the low velocity impact tests

The following graphic represents the velocity vs time for all specimens. The continuous line represents the 8 [J] impact energy and the dash live represents the 16 [J] impact energy.

Impact Energy: 8J

Table 37 shows that the velocity of the four specimens is identical. For A2 and A1 tests, the rate at which the impactor moves upwards is faster. In the H1 test, the impactor rises at a nearly constant pace, while in the H2 test, the impactor slows down.

Table 37 Velocity at impact of the test specimen at 8 [J] impact energy

Test Specimen	Velocity at impact [m/s]
H1	2.066
H2	2.088
A1	2.066
A2	2.069

Impact Energy: 16J

Once again, the velocity impact is consistent across all testing. Looking at the image in table 38, it is evident that the impactor rises at the same pace for each specimen.

Table 38 Velocity at impact of the test specimen at 16 [J] impact energy

Test Specimen	Velocity at impact [m/s]
H3	2,915
H4	2,915
A3	2,922
A4	2,922

5.3.3. Post-test

In this part, there are two issues connected with the post-test analysis: impactor-related dent depth and the recovery of the test specimen during the next four weeks. It was first conducted half an hour after the test, then twenty-four hours after and then once a week for the four weeks stated.

The depth was first measured right after the test. Picture 67 displays the depth for every test specimen, in both levels. It is curious to see the hexagonal core has a lower depth for the 8 [J] impact level, whereas in the 16 [J] impact level, the opposite happens. This suggests that auxetic core offer more resistance to indentation failure in higher levels of energy, in comparison to the hexagonal cored. More different levels of energy should be test out to support this conclusion.

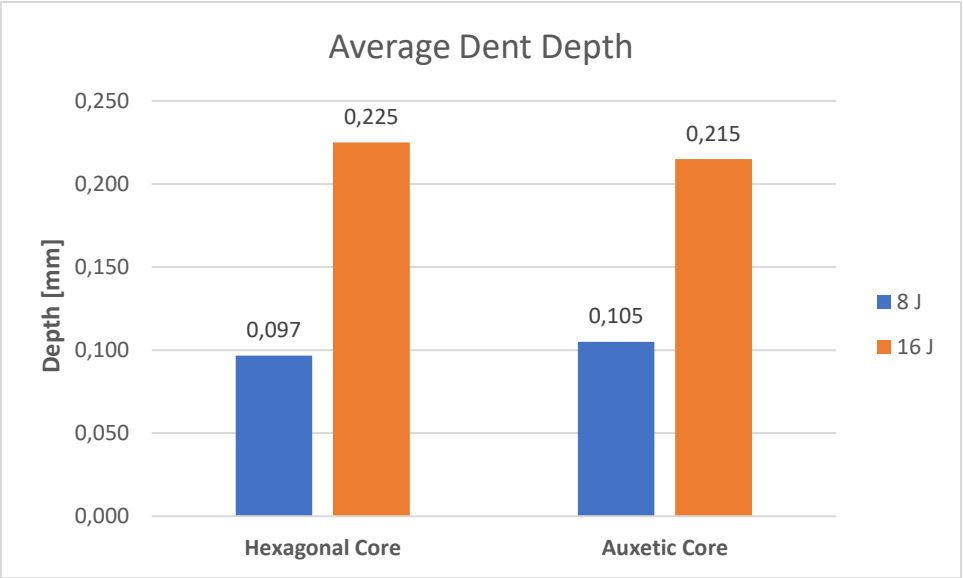

Figure 67 Average Dent Depth for the hexagonal and Auxetic core at 8 [J] and 16 [J] impact energy

Picture 63 shows the development from the impact occurrence of the residual indentation. The residual indentation lessens as the time progresses for all specimens.

For both cores, the evolution is very similar in the lower level of impact energy. The differences are more pronounced in the first few weeks; however, the difference is essentially nothing between week three and week four.

The hexagonal core decreased considerably in the first week for 16 [J] impact energy and then stabilised. The auxetic core reveals a fast recovery, which lasts until the first and during the second week.

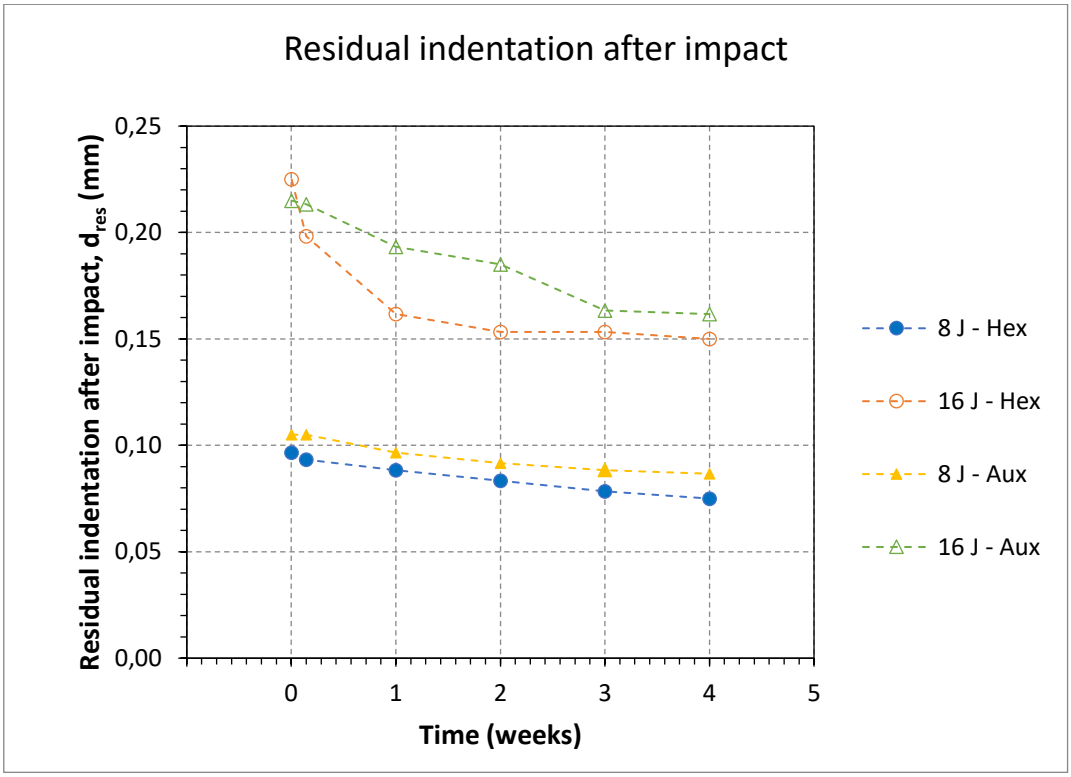

Figure 68 Residual indentation after impact for the hexagonal and Auxetic core at 8 [J] and 16 [J] impact energy

5.3.4. Numerical Results

The experimental results will be compared to the numerical data in this section. First, the two cores, independently, and then the two impact energy levels. The graphs of force, energy and velocity versus time, as well as certain key parameters mentioned in the last section will be displayed.

Hexagonal Core

The following image displays the force vs time with the two hexagonal core test specimens and the curve from the FEM analysis. In table 39, the values concerning the maximum force for the experimental and numerical data are seen. In each analysis, the impact energy for 8 [J] comes first, followed by the impact energy for 16 [J].

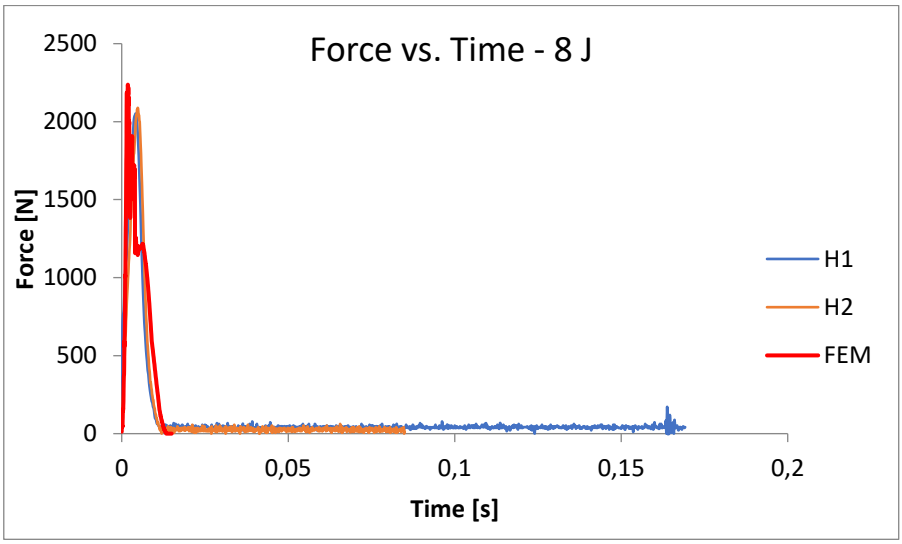

Figure 69 Force vs Time - hexagonal Core - numerical and experimental test - 8 [J]

Table 39 Maximum force for the hexagonal core at 8 [J] impact energy - experimental and numerical

Data	Maximum Force [N]
Experimental (average)	2070.3
Numerical	2237.3

Although the curve differs slightly from the experimental data because it contains numerous "peaks," the numerical data's maximum force results are just 8 [%] higher. In both analyses, the contact time is likewise close.

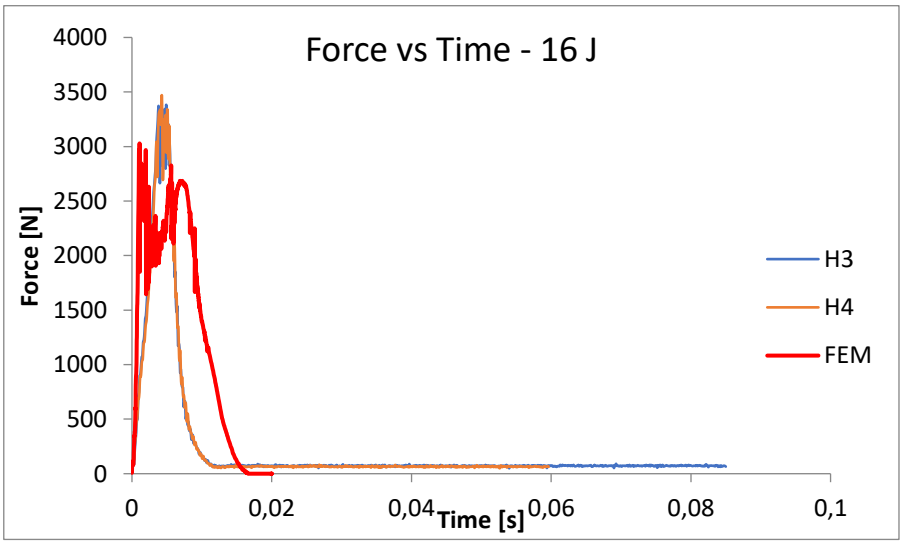

Figure 70 Force vs Time - hexagonal Core - numerical and experimental test - 16 [J]

Table 40 Maximum force for the hexagonal core at 16 [J] impact energy - experimental and numerical

Data	Maximum Force [N]
Experimental (average)	3427.02
Numerical	3028.50

The curves are slightly different with larger impact energy, and the maximum force in the numerical analysis is smaller in this instance, around 12 [%]. For the FEM analysis, the contact time is longer.

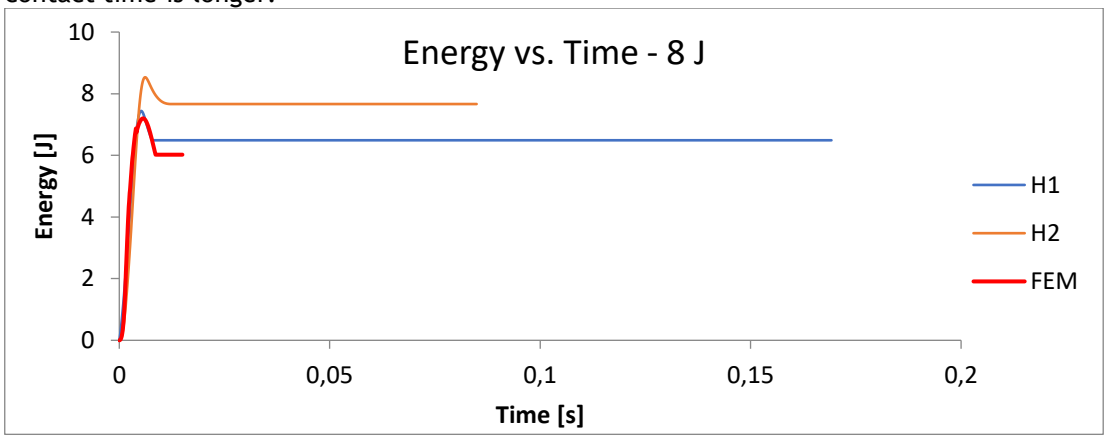

Figure 71 Force vs Time - hexagonal Core - numerical and experimental test - 8 [J]

Table 41 Impacted, Absorbed Energy and ratio Absorbed Energy and Impact Energy of hexagonal core - numerical and experimental 8 [J]

Data	Impacted Energy [J]	Absorbed Energy [J]	Absorbed Energy/Impacted Energy [%]
Experimental (average)	7.94	7.05	89
Numerical	7.20	6.02	84

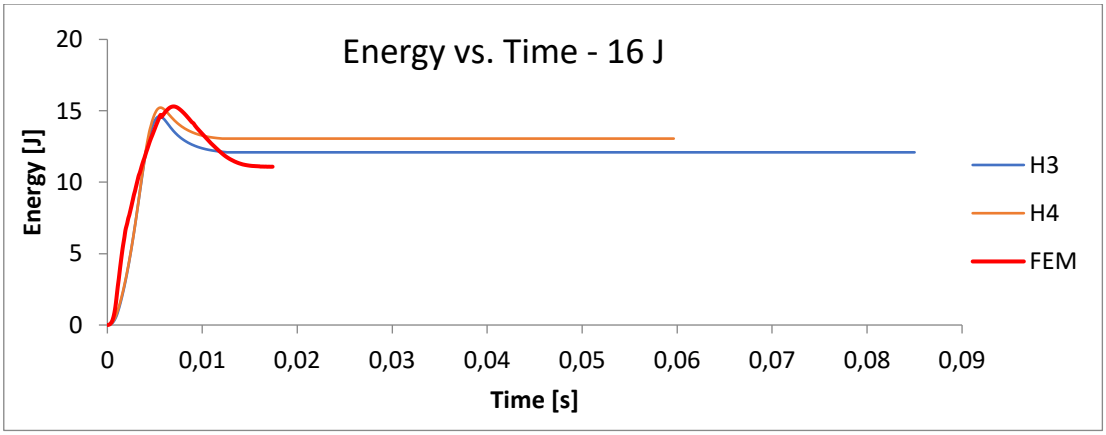

Figure 72 Energy vs Time - hexagonal Core - numerical and experimental test - 16 [J]

The energy vs. time graph demonstrates that the test specimen H2 and the FEM data for the impacted energy are very similar. The numerical data for absorbed energy shows lower values. The absorbed and impacted energy ratios are nearly identical.

Table 42 Impacted, Absorbed Energy and ratio Absorbed Energy and Impact Energy of hexagonal core - numerical and experimental 16 [J]

Data	Impacted Energy [J]	Absorbed Energy [J]	Absorbed Energy/Impacted Energy [%]
Experimental (average)	14.92	12.57	85
Numerical	15.31	11.08	72

The impacted energy is similar in both studies, albeit the test specimens absorbed more energy in the experimental data, roughly 12 [%] more than the numerical data.

On the ascendent path, the numerical statistics reflect less absorbed energy, which is responsible for a higher velocity in the impactor, in both experiments: 8 [J] and 16 [J]. The following pictures illustrate this.

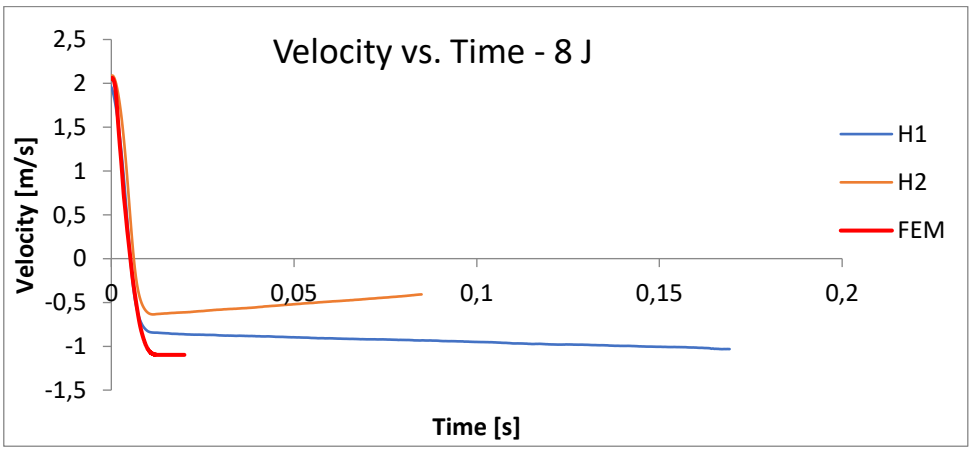

Figure 73 Velocity vs Time - hexagonal Core - numerical and experimental test - 8 [J]

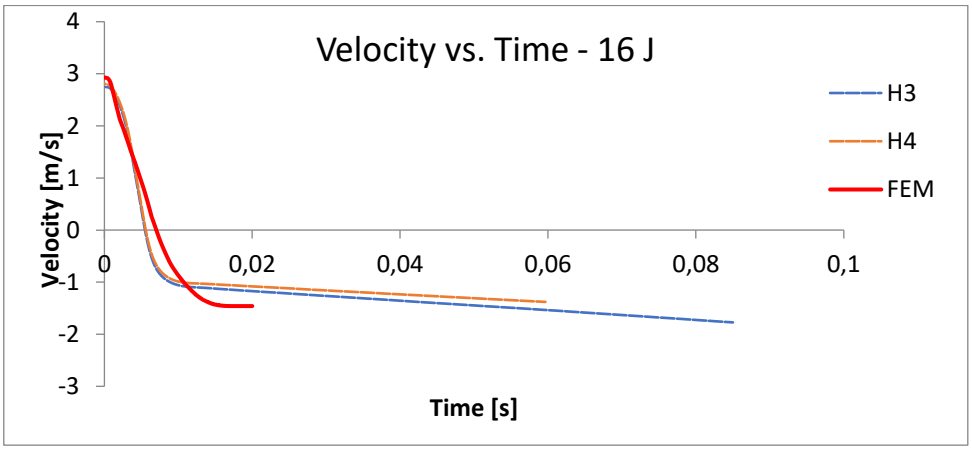

Figure 74 Velocity vs Time - hexagonal Core - numerical and experimental test - 16 [J]

Auxetic Core

The auxetic core's experimental and numerical data will be compared using the same model as in the previous section.

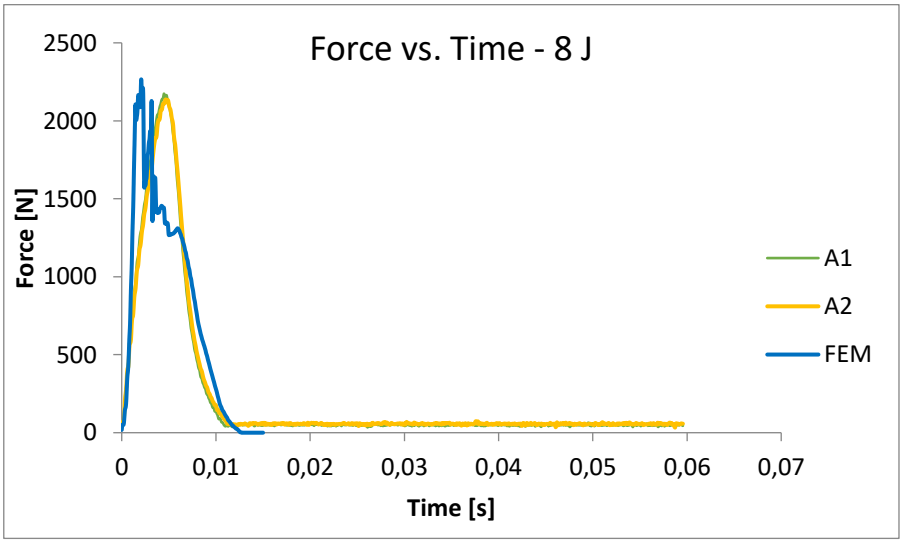

Figure 75 Force vs Time - auxetic Core - numerical and experimental test - 8 [J]

Table 43 Maximum force for the auxetic core at 8 [J] impact energy - experimental and numerical

Data	Maximum Force [N]
Experimental (average)	2155.25
Numerical	2265.84

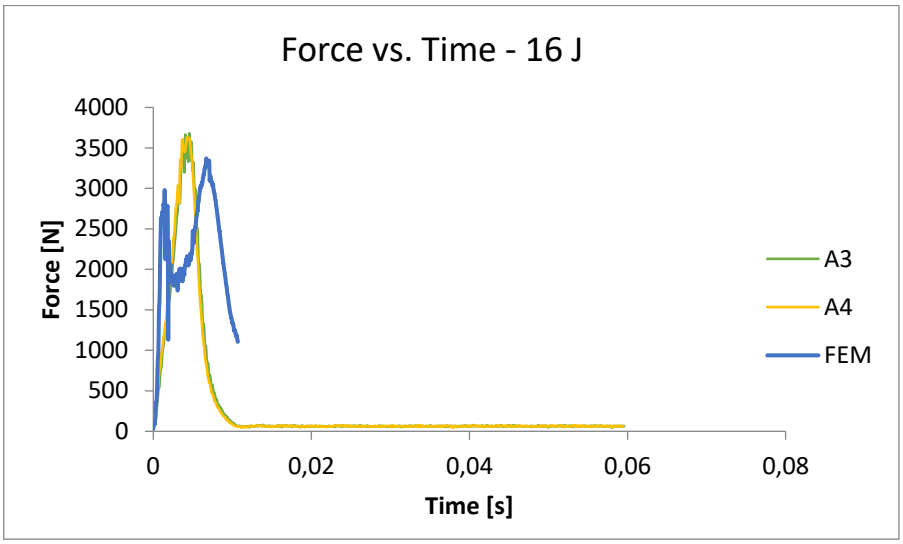

Figure 76 Force vs Time - auxetic Core - numerical and experimental test - 16 [J]

Table 44 Maximum force for the auxetic core at 16 [J] impact energy - experimental and numerical

Data	Maximum Force [N]
Experimental (average)	3653.5
Numerical	3369.97

Although the curves are similar, there are "many peaks" in the numerical data in this core. The maximum force in the FEM study is slightly higher, although only by 5 [%].

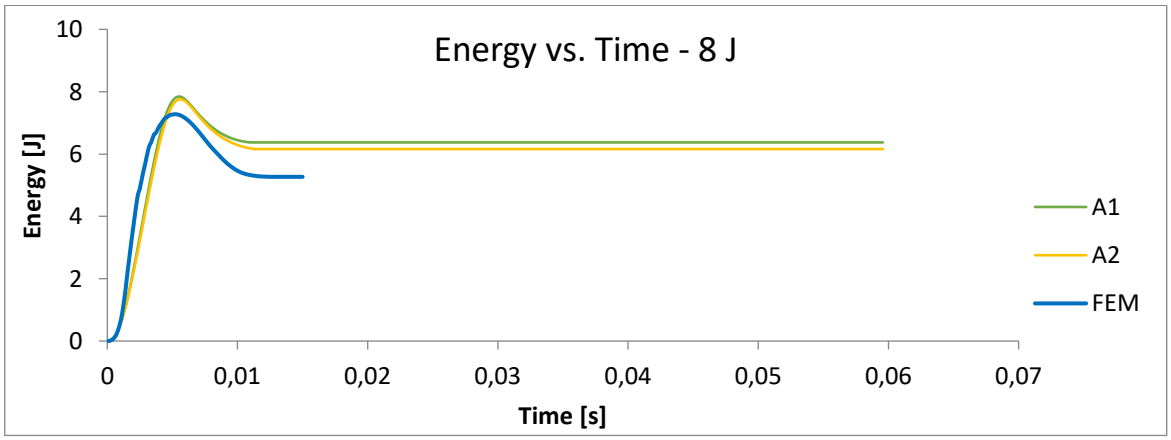

Figure 77 Energy vs Time - auxetic Core - numerical and experimental test - 8 [J]

The curves, as well as the difference in maximum forces, are more distinct in this situation. The experimental data shows an increase of 8 [%] in force.

Table 45 Impacted, Absorbed Energy and ratio Absorbed Energy and Impact Energy of hexagonal core - numerical and experimental 8 [J]

Data	Impacted Energy [J]	Absorbed Energy [J]	Absorbed Energy/Impacted Energy [%]
Experimental (average)	7.80	6.27	80
Numerical	7.28	5.27	72

For the experimental results, the absorbed energy is 16 [%] higher. The impacted energy and the ratio are both similar.

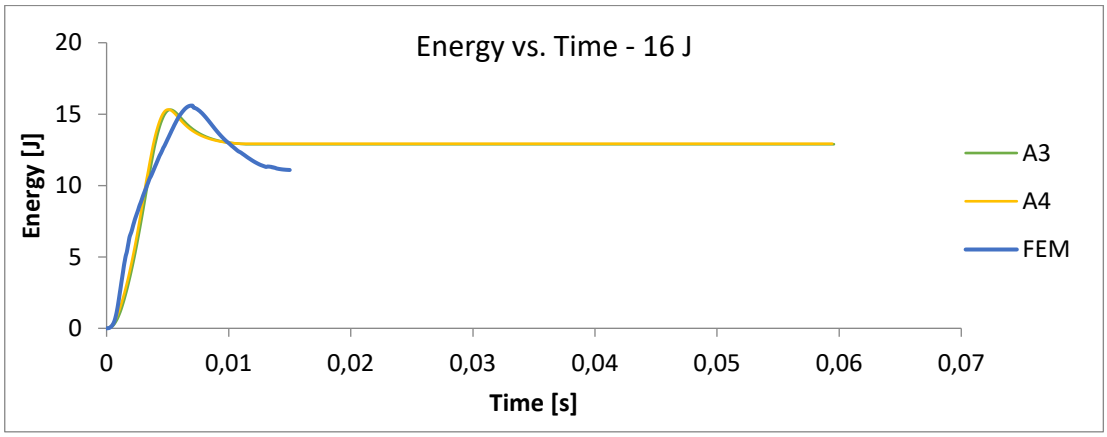

Figure 78 Energy vs Time - auxetic Core - numerical and experimental test -16 [J]

Table 46 Impacted, Absorbed Energy and ratio Absorbed Energy and Impact Energy of hexagonal core - numerical and experimental 8 [J]

Data	Impacted Energy [J]	Absorbed Energy [J]	Absorbed Energy/Impacted Energy [%]
Experimental (average)	15.31	12.91	84
Numerical	15.59	11.08	71

In terms of energy, the results of numerical and experimental data are more similar than in the previous graph. In the simulation, the impacted energy is higher, but the test specimen absorbs less energy, just like the hexagonal core.

As a result, it is plausible to assume that the end velocity in the FEM analysis is higher: the test specimen absorbs less energy, leaving the impactor with a higher kinetic energy. The graphs below show the velocity versus time throughout the encounter at the 8 and 16 [J].

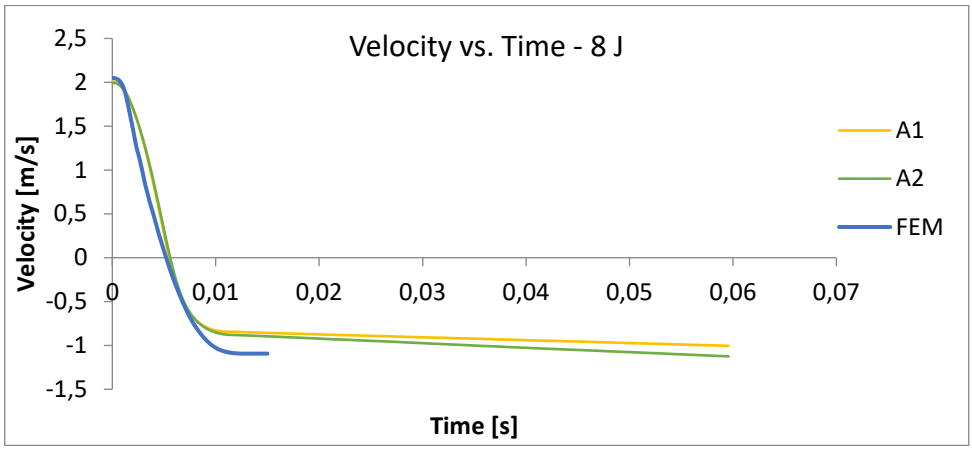

Figure 79 Velocity vs Time - auxetic Core - numerical and experimental test – 8 [J]

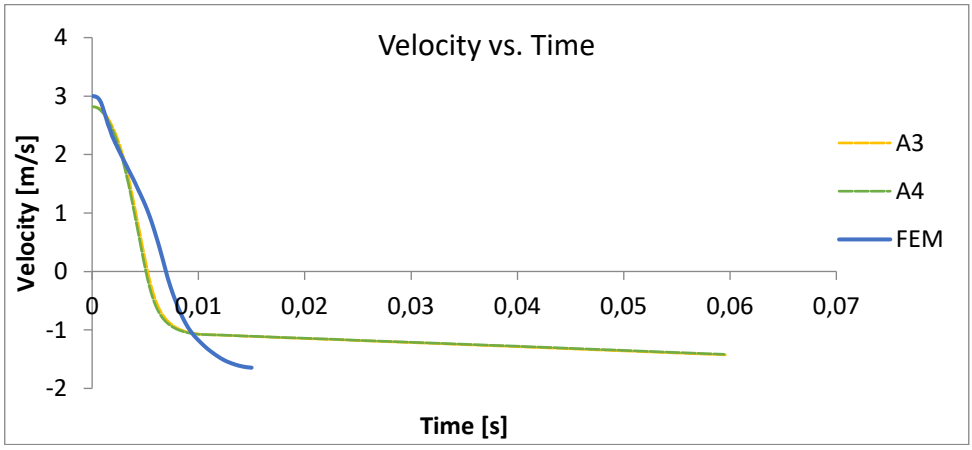

Figure 80 Velocity vs Time - auxetic Core - numerical and experimental test – 16 [J]

All the numerical data agrees well with the experimental results. There isn't a discrepancy between the data in the tables that is greater than 16 [%]. In most circumstances, the percentages range from 3 to 10 [%].

A comparison of the FEM data for the hexagonal and auxetic core will now be shown.

Hexagonal Core versus Auxetic Core

The next graphics compare the hexagonal and auxetic core in terms of force, energy, and velocity versus the time.

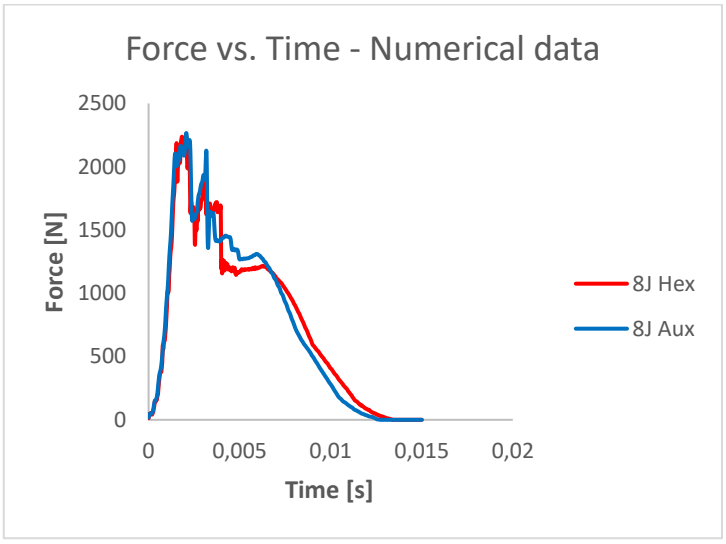

Figure 81 Force vs Time - auxetic and hexagonal Cores - numerical data - 8 [J]

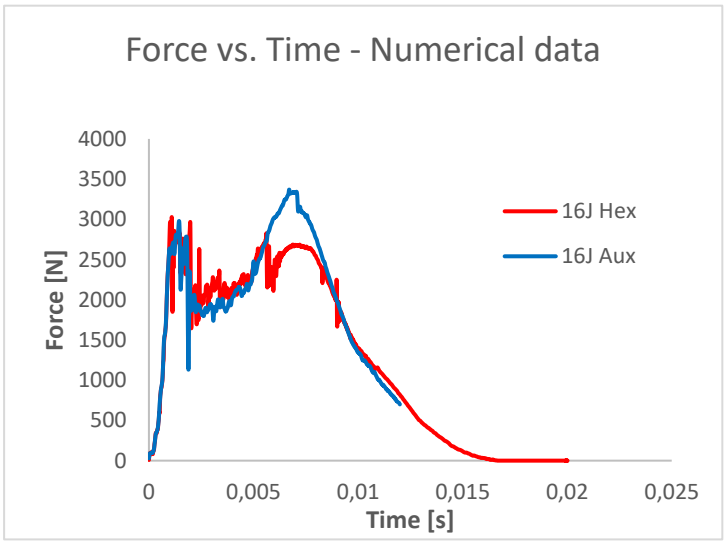

Figure 82 Force vs Time - auxetic and hexagonal Cores - numerical data - 16 [J]

There is not much of a difference in force for 8 [J] impact energy. Although the auxetic has a larger maximum force, the hexagonal core exhibits somewhat higher values at first in the higher impact energy, i.e., at 16 [J].

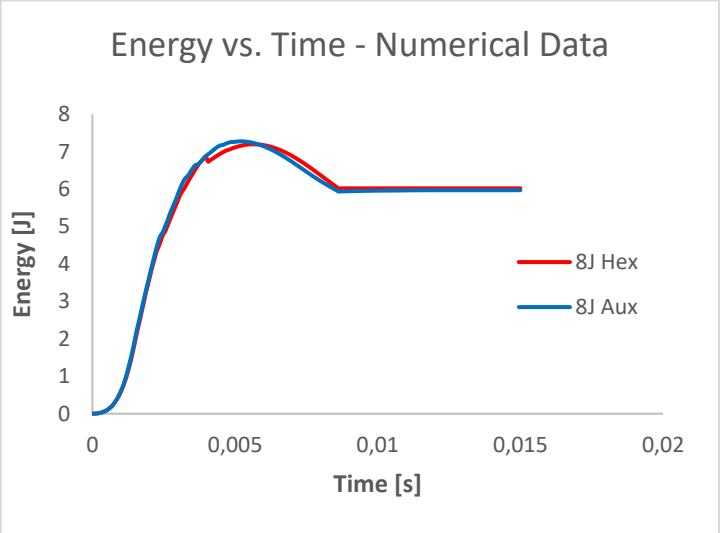

Figure 83 Energy vs Time - auxetic and hexagonal Cores - numerical data - 8 [J]

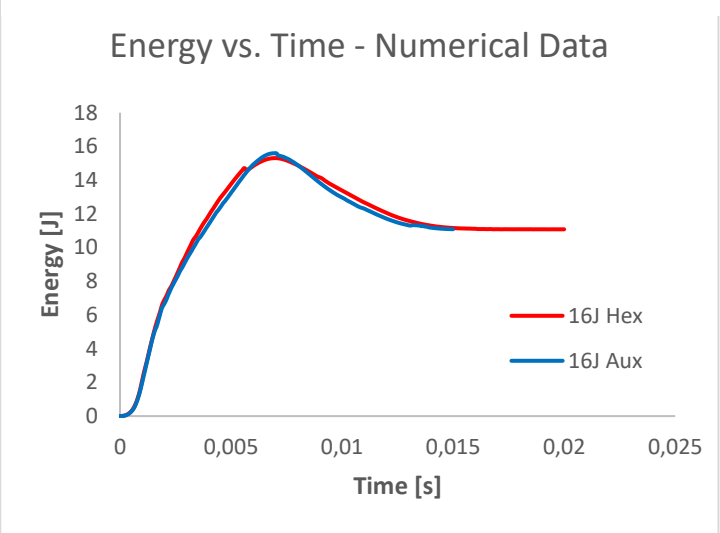

Figure 84 Energy vs Time - auxetic and hexagonal Cores - numerical data - 16 [J]

For both impact energies, the images are very similar. The impacted energy was similar between test specimens in the experimental data, while the absorbed energy was more varied.

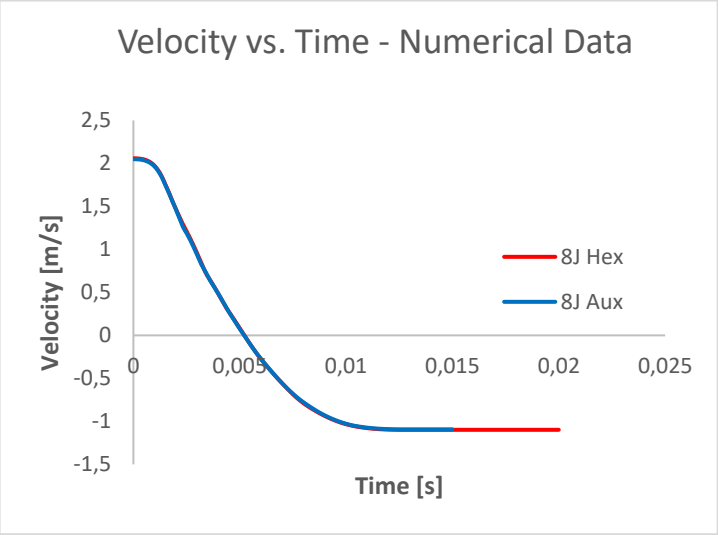

Figure 85 Velocity vs Time - auxetic and hexagonal Cores - numerical data - 8 [J]

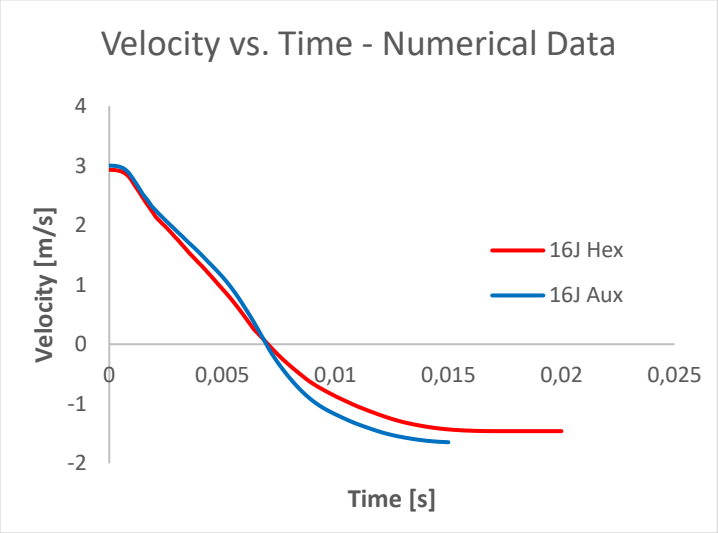

Figure 86 Velocity vs Time - auxetic and hexagonal Cores - numerical data - 16 [J]

The pictures almost overlap at lower energies; however, the hexagonal core gives the impactor a lower end velocity at the 16 [J] impact energy.

5.4. Summary of the Properties

Finally, the summary of the mechanical specific properties obtained from tests are displayed in tables 47, 48 and 49. These three tables were elaborated to facilitate the comparison between hexagonal and auxetic cores and between the cork cores and other typical cores.

Table 47 summarizes three parameters of the three-point bending test from hexagonal and auxetic core.

Table 47 Mechanical properties from the Three Point Bending Test

Three Point Bending Test						
Core	**Flexural Rigidity [N.mm^2]**	**Specific Flexural Rigidity [N·m^5/kg]**	**Transverse Shear Rigidity [N]**	**Specific Transverse Shear Rigidity [N·m^3/kg]**	**Shear Modulus [MPa]**	**Specific Shear Modulus [N·m/kg]**
Hexagonal Core	2.12 x 10^8	1.38	1460.1	9.5	1.66	10849.7
Auxetic Core	2.11 x 10^8	1.32	2635.8	10.2	1.82	11375.0

Table 48 summarizes three parameters of the compression test from hexagonal and auxetic core. The properties are divided into two parts in order to facilitate the reading and include all information.

Table 48 Mechanical Properties from Compression Test

Compression Test				
Core	**Compression Modulus [MPa]**	**Specific Compression Modulus [N·m/kg]**	**Compression Strength [MPa]**	**Specific Compression Strength [N·m/kg]**
Hexagonal Core	2.33	15235.3	0.054	352.9
Auxetic Core	2.83	17700.0	0.067	418.75

Core	Compressive Stress at 2 % [MPa]	Specific Compressive Stress at 2 % [N·m/kg]	Compressive Stress at 10 % [MPa]	Specific Compressive Stress at 10 % [N·m/kg]
Hexagonal Core	0.061	398.7	0.136	888.89
Auxetic Core	0.093	581.3	0.174	1078.5

Finally, table 49 includes the peak force and the ratio absorbed energy to impacted energy recorded in the low velocity impact test.

Table 49 Mechanical Properties from Low Velocity Impact Test

Low Velocity Impact Test		
Core	**Peak Force [N]**	**Absorbed Energy/ Impacted Energy [%]**
Hexagonal Core, 8 [J]	2070.3	89
Auxetic Core, 8 [J]	2155.3	80
Hexagonal Core, 16 [J]	3427.0	85
Auxetic Core, 16 [J]	3656.5	84

Chapter 6: Conclusions and Future Work

6.1. Conclusions

The major goal of this project was to demonstrate the properties of cork as a sustainable and renewable core material. In addition, a comparison was made between an auxetic core and a hexagonal core. To confirm the experimental results, a numerical analysis was carried out.

The core and the skins are the two parts of the sandwich structures. The tensile and compressive stresses are supported by the skins, while shear stress is handled by the core.

Honeycomb cores are designed to lower the weight of a sandwich without affecting the final structure's qualities. As a result, two types of honeycombs were tested: hexagonal honeycomb cores, which are the most prevalent, and auxetic holes, which are re-entrant form types. Due of the different Poisson ratios, and to investigate how the geometry of the cell would affect the honeycomb properties, the auxetic material was chosen.

In terms of the conclusions drawn from the different types of cores, the auxetic core appeared to outperform the hexagonal core marginally, especially in compressive and flexural circumstances. The auxetic core's compression and shear modulus were slightly higher than the hexagonal core's. This could be because the applied forces are perpendicular to the sandwich, and the honeycomb core's holes create walls with different angles for the hexagonal and auxetic cores. Furthermore, due to the design of the cell, the auxetic core should have a different Poisson ratio, which could affect the final qualities.

When it comes to impact energy absorption, the results for both cores are similar in impact tests. This makes sense because the hexagonal and auxetic holes in the core have the same area, hence the amount of cork used to absorb the energy is roughly the same.

The mechanical tests performed in the two cores appear to be in good agreement with the numerical models.

In comparison with the common core materials, honeycomb core corks have the lowest specific properties of all of the materials. As a result, cork cores should be used in applications with lower compressive and shear strengths, as well as thermal, acoustic, and vibrational insulation. It would be a "greener" option for these kinds of functions.

6.2. Future Work

Future research should concentrate on determining an optimal cell form, as this has an impact on honeycomb properties. The optimal outcome should be determined by analysing triangular, square, and other shapes.

In addition, it would be interesting to observe how a “obliquely” honeycomb, i.e., a honeycomb with obliquely holes instead of vertical holes, would perform under compression, flexural, and impact stresses. The goal would be to imitate oblique loading without really delivering the load in an oblique manner.

Aside from the honeycomb cork mechanical studies, additional sectors such as thermal insulation, acoustic performance and vibration insulation should be investigated further.

Finally, it is crucial to note that cork is a sustainable material, despite the fact that the skins utilised in this project, namely carbon fibre prepregs, are not. Other skins made from renewable resources, such as basalt fibres, might be used with cork to form a complete renewable material sandwich structure.

Chapter 7: References

Abdullah, M. K. F. S. A. M. F., Azman, A. H., Hui, D., & Singh, S. S. K. (2021). Review of current trends for metal-based sandwich panel: Failure mechanisms and their contribution factors. *Engineering Failure Analysis, 123*. doi:https://doi.org/10.1016/j.engfailanal.2021.105302

Alphonse, M., & Chandra, V. K. B. R. V. G. K. R. S. U. K. B. V. S. L. V. R. (2021). Mechanical behavior of sandwich structures with varying core material – A review. *Materials Today: Proceedings*. doi:https://doi.org/10.1016/j.matpr.2020.11.722

Andami, H., & Toopchi-Nezhad, H. (2020). Performance assessment of rigid polyurethane foam core sandwich panels under blast loading. *International Journal of Protective Structures, 11*(1), 109-130. doi:https://doi.org/10.1177/2041419619858091

Arbintarso, E. S., Datama, H. F., Aviyanto, R. N. W., Prasetya, B., Purwokusumo, U. S. A. B., Aditiawan, B., . . . Adi, R. B. S. (2019). The Bending Stress on GFRP Honeycomb Sandwich Panel Structure fora Chassis Lightweight Vehicle. *IOP Conference Series: Materials Science and Engineering, 506*. doi:10.1088/1757-899X/506/1/012050

Aster. (2021). What is Polypropylene spunbond Nonwoven? Retrieved from http://www.astersrl.eu/en/cms_pg.php?pgid=35&name=What-is-the-polypropylene-spunbond-nonwoven 02/08/2021

Avillez, A. d. C. F., Rodrigues, V., A, F. G. d. S., Santos, F., Rebelo, F., Jorge, M. N., & Aires, N. (2020). *The Cork Sector: from the Forest to th Consumer Final Report: Extended Summary*. Retrieved from www.apcor.pt:

B. Castanie, C. Bouvet, Y. Aminanda, J.-J. Barrau, & Thevenet, P. (2006). *Modelling of low-energy/low-velocity impact on Nomex honeycomb sandwich structures with metallic skins*. Paper presented at the ASME 8th Biennial Conference on Engineering Systems Design and Analysis, Torino, Italy. https://www.researchgate.net/publication/222561915_Modelling_of_low_energylow_velocity_impact_on_Nomex_honeycomb_sandwich_structures_with_metallic_skins

B. Soares, L. Reis, & Sousa, L. (2011). Cork composites and their role in sustainable development. *Procedia Engineering, 10*, 3214-3219. doi:https://doi.org/10.1016/j.proeng.2011.04.531

Belleville, N. J. K. B., & Ozarska, B. K. G. B. (2016). Mechanical properties of Papua New Guinea balsa wood. *Eur. J. Wood Prod*(74), 83-89. doi:10.1007/s00107-015-0983-0

Benzaama, A., Mokhtari, M. M., Benzaama, H., Gouasmi, S., & Tamine, T. (2018). Using XFEM technique to predict the damage of unidirectional CFRP composite notched under tensile load. *Advances in Aircraft and Spacecraft Science, 5*(1), 129-139. doi:https://doi.org/10.12989/aas.2018.5.1.129

Bharath, H. S., Bonthu, D., Gururaja, S., Prabhakar, P., & Doddamani, M. (2021). Flexural response of 3D printed sandwich composite. *Composite Structures, 263*. doi:https://doi.org/10.1016/j.compstruct.2021.113732

Bird, B., Stewart, W. E., & Lightfoot, E. N. (2002). *Transport Phenomena* (Second Edition ed.): University of Wisconsin-Madison. ISBN 0-471-41077-2

Biron, M. (2013). Thermoplastics and Thermoplastic Composites. In M. Biron (Ed.), *Plastics Design Library* (Second ed., pp. 769-829). In Plastics Design Library: William Andrew Publishing. ISBN 9781455778980

Cabrera, N. O., Alcock, B., & Peijs, T. (2008). Design and manufacture of all-PP sandwich panels based on co-extruded polypropylene tapes. *Composites Part B: Engineering, 39*(7-8), 1183-1195. doi:https://doi.org/10.1016/j.compositesb.2008.03.010

Caliskan, U., & Apalak, M. K. (2017). Low velocity bending impact behavior of foam core sandwich beams: Experimental. *Composites Part B: Engineering, 112*, 158-175. doi:https://doi.org/10.1016/j.compositesb.2016.12.038

Campbell, F. C. (2010). *Structural Composite Materials*: ASM International. ISBN-13: 978-1-61503-037-8

Carlsson, L. A., & Kardomateas, G. A. (2011). *Structural and Failure Mechanics of Sandwich Composites* (Vol. 121): Springer. 978-1-4020-3225-7

Chai, G. B., & Zhu, S. (2011). A Review of Low-velocity Impact on Sandwich Structures. *The Journal of Materials: Design and Applications, 255*(4), 207-230. doi:https://doi.org/10.1177/1464420711409985

Chu, S., Gao, L., Xiao, M., & Li, H. (2019). Design of sandwich panels with truss cores using explicit topology optimization. *Composite Structures, 210*, 892-905. doi:https://doi.org/10.1016/j.compstruct.2018.12.010

Cripps, D. (2019). Wood Cores. *NetComposites*. Retrieved from https://netcomposites.com/guide/core-materials/wood-cores/ 14/08/2021

Daniel, I. M. (2009). Dynamic Failure of Materials and Structures. In A. Shukla, G. Ravichandran, & Y. D. S. Rajapakse (Eds.), *Impact Response and Damage Tolerance of Composite Sandwich Structures* (pp. 191-233): Springer, Boston, MA. 978-1-4419-0445-4

Daniel, I. M., Gdoutos, E. E., Abot, J. L., & Wang, K.-a. (2003). Deformation and Failure of Composite Sandwich Structures. *Journal of THERMOPLASTIC COMPOSITE MATERIALS, 16*(4), 345-364. doi:10.1177/089270503030670

Datasheet - AluNID. Retrieved from https://www.alucoat-conversion.com/aluminium-honeycomb-core/ 14/08/2021

Davies, J. M. (2001). *Lightweight Sandwich Construction*: Blackwell Science Ltd. ISBN: 9780470690253

Deb, A., & Shivakumar, N. D. (2009). An Experimental Study on Energy Absorption Behavior of Polyurethane Foams. *Journal of REINFORCED PLASTICS AND COMPOSITES, 28*. doi:https://doi.org/10.1177/0731684408094220

Devezas, O. C. J. M. S. T., Silva, A., & Gil, L. (2009). Cork agglomerates as an ideal core material in lightweight structures. *Materials and Design, 31*, 425-432. doi:10.1016/j.matdes.2009.05.039

DragonPlate. (2019). Carbon Fiber 101: What do Isotropic, Quasi-Isotropic, and Anisotropic Mean? *DragonPlate*. Retrieved from https://dragonplate.com/carbon-fiber-101-what-do-isotropic-quasi-isotropic-and-anisotropic-mean 29/4/2021

Edupack (2020). from Granta Edupack

Engelsmann, S., Spalding, V., & Peters, S. (2010). *Plastics : In architecture and construction*: Birkhäuser. ISBN: 9783034611855

Evans, H. N. G. W. N. A. F. A. G. (2003). Fabrication and structural performance of periodic cellular metal sandwich structures. *Composites Science and Technology, 63*(16), 2331-2343. doi:https://doi.org/10.1016/S0266-3538(03)00266-5

Eyma, J. S. F., Luycker, E. D., Cantarel, A., Bouvet, C., & Castanie, B. (2019). Experimental investigation of compression and compression after impact of wood-based sandwich structures. *Composite Structures, 220*, 236-249. doi:https://doi.org/10.1016/j.compstruct.2019.03.095

F.A.O. Fernandes, R.T. Jardin, A.B. Pereira, & Sousa, R. J. A. d. (2015). Comparing the mechanical performance of synthetic and natural cellular materials. *Materials & Design, 82*, 335-341. doi:https://doi.org/10.1016/j.matdes.2015.06.004

Gil, L. (2007). *A cortiça como material de construção*. www.realcork.org: APCOR – Associação Portuguesa de Cortiça.

Gil, L. (2009). Cork Composites: A Review. *Materials, 2*. doi:10.3390/ma2030776

Hamzah, A. F., Al-kawaz, A. E., & Hamzah, A. S. (2020). Effect of Cell Shape on Flexural Strength of Honey Comb Structure. *TEST Engineering & Management*, 14982 – 14991.

He, Y. R. J. L. W. L. W. (2018). Effects of geometric configurations of corrugated cores on the local impact and planar compression of sandwich panels. *Composites Part B: Engineering, 152*, 324-335. doi:https://doi.org/10.1016/j.compositesb.2018.08.130

Heimbs, S. (2012). Foldcore Sandwich Structures and Their Impact Behaviour: An Overview. In *Dynamic Failure of Composite and Sandwich Structures* (Vol. 192, pp. 491-544): Springer, Dordrecht. ISBN: 978-94-007-5329-7

Hu, J. S., & Wang, B. L. (2021). Crack growth behavior and thermal shock resistance of ceramic sandwich structures with an auxetic honeycomb core. *Composite Structures, 260*(12). doi:10.1016/j.compstruct.2020.113256

Jędral, A. (2019). Review of Testing Methods dedicated for Sandwich structures with Honeycomb Core. *TRANSACTIONS ON AEROSPACE RESEARCH, 2*(255), 1-14. doi:10.2478/tar-2019-0006

Junior, S. A. R., Ferracane, J. L., & Bona, Á. D. (2008). Flexural strength and Weibull analysis of a microhybrid and a nanofill composite evaluated by 3- and 4-point bending tests. *Dental Materials, 24*(3), 426-431. doi:10.1016/j.dental.2007.05.013

Ke, S. A. J. Z. P. F. D. Y. Z. W. M. (2020). Processing technologies for Nomex honeycomb composites (NHCs): A critical review. *Composite Structures, 250*. doi:https://www.sciencedirect.com/science/article/pii/S0263822319345246#:~:text=https%3A//doi.org/10.1016/j.compstruct.2020.112545

Keller, C. W. N. V. A. P. V. T. (2020). Mechanical properties of a balsa wood veneer structural sandwich core material. *Construction and Building Materials, 265*. doi:https://doi.org/10.1016/j.conbuildmat.2020.120193

Krause, R. S. D. (2014). *Numerical Modelling of Nomex Honeycomb Core for Detailed Analyses of Sandwich Panel Joints* Paper presented at the 11th. World Congress on Computational Mechanics (WCCM XI), Barcelona, Spain. Retrived from https://www.researchgate.net/publication/264236898_Numerical_modelling_of_Nomex_honeycomb_cores_for_local_analyses_of_sandwich_panel_joints

Kroplin, L. A. A. F. J. B.-H. (2008). Numerical modelling of honeycomb core crush behaviour. *Engineering Fracture Mechanics, 75*, 2616-2630. doi:https://doi.org/10.1016/j.engfracmech.2007.03.008

Lascano, D., Guillen-Pineda, R., Quiles-Carrillo, L., Ivorra-Martínez, J., Balart, R., Montanes, N., & Boronat, T. (2021). Manufacturing and Characterization of Highly Environmentally Friendly Sandwich Composites from Polylactide Cores and Flax Polylactide Faces. *Polymers, 13*(3). doi: https://doi.org/10.3390/polym13030342

Li, B. L. Z., Zhou, J., Ye, L., & Li, E. (2015). Damage localization in composite lattice truss core sandwich structures based on vibration characteristics. *Composite Structures, 126*, 34-51. doi:https://doi.org/10.1016/j.compstruct.2015.02.046

Liang, A. I. A. H. R. (2017). Design and modeling of auxetic and hybrid honeycomb structures for in-plane property enhancement. *Materials & Design, 117*, 72-83. doi:https://doi.org/10.1016/j.matdes.2016.12.067

Linul, C. V. C. S. L. M. E. (2020). Mechanical characterization of lightweight foam-based sandwich panels. *Materials Today: Proceedings, 45*(5), 4166-4170. doi:https://doi.org/10.1016/j.matpr.2020.12.035.

Liu, J., Tao, J., Li, F., & Zhao, Z. (2021). Flexural properties of a novel foam core sandwich structure reinforced by stiffeners. *Construction and Building Materials, 235*. doi:https://doi.org/10.1016/j.conbuildmat.2019.117475

Ma, G. Z. L., Wang, B., & Wu, L. (2012). Mechanical behaviour of CFRP sandwich structures with tetrahedral lattice truss cores. *Composites Part B: Engineering, 43*(2), 471-476. doi:https://doi.org/10.1016/j.compositesb.2011.11.017

Manrique, Y. J. A. (2016). *Supercritical fluid extraction and fractionation of bioactive natural products from cork*. (Doctor of Philosoph Thesis), Universidade do Porto, Retrieved from https://hdl.handle.net/10216/103555 https://hdl.handle.net/10216/103555

Masters, I. G., & Evans, K. E. (1996). Models for the elastic deformation of honeycombs *Composite Structures, 35*, 403-422. doi:https://doi.org/10.1016/S0263-8223(96)00054-2.

Materials & Processes: Composites part design. (2016). *Composites World*. Retrieved from https://www.compositesworld.com/articles/part-design-criteria 29/04/2021

McCormack, T. M., Ronald, E. M., Kesler, O., & Gibson, L. (2001). Failure of sandwich beams with metallic foam cores. *International Journal of Solids and Structures, 38*, 4901-4920. doi:https://doi.org/10.1016/S0020-7683(00)00327-9

McDaniels, R. (2017). The Physics of Fatigue- Part 1 – Nucleation. *Vextec.com*. Retrieved from https://vextec.com/the-physics-of-fatigue-nucleation/

McGugan, M., Larsen, G. C., Bent F. Sørensen, Borum, K. K., & Engelhardt, J. (2008). *Fundamentals for remote condition monitoring of offshore wind turbines*. Core: Danmarks Tekniske Universitet, Risø Nationallaboratoriet for Bæredygtig Energi. ISBN: 978-87-550-3662-8

Miranda, A., Leite, M., Reis, L., Copin, E., Vaz, M., & Deus, A. (2021). Evaluation of the influence of design in the mechanical properties of honeycomb cores used in composite panels. *Proceedings of the Institution of Mechanical Engineers, Part L: Journal of Materials: Design and Applications, 235*(6), 1325-1340. doi:10.1177/1464420720985191

Mirza, M. K. K. T. B. S. (2012). Experimental investigation of in-plane and out-of-plane crushing of aluminum honeycomb. *Materials Science and Engineering A, 539*, 135-142. doi:https://doi.org/10.1016/j.msea.2012.01.070

Najafi, M., & Eslami-Farsani, R. (2021). Design and characterization of a multilayered hybrid cored-sandwich panel stiffened by thin-walled lattice structure. *Thin-Walled Structures, 161*(107419). doi:https://doi.org/10.1016/j.tws.2021.107514

Njuguna, J. (2016). *Lightweight Composite Structures in Transport : Design, Manufacturing, Analysis and Performance*: Woodhead Publishing. 978-1-78242-325-6

Nomex® honeycomb - commercial. (2017, Last Update). Retrieved from https://www.schuetz-composites.net/en/sandwich-panels/standard-panels/

Palomba, G., & Epasto, V. C. G. (2019). Collapse modes of aluminium honeycomb sandwich structures under fatigue bending loading. *Thin-Walled Structures, 145*. doi:https://doi.org/10.1016/j.tws.2019.106363

Pereira, A. B., & Fernandes, F. A. O. (2019). Sandwich Panels Bond with Advanced Adhesive Films. *Journal of Composites Science, 3*(3). doi:10.3390/jcs3030079

Pereira, H. (1988). Chemical composition and variability of cork from Quercus suber L. . *Wood Science and Technology, 22*, 211-218. doi:10.1007/BF00386015

Pereira, H. (2015). The Rationale behind Cork Properties: A Review of Structure and Chemistry. *BioResources, 10*(3), 6207-6229.

Petras, A. (1999). *Design of Sandwich Structures*. (Doctor of Philosophy Thesis), Cambridge Universit, Core. https://doi.org/10.17863/CAM.13989

Polycarbonate honeycomb core. (2020, Last Update). *CEL Components S.r.l.* Retrieved from https://www.honeycombpanels.eu/en/products/honeycomb/polycarbonate-honeycomb-core

Polypropylene honeycomb core (2017, Last Update). *PP8.80/PP8-80T30/PP8-80T30F75/PP8-120T30*. Retrieved from https://www.schuetz-composites.net/en/sandwich-panels/standard-panels/

Rejab, Q. M. M. R. M., Siregar, J. P., & Guan, Z. (2021). A review of the recent trends on core structures and impact response of sandwich panels. *JOURNAL OF COMPOSITE MATERIALS, 55*(18), 1-43. doi:https://doi.org/10.1177/0021998321990734

Sadek, S. H. M. (2016). *Aluminum foam sandwich with adhesive bonding: computational modelling*. (Master Thesis), University of Porto, https://doi.org/10.1080/00218464.2016.1200975

Schiffer, S. Y. A., Cantwell, W. J., & Kim, T.-Y. (2021). Detection of core-skin disbonds in honeycomb composite sandwich structures using highly nonlinear solitary waves. *Composite Structures, 256*(113071). doi:https://doi.org/10.1016/j.compstruct.2020.113071

Schubel, P. M., Luo, J.-J., & Daniel, I. M. (2007). Impact and post impact behavior of composite sandwich panels. *Composites Part A: Applied Science and Manufacturing, 38*(3), 1051-1057. doi:https://doi.org/10.1016/j.compositesa.2006.06.022

Sergi, C., Boria, S., Sarasini, F., Russo, P., Vitiello, L., Barbero, E., . . . Tirillò, J. (2021). Experimental and finite element analysis of the impact response of agglomerated cork and its intraply hybrid flax/basalt sandwich structures. *Composite Structures, 272*. doi:https://doi.org/10.1016/j.compstruct.2021.114210

Silva, S. P., Sabino, M. A., Fernandes, E. M., Correlo, V. M., & Reis, L. F. B. R. L. (2005). Cork: properties, capabilities and applications. *International Materials Reviews, 50*(6), 345-365. doi:10.1179/174328005X41168

Sun, S. S. B. C. Z. (2018). Equivalent properties of composite sandwich panels with honeycomb–grid hybrid core. *Journal of Sandwich Structures & Materials, 22*(6), 1859-1878. doi:https://doi.org/10.1177/1099636218789615

Wadley, D. T. Q. V. S. D. H. N. G. (2007). Truss Waviness Effects in Cellular Lattice Strcutures. *Journal of Mechanics of Materials and Strucutures, 2*(9), 1657–1675. doi:10.2140/jomms.2007.2.1657

Wang, F. Z. G. L. D. R. Z. (2010). Plastic Deformation, Failure and Energy Absorption of Sandwich Structures with Metallic Cellular Cores. *International Journal of Protective Structures, 1*, 507-541. doi:https://doi.org/10.1260/2041-4196.1.4.507

William D. Callister, J., & Rethwisch, D. G. (2007). *Materials Science and Engineering* (8th edition ed.). ISBN: 978-0-470-41997-7

Xiong, J., Du, Y., Mousanezhad, D., Asl, M. E., Norato, J., & Vaziri, A. (2018). Sandwich Structures with Prismatic and Foam Cores: A Review. *Advance Engineering Materials, 21*(1). doi:10.1002/adem.201800036

Xue, J., Wang, W., Zhang, J.-Z., & Wu, S.-J. (2015). Progressive failure analysis of the fiber metal laminates based on chopped carbon fiber strands. *Journal of REINFORCED PLASTICS AND COMPOSITES, 34*(5), 364-376. doi: 10.1177/0731684415571659

Yan, J. (2013). *Vibration and Acoustic Properties of Honeycomb Sandwich Structures Subject to Variable Incident Plane Wave Angle Pressure Loads.* (Master Thesis), Graduate School of Clemson University, Retrieved from https://tigerprints.clemson.edu/all_theses/1668 https://tigerprints.clemson.edu/all_theses/1668

Yan, L., Zhu, K., Chen, N., Zheng, X., & Quaresimin, M. (2021). Energy-absorption characteristics of tube-reinforced absorbent honeycomb sandwich structure. *Composite Structures, 255*. doi:https://doi.org/10.1016/j.compstruct.2020.112946

Yu, J., Wang, E., Li, J., & Zheng, Z. (2008). Static and low-velocity impact behavior of sandwich beams with closed-cell aluminum-foam core in three-point bending. *International Journal of Impact Engineering, 35*(8), 885-894. doi:10.1016/j.ijimpeng.2008.01.006

Yuan, W., Song, H., & Huang, C. (2016). Failure maps and optimal design of metallic sandwich panels with truss cores subjected to thermal loading. *International Journal of Mechanical Sciences, 115-116*, 56-67. doi:10.1016/j.ijmecsci.2016.06.006

Zaid, N. Z. M., Rejab, M. R. M., & Mohamed, N. A. N. (2016). Sandwich Structure Based On Corrugated-Core: A Review. *MATEC Web Conf., 74*, 00029. doi:10.1051/matecconf/20167400029

Zenkert, D. (1995). An Introduction to Sandwich Structures. In (Student Edition ed.): Engineering Materials Advisory Services Ltd. . ISBN: 978-0947817770

Zenkert, S. K. D. (2009). Corrugated all-composite sandwich structures. Part 1: Modeling. *Composites Science and Technology, 69*(7-8), 913-919. doi:https://doi.org/10.1016/j.compscitech.2008.11.030

Zenkert, S. K. D. T. D. (2009). Corrugated all-composite sandwich structures. Part 2: Failure mechanisms and experimental programme. *Composites Science and Technology, 69*(7-8), 920-925. doi:10.1016/j.compscitech.2008.11.035

Zhang, Y., Yan, L., Zhang, C., & Guo, S. (2021). Low-velocity impact response of tube-reinforced honeycomb sandwich structure. *Thin-Walled Structures, 158*(107188). doi:https://doi.org/10.1016/j.tws.2020.107188

Zhao, F.-L. J. M., & Park, M. P. S.-J. (2019). Recent Trends of Foaming in Polymer Processing: A Review. *Polymers, 11*(6). doi:10.3390/polym11060953

Zhou, S. A. M. (2016). Compressive response of sandwich plates to water-based impulsive loading. *International Journal of Impact Engineering, 93*. doi:https://doi.org/10.1016/j.ijimpeng.2016.03.007

Zimmermann, N., & Wang, P. H. (2020). A review of failure modes and fracture analysis of aircraft composite materials. *Engineering Failure Analysis, 115*(104692). doi:https://doi.org/10.1016/j.engfailanal.2020.104692.

Appendixes

The abstract of an article presented in the conference MECHCOMP7 - 7th International Conference on Mechanics of Composites, Faculty of Engineering, University of Porto, Portugal, 1-3 September 2021, based on this thesis, is shown below.

Honeycomb sandwich structures made with cork

Mafalda Esteves, Francisco Rede, Paulo Nóvoa, António Torres Marques*

*marques@fe.up.pt

The increasing enviromental concern and the systematic search for new and sustainable solutions, allowed the application of cork in fields and areas where once seemed impossible for it to fit. Cork is a natural resource used by Humanity for over 5000 years and it has, currently, a well-noted importance and the most diverse applications from bottling to aeronautical industry. As Portugal is the world's leading exporter of cork, its investment brings direct economic benefits, as well as the creation of new factories, thus generating higher employment. The majority of the cork is used under the form of composites that added to other materials can become parts and pieces of great mechanical endurance and durability. Cork is also well known for its thermal, acoustic and vibration isolation properties. From the structural point of view, its integration as a core of composite sandwiches has also shown very interesting results. Mainly, due to the combination of the low density of cork, along with the properties of the face-sheets - usually composed by fibers - which confer mechanical characteristics similar to those of structures with polymeric cores. This paper aims to present the advantages that can arise from changes in the core structure of a sandwich construction with fiberglass composite face-sheets. In this study, a low-density cork board (150 kg/m^3) was used to produce both a cylinder honeycomb, a hexagonal honeycomb and na auxetic cork core. The mechanical properties of the obtained composites were compared with other well-known materials and composites.

To find the optimized structure, a few simulations were carried out using the software ABAQUS CAE. The simulations were based on four different mechanical tests, according to the standards, namely: ASTM C393/393M-11 for the bending test; ASTM C365/C365M-11a for the compression test; ASTM D7136/D7136M-0.5 for the low-

velocity impact and finally, ASTM C 273 – 00 for the shear core test. To choose the dimensions of the honeycomb cell size, the three tests simulated were a three-point bending test, a compression test, and a low velocity impact test, using cork NL10. Since the comparison is between cell sizes, the elastic properties (modulus and Poisson ratio) were taken from a database, CES Edupack. A comparison of sandwich core will be made mainly evaluating the possible advantages of an auxetic core.

TECHNICAL DATA SHEET
No. CFA-005

TORAYCA®

T700S DATA SHEET

Highest strength, standard modulus fiber available with excellent processing characteristics for filament winding and prepreg. This never twisted fiber is used in high tensile applications like pressure vessels, recreational, and industrial.

FIBER PROPERTIES

		English	Metric	Test Method
Tensile Strength		711 ksi	4,900 MPa	TY-030B-01
Tensile Modulus		33.4 Msi	230 GPa	TY-030B-01
Strain		2.1 %	2.1 %	TY-030B-01
Density		0.065 lbs/in^3	1.80 g/cm^3	TY-030B-02
Filament Diameter		2.8E-04 in.	7 µm	
Yield	6K	3,724 ft/lbs	400 g/1000m	TY-030B-03
	12K	1,862 ft/lbs	800 g/1000m	TY-030B-03
	24K	903 ft/lbs	1,650 g/1000m	TY-030B-03
Sizing Type & Amount	50C	1.0 %		TY-030B-05
	60E	0.3 %		TY-030B-05
	F0E	0.7 %		TY-030B-05
	Twist	Never twisted		

FUNCTIONAL PROPERTIES

CTE	-0.38	$\alpha \cdot 10^{-6}$/°C
Specific Heat	0.18	Cal/g·°C
Thermal Conductivity	0.0224	Cal/cm·s·°C
Electric Resistivity	1.6 x 10^{-3}	Ω·cm
Chemical Composition: Carbon	93	%
Na + K	<50	ppm

COMPOSITE PROPERTIES*

Tensile Strength	370 ksi	2,550 MPa	ASTM D-3039
Tensile Modulus	20.0 Msi	135 GPa	ASTM D-3039
Tensile Strain	1.7 %	1.7 %	ASTM D-3039
Compressive Strength	215 ksi	1,470 MPa	ASTM D-695
Flexural Strength	245 ksi	1,670 MPa	ASTM D-790
Flexural Modulus	17.5 Msi	120 GPa	ASTM D-790
ILSS	13 ksi	9 kgf/mm^2	ASTM D-2344
90° Tensile Strength	10.0 ksi	69 MPa	ASTM D-3039

* Toray 250°F Epoxy Resin. Normalized to 60% fiber volume.

T700S

COMPOSITE PROPERTIES**

Tensile Strength	355 ksi	2,450 MPa	ASTM D-3039
Tensile Modulus	18.0 Msi	125 GPa	ASTM D-3039
Tensile Strain	1.7 %	1.7 %	ASTM D-3039
Compressive Strength	230 ksi	1,570 MPa	ASTM D-695
Compressive Modulus	--- Msi	--- GPa	ASTM D-695
In-Plane Shear Strength	14 ksi	98 MPa	ASTM D-3518
ILSS	15.5 ksi	11 kgf/mm^2	ASTM D-2344
90˚ Tensile Strength	10.0 ksi	70 MPa	ASTM D-3039

** Toray Semi-Toughened 350˚F Epoxy Resin. Normalized to 60% fiber volume.

See Section 4 for Safety & Handling information. The above properties do not constitute any warranty or guarantee of values. These values are for material selection purposes only. For applications requiring guaranteed values, contact our sales and technical team to establish a material specification document.

PACKAGING

The table below summarizes the tow sizes, twists, sizing types, and packaging available for standard material. Other bobbin sizes may be available on a limited basis.

Tow Sizes	Twist[1]	Sizing	Bobbin Net Weight (kg)	Bobbin Type[2]	Bobbin Size (mm) a	b	c	d	e	Spools per Case	Case Net Weight (kg)
6K	C	50C	2.0	III	76.5	82.5	280	140	252	12	24
12K	C	50C	6.0	III	76.5	82.5	280	200	252	4	24
	C	60E	6.0	III	76.5	82.5	280	200	252	4	24
	C	F0E	6.0	III	76.5	82.5	280	200	252	4	24
24K	C	50C	6.0	III	76.5	82.5	280	200	252	4	24
	C	60E	6.0	III	76.5	82.5	280	200	252	4	24
	C	F0E	6.0	III	76.5	82.5	280	200	252	4	24

1 **Twist** A: Twisted yarn B: Untwisted yarn made from a twisted yarn through an untwisting process C: Never twisted yarn

2 **Bobbin Type** See Diagram below

TYPE I

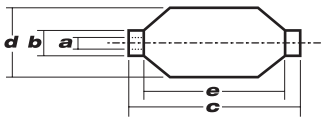

TYPE II

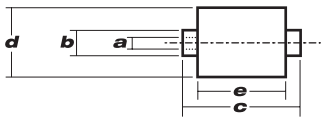

TYPE III

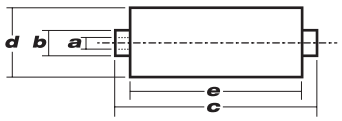

TORAY CARBON FIBERS AMERICA, INC.
6 Hutton Centre Drive, Suite #1270, Santa Ana, CA 92707 TEL: (714) 431-2320 FAX: (714) 424-0750
Sales@Toraycfa.com Technical@Toraycfa.com www.torayusa.com

Composite Materials (Italy) s.r.l. – Socio Unico
Via Quasimodo, 33 – 20025 Legnano (MI) ITALY
Phone: +39 0331.467.555
Fax: +39 0331.467.777
E-mail: info@composite-materials.it
www.composite-materials.it

CIT HS160 T700 REM UD tape 36%

MECHANICAL PROPERTIES OF PREPREG LAMINATES

Test carried out on a UD *REM TAPE – T700 Carbon Prepreg*
(Standard cure cycle: 1 hours @ 125°C).

Cured Material Property	Unit	Actual Values
Tensile Modulus 0°	GPa	123.0
Tensile Strength 0°	MPa	2294
Tensile Strain	%	1.72
Compression Modulus 0°	GPa	109.8
Compression Strength 0°	MPa	1152
Flexural Modulus 0°	GPa	134.0
Flexural Strength 0°	MPa	1850
Inter-laminar Shear Strength	MPa	81.5
Cured Ply Thickness	mm	0.164

Laminates Cure condition: 2 hours @ 135°C

This information is properties of Composite Materials (Italy) s.r.l and correspond to the present knowledge and are without any legal binding. The values of the cured properties may change due to processing conditions. Modifications due to technical progress or commercial policy change are possible.

REM
EPOXY MATRIX

GENERAL FEATURES

REM a general use epoxy matrix, suitable to impregnate carbon, glass fabric and unidirectional. It can be processed both by hot press and autoclave cure.

MAIN CHARACTERISTICS

- Maximum Tg of 125°C (257°F).
- Suitable to impregnate a very wide range of support (UD, fabrics and multi-axial - carbon, glass, aramid and hybrids).
- Versatile in different manufacturing process and wide range of temperatures.

QUICK REFERENCE TIPS

It is suggested to vent the vacuum in autoclave process according to the curing cycle shown in the following pages in order to get the highest mechanical behaviour and to avoid both irregularities and pin holes on the surface.

The REM series is available in the following variants:

- **REMT**: higher viscosity for fabric prepregs
- **EU334**: modified tack, for high modulus fiber unidirectional prepreg
- **EU340**: higher viscosity
- **EU432**: modified tack for high modulus fiber unidirectional prepreg and low resin content

www.composite-materials.it

OPERATIONAL INSTRUCTIONS

CURE PROCESS RECOMMENDATIONS

This epoxy matrix system can be processed under a very wide range of temperature*. Just as indication, see below curing cycle:

Temperature °C (°F)	Time	Tg °C (°F) DSC	Tg °C (°F) E' DMA
125 (257)	60'	125 (257)	132.5 (271)

**Personalized cure cycle can be developed with CIT Technical Department, in order to fulfil customer manufacturing process optimization.*

AUTOCLAVE

Once determined the processing temperature and corresponding cure time, use these processing parameters in the following cure cycle:

Step	Temperature °C (°F)	Time (min)	Heating rate to isothermal °C/min (°F/min)	Pressure bar (psi)
1	25 (77)	–	–	Vacuum -0.8 (-11.6)
2	125 (257)	–	1÷3 (1.8÷5.4)	3÷7 (43÷102)
3	125 (257)	60	–	3÷7 (43÷102)
4	70 (158)	–	3÷5 (5.4÷9.0)	3÷7 (43÷102)
5	25 (77)	–	–	–

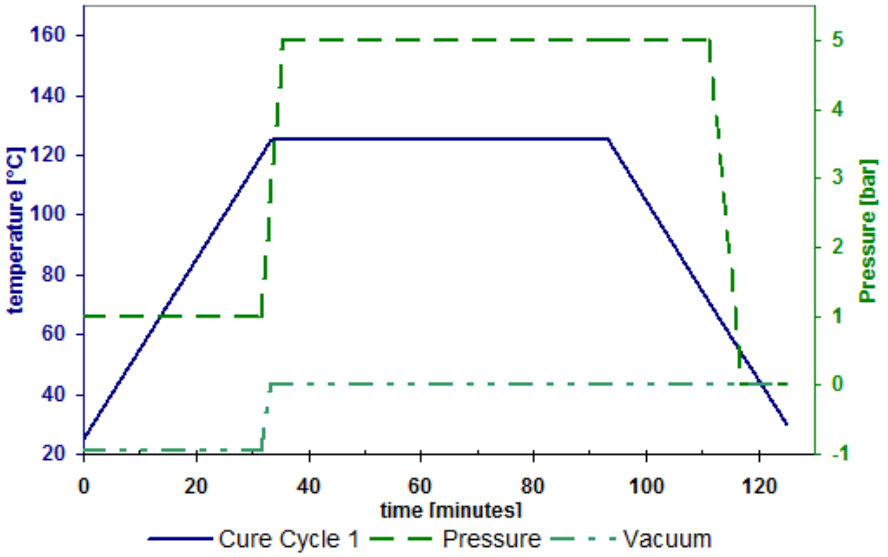

www.composite-materials.it

RESIN MATRIX

GENERAL PROPERTIES

Property	Unit	Value	Standard
Storage life @ -18°C (0°F)	months	12	
Out life @ 23°C (73°F)	days	30	
Prepreg volatiles	%wt	<1	ASTM D3530-97R03
Cured resin density	g/cm^3	1.20	ASTM D792-00
Tg (DSC)	°C (°F)	125 (257)	ASTM D3418-03
Tg E' (DMA)*	°C (°F)	115 (257)	ASTM E1640-09
Tg Peak Tan δ (DMA)*	°C (°F)	132,5 (270,5)	ASTM E1640-09
Tack		medium	
Elastic Modulus	GPa	3.36	ASTM D790-03

**Laminate Fully Cured 60'@125°C*

THERMO-MECHANICAL DMA ANALYSIS

DMA trace of REM laminate cured for 60' @ 125°C.

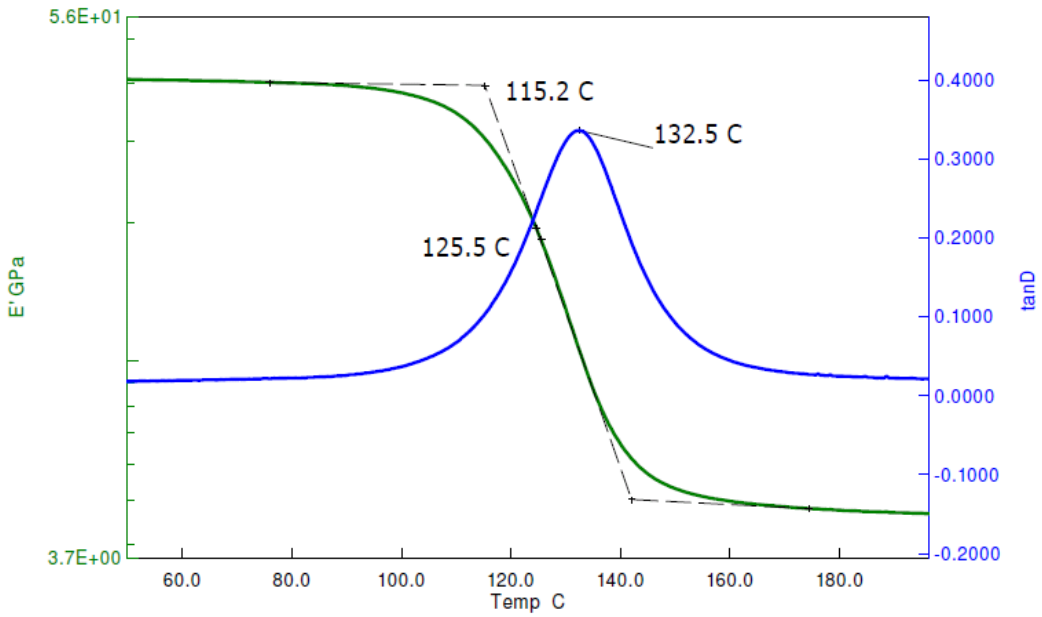

DMA Analysis (1Hz)

www.composite-materials.it

composite materials italy

VISCOSITY PROFILE

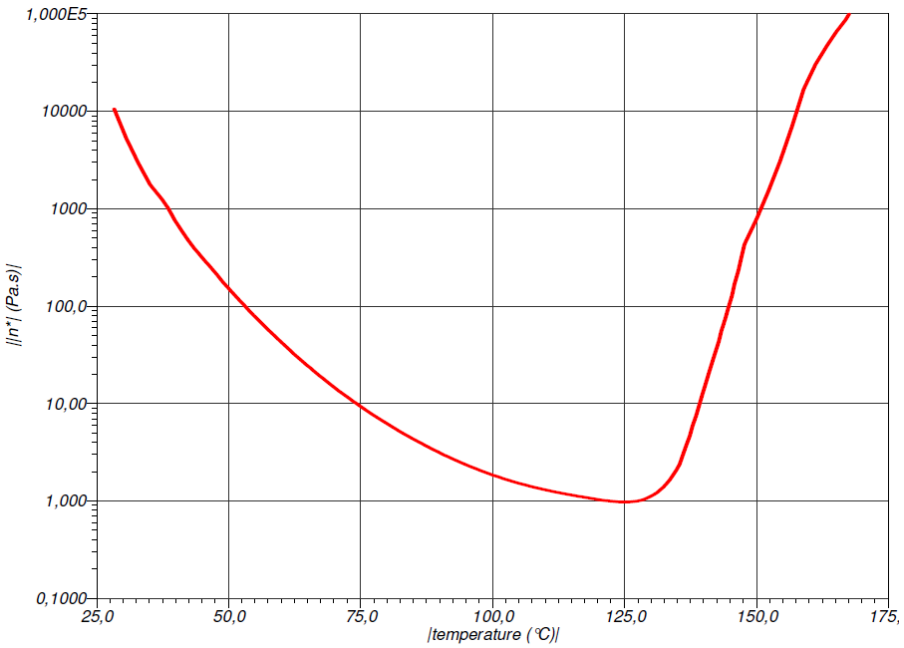

Viscosity profile: temperature vs complex viscosity

Resin complex viscosity is measured under 3°C/min heating rate, 1Hz oscillating frequency.

GEL TIME

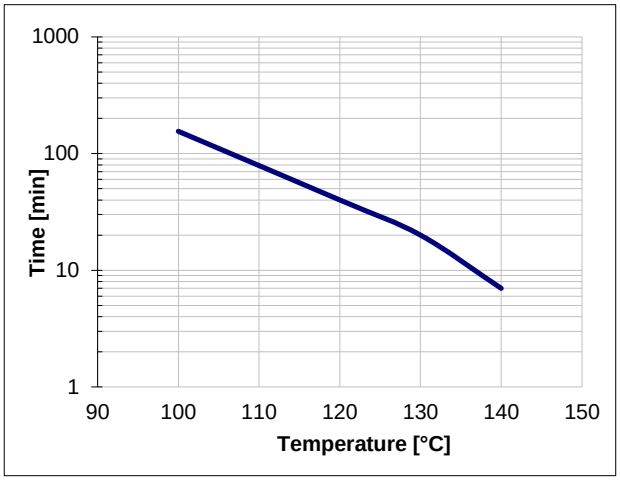

Temperature °C (°F)	Gel Time (min)
100 (212)	155
120 (248)	40
130 (266)	20
140 (284)	7

www.composite-materials.it

CURED PREPREG

Test carried out on a UD REM TAPE – 12KT700 Carbon Fiber at 36%wt resin content (54% fiber volume). Values are then normalized to 60% F.V.

Cured Material Property	Unit	Value Actual 54%F.V.	Value Normalized 60%F.V.	Standard
Tensile Modulus	GPa (Msi)	123 (17.8)	136 (19.8)	ASTM D3039-00
Tensile Strength	MPa (ksi)	2294 (333)	2549 (370)	
Poisson's ratio	–	0.34	–	
Flexural Modulus	GPa (Msi)	134 (19.5)	149 (21.7)	ASTM D790-03
Flexural Strength	MPa (ksi)	1857 (269)	2063 (299)	
Interlaminar Shear Strength	MPa (ksi)	81.5 (11.8)	–	ASTM D2344-00
Interlaminar Fracture Toughness G_{IC}	J/m^2 ($lb\text{-}in/in^2$)	800 (4.57)	–	ASTM D5528-01

(*) at 5% calculated shear strain

www.composite-materials.it

SAFETY CONSIDERATIONS

- This product contains epoxy resin.
- May cause allergic reaction.
- Avoid prolonged contact with skin.
- The use of latex gloves for handling is suggested.
- It is also suggested to work in an aerated environment.
- Scraps are to be cured and discarded following national law.

Note: For further information check the Material Safety Data Sheet.

DELIVERY FORM AND PACKAGING

The ***prepreg fabrics*** are rolled on 75 mm of diameter cardboard cores with release paper on one side and polyethylene film separator on the other side.
It is delivered on rolls sealed in waterproof plastic bag and packed in cardboard boxes.

Standard width: 100 cm. ***Standard length:*** 50 m.

The ***prepreg UD*** are rolled on 300 mm of diameter cardboard cores with release paper on one side (or no flat polyethylene film as alternative) and no flat polyethylene film separator on the other side.
It is delivered on rolls sealed in waterproof plastic bag and packed in cardboard boxes.

Standard width: 60cm (from 30cm up to 90cm).
Standard length: 100 m.

HANDLING AND CONDITIONING

- Stock rolls at -18 °C, sealed in original packages.
- Shop life at 23°C refers to rolls sealed in original packages.
- Before the use of the prepreg, get out the roll from the freezer and let it warm up to room temperature for 6 hours sealed in its original package.

IMPORTANT NOTICE:

The data and statements supplied in this datasheet are met to provide an overview of this product and its properties. Users should perform their own verification and testing to determine suitability of this material for their specific end use applications. NO WARRANTY OF FITNESS FOR A PARTICULAR PURPOSE IS EXPRESSED OR IMPLIED. Nothing herein is to be taken as permission to practice any patented invention without a licence.

Copyright Composite Materials (Italy) s.r.l., December 2015, All rights reserved. RDS 15.016, Rev.01

Toray Group
Composite Materials (Italy) s.r.l. - Socio Unico
Via Quasimodo, 33 - 20025 Legnano (MI) ITALY
Capitale Sociale € 100.000 I.V. - R.E.A. MI n° 2052698
Iscrizione Registro Imprese C. F. n° 08844870967
P.IVA IT08844870967
Phone: +39 0331.467.555 • Fax: +39 0331.467.777
E-mail: info@composite-materials.it
www.composite-materials.it

CORECORK

AMORIM
CORK COMPOSITES

NL10

Material Data Sheet

Flexibility and excellent conformability make **NL10** possible to be easily integrated into fast production cycles.

This product can be processed by hand layup, vacuum bagging and infusion processes and will withstand manufacturing temperatures up to 150ºC.

The unique properties of **NL10** such as: a closed air filled cell structure, low water absorption, rot resistance and high level of noise and vibration attenuation make it an excellent core material for the composites industry - perfectly aligned with the new green classifications.

MECHANICAL PROPERTIES OF THE CORE MATERIAL		
DENSITY (Kg/m^3)	ASTM C271	120-180
COMPRESSIVE STRENGHT (MPa)	ASTM C365	0,3*
COMPRESSIVE MODULUS (MPa)	ASTM C365	5,1*
TENSILE STRENGHT (MPa)	ASTM C297	0,6*
SHEAR STRENGHT (MPa)	ASTM C273	0,9*
SHEAR MODULUS (MPa)	ASTM C273	5,9*
THERMAL CONDUCTIVITY (W/mK)	ASTM E1530	0,042*
LOSS FACTOR (at 1KHz)	ASTM E756	0,022*

MECHANICAL PROPERTIES OF THE CORE MATERIAL IN A COMPOSITE [1]		
FLEXURAL STRENGHT AT YIELD (MPa)	ASTM D790	37*
FLEXURAL MODULUS (GPa)	ASTM D790	3,5*
SHEAR STRENGHT AT YIELD (MPa)	ASTM C392	0,8*
SHEAR MODULUS (MPa)	ASTM C392	44*
COMPRESSIVE STRENGHT AT YIELD (MPa)	ASTM C365	1,2*
COMPRESSIVE MODULUS (MPa)	ASTM C365	19*
WATER ABSORPTION (%)	ASTM C272	<4*
PANEL DENSITY	-	0,600*

[1] Samples made by Infusion (0.6 bar) with epoxy resin ref. SR8100/cat ref. SD8824 and two layers of 300g/m^2 glass fibre roving, on each side, sandwich thickness: 6,5 mm; cure at 60ºC; samples tested after 5 days of manufacturing.
* Typical values

Lightweight

Vibration damping

Thermal insulation

Sustainable and energy efficient

KEY FEATURES

- Good drapeability
- Print blocking capability
- Stable material
- Lower resin consumption
- Resin compatibility (Excelent for: Epoxy, Polyester, Phenolic, Vynilester and Polyurethane)

PROCESS GUIDELINES	
RESIN UPTAKE (*) (per m^2 at 1mm)	270g
MAXIMUM PROCESSING TEMPERATURE	180ºC
VACUUM BAG PROCESSING	up to 150ºC
AUTOCLAVE CURE PROCESSING	possible
COEFFICIENT OF THERMAL EXPANSION (ASTM E831-06)	aprox. 110 X 10-6/ºC at RT

AMORIM
CORK COMPOSITES

The data provided in this Material Data Sheet represents typical values. This information is not intended to be used as a purchasing specification and does not imply suitability for use in a specific application. Failure to select the proper sealing product may result in either product damage or personal injury. Please contact Amorim Cork Composites regarding recommendations for specific applications. Amorim Cork Composites expressly disclaims all warranties, including any implied warranties or merchantability or of fitness for a particular purpose. Amorim Cork Composites is not liable for any indirect, special, incidental, consequential, or punitive damages as a result of using the information listed in this material data sheet, any of its brochures, its products or any future use or re-use of them by any person or entity. **For contractual purposes, please request our Product Specifications Sheet (PDA).**

www.amorimcorkcomposites.com

CORECORK

AMORIM
CORK COMPOSITES

NL20

Material Data Sheet

Flexibility and excellent conformability make **NL20** possible to be easily integrated into fast production cycles.

This product can be processed by hand layup, vacuum bagging and infusion processes and will withstand manufacturing temperatures up to 150ºC.

The unique properties of **NL20** such as: a closed air filled cell structure, low water absorption, rot resistance and high level of noise and vibration attenuation make it an excellent material for to the composites industry - perfectly aligned with the new green classifications.

MECHANICAL PROPERTIES OF THE CORE MATERIAL		
DENSITY (Kg/m^3)	ASTM C271	170-235
COMPRESSIVE STRENGHT (MPa)	ASTM C365	0,5*
COMPRESSIVE MODULUS (MPa)	ASTM C365	6,0*
TENSILE STRENGHT (MPa)	ASTM C297	0,7*
SHEAR STRENGHT (MPa)	ASTM C273	0,9*
SHEAR MODULUS (MPa)	ASTM C273	5,9*
THERMAL CONDUCTIVITY (W/mK)	ASTM E1530	0,044*
LOSS FACTOR (at 1KHz)	ASTM E756	0,043*

MECHANICAL PROPERTIES OF THE CORE MATERIAL IN A COMPOSITE [1]		
FLEXURAL STRENGHT AT YIELD (MPa)	ASTM D790	56*
FLEXURAL MODULUS (GPa)	ASTM D790	4*
SHEAR STRENGHT AT YIELD (MPa)	ASTM C392	0,9*
SHEAR MODULUS (MPa)	ASTM C392	41*
COMPRESSIVE STRENGHT AT YIELD (MPa)	ASTM C365	2,2*
COMPRESSIVE MODULUS (MPa)	ASTM C365	23*
WATER ABSORPTION (%)	ASTM C272	<4*
PANEL DENSITY	-	0,560*

[1] Samples made by Infusion (0.6 bar) with epoxy resin ref. SR8100/cat ref. SD8824 and two layers of 300g/m^2 glass fibre roving, on each side, sandwich thickness: 6,5 mm; cure at 60ºC; samples tested after 5 days of manufacturing.
* Typical values

Lightweight

Vibration damping

Thermal insulation

Sustainable and energy efficient

KEY FEATURES

- Good drapeability
- Print blocking capability
- Stable material
- Lower resin consumption
- Resin compatibility (Excelent for: Epoxy, Polyester, Phenolic, Vynilester and Polyurethane)

PROCESS GUIDELINES	
RESIN UPTAKE (*) (per m^2 at 1mm)	170g
MAXIMUM PROCESSING TEMPERATURE	180ºC
VACUUM BAG PROCESSING	up to 150ºC
AUTOCLAVE CURE PROCESSING	possible
COEFFICIENT OF THERMAL EXPANSION (ASTM E831-06)	aprox. 110 X 10-6/ºC at RT

AMORIM
CORK COMPOSITES

The data provided in this Material Data Sheet represents typical values. This information is not intended to be used as a purchasing specification and does not imply suitability for use in a specific application. Failure to select the proper sealing product may result in either product damage or personal injury. Please contact Amorim Cork Composites regarding recommendations for specific applications. Amorim Cork Composites expressly disclaims all warranties, including any implied warranties or merchantability or of fitness for a particular purpose. Amorim Cork Composites is not liable for any indirect, special, incidental, consequential, or punitive damages as a result of using the information listed in this material data sheet, any of its brochures, its products or any future use or re-use of them by any person or entity. **For contractual purposes, please request our Product Specifications Sheet (PDA).**

www.amorimcorkcomposites.com

CORECORK

AMORIM
CORK COMPOSITES

NL25

Material Data Sheet

Flexibility and excellent conformability make **NL25** possible to be easily integrated into fast production cycles.

This product can be processed by hand layup, vacuum bagging and infusion processes and will withstand manufacturing temperatures up to 150ºC.

The unique properties of **NL25** such as: a closed air filled cell structure, low water absorption, rot resistance and high level of noise and vibration attenuation make it an excellent core material for the composites industry - perfectly aligned with the new green classifications.

MECHANICAL PROPERTIES OF THE CORE MATERIAL		
DENSITY (Kg/m^3)	ASTM C271	220-260
COMPRESSIVE STRENGHT (MPa)	ASTM C365	0,6*
COMPRESSIVE MODULUS (MPa)	ASTM C365	6,9*
TENSILE STRENGHT (MPa)	ASTM C297	0,7*
SHEAR STRENGHT (MPa)	ASTM C273	1,0*
SHEAR MODULUS (MPa)	ASTM C273	6,0*
THERMAL CONDUCTIVITY (W/mK)	ASTM E1530	0,046*
LOSS FACTOR (at 1KHz)	ASTM E756	0,062*

MECHANICAL PROPERTIES OF THE CORE MATERIAL IN A COMPOSITE [1]		
FLEXURAL STRENGHT AT YIELD (MPa)	ASTM D790	63*
FLEXURAL MODULUS (GPa)	ASTM D790	4,3*
SHEAR STRENGHT AT YIELD (MPa)	ASTM C392	0,9*
SHEAR MODULUS (MPa)	ASTM C392	38*
COMPRESSIVE STRENGHT AT YIELD (MPa)	ASTM C365	2,5*
COMPRESSIVE MODULUS (MPa)	ASTM C365	26*
WATER ABSORPTION (%)	ASTM C272	<4*
PANEL DENSITY	-	0,630*

[1] Samples made by Infusion (0.6 bar) with epoxy resin ref. SR8100/cat ref. SD8824 and two layers of 300g/m^2 glass fibre roving, on each side, sandwich thickness: 6,5 mm; cure at 60ºC; samples tested after 5 days of manufacturing.

* Typical values

Lightweight

Vibration damping

Thermal insulation

Sustainable and energy efficient

KEY FEATURES

- Good drapeability
- Print blocking capability
- Stable material
- Lower resin consumption
- Resin compatibility (Excelent for: Epoxy, Polyester, Phenolic, Vynilester and Polyurethane)

AMORIM
CORK COMPOSITES

The data provided in this Material Data Sheet represents typical values. This information is not intended to be used as a purchasing specification and does not imply suitability for use in a specific application. Failure to select the proper sealing product may result in either product damage or personal injury. Please contact Amorim Cork Composites regarding recommendations for specific applications. Amorim Cork Composites expressly disclaims all warranties, including any implied warranties or merchantability or of fitness for a particular purpose. Amorim Cork Composites is not liable for any indirect, special, incidental, consequential, or punitive damages as a result of using the information listed in this material data sheet, any of its brochures, its products or any future use or re-use of them by any person or entity. **For contractual purposes, please request our Product Specifications Sheet (PDA).**

www.amorimcorkcomposites.com